CRYSTALLINE FORMS OF SELECTED AGROCHEMICAL ACTIVES: DESIGN AND SYNTHESIS OF COCRYSTALS

BY

ELISA NAUHA

Academic dissertation
for the degree of
Doctor of Philosophy

To be presented, by permission of the Faculty of Mathemathics and Science of the University of Jyväskylä, for public examination in Auditorium YAA303, on January 13th 2012, at 12 noon.

UNIVERSITY OF JYVÄSKYLÄ

ABSTRACT

The research described in this disseration covers the crystal form screening of two analogous agrochemical actives, thiophanate-methyl and thiophanate-ethyl, as well as the discovery of seven 4-hydroxybenzoic acid cocrystals of selected agrochemical actives. Polymorphs are crystal forms of a compound that have the same composition, but a different arrangement of molecules. Cocrystals are molecular crystals composed of two or more compounds, and refer mainly to crystals which contain compounds that are solids at standard conditions. Solvates are forms that have molecules of solvent in the crystal lattice and these include hydrates, in which the solvent is water. The crystal forms of organic compounds are investigated especially in the pharmaceutical and other specialty chemical industries for better processing and activity of the compounds as well as for intellectual property reasons.

Thiophanate-methyl was found to crystallize as two polymorphs and fourteen solvates, while thiophanate-ethyl was found to crystallize as four polymorphs and seven solvates. Identification of the forms was achieved mostly with powder X-ray diffraction, but methods such as IR spectroscopy, solid state NMR spectroscopy and thermogravimetric analysis were also used. The crystal structures of most of the crystal forms were determined by single crystal X-ray diffraction, allowing the inspection of intermolecular interactions such as hydrogen bonding. Reliable hydrogen bonding motifs were identified and used as supramolecular synthons in the design of new cocrystal forms. Three cocrystals of thiophanate-methyl and eight cocrystals of thiophanate-ethyl were found. The seven cocrystal forms of agrochemical actives with 4-hydroxybenzoic acid show better properties in comparison to the pure forms, and highlight the importance of cocrystallization in industrial applications.

The design and synthesis of cocrystals as well as the analysis of packing and hydrogen bonding in crystal structures is reviewed in the literature part of this thesis.

Keywords: polymorph, cocrystal, solvate, supramolecular synthon, agrochemical, X-ray crystallography, supramolecular chemistry, structural chemistry

Author's address   Elisa Nauha
Department of Chemistry
Nanoscience Center
P.O. Box 35
40014 University of Jyväskylä
Finland
elisa.k.nauha@jyu.fi

Supervisor   Professor Maija Nissinen
Department of Chemistry
Nanoscience Center
University of Jyväskylä
Jyväskylä, Finland

Reviewers   Professor Fabrizia Grepioni
Department of Chemistry
University of Bologna
Bologna, Italy

Professor Joel Bernstein
Faculty of Science
New York University Abu Dhabi
Abu Dhabi, United Arab Emirates

Opponent   Professor Katharina Fromm
Department of Chemistry
University of Fribourg
Fribourg, Switzerland

PREFACE

This work was carried out at the Department of Chemistry, University of Jyväskylä, Finland and partly at BASF SE in Ludwigshafen, Germany between 2007 and 2011.

Jyväskylä, December 15th 2011

Elisa Nauha

LIST OF ORIGINAL PUBLICATIONS

This dissertation is based on the original publications listed below and they are herein referred to by their Roman numerals.

I   E. Nauha, H. Saxell, M. Nissinen, E. Kolehmainen, A. Schäfer, and R. Schlecker, Polymorphism and versatile solvate formation of thiophanate-methyl, *CrystEngComm* 11 (2009), 2536-2547. DOI: 10.1039/b905511h.

II   E. Nauha, A. Ojala, H. Saxell and M. Nissinen, Comparison of the polymorphs and solvates of two analogous fungicides - a case study of the applicability of a supramolecular synthon approach in crystal engineering, *CrystEngComm* 13 (2011), 4956-4964. DOI: 10.1039/C1CE05077J.

III   E. Nauha, E. Kolehmainen and M. Nissinen, Packing incentives and a reliable N-H···N-pyridine synthon in co-crystallization of bipyridines with two agrochemical actives. *CrystEngComm* 13 (2011), 6531-6537. DOI:10.1039/C1CE05730H.

IV   E. Nauha and M. Nissinen, Co-crystal design using a pyridine-amine synthon for an agrochemical active containing a thioamide group, *J. Mol. Struct.* 1006 (2011), 566-569 DOI: 10.1016/j.molstruc.2011.10.004.

V   H. E. Saxell, R. Israels, A. Schäfer, M. Bratz, H. W. Höffken, I. Brode, E. Nauha, M. Nissinen, Crystalline complexes of 4-hydroxy benzoic acid and selected pesticides, *US. Pat.*, WO/2011/054741, 28.10.2010, (2011).

AUTHOR'S CONTRIBUTION

For papers I-IV the author is the primary author, and has carried out all the crystallization work and most of the X-ray crystallographic work for paper I and all the X-ray crystallographic work for papers II-IV. For patent V the author planned and carried out most of the screening experiments and did part of the X-ray crystallographic work.

ABBREVIATIONS

1,2-DCB	1,2-dichlorobenzene
1,2-DCE	1,2-dichloroethane
AI	active ingredient
API	active pharmaceutical ingredient
BPD	binary phase diagram
CH-one	cyclohexanone
CSD	Cambridge Structural Database
COSP	corresponding ordered set of points
DABCO	1,4-diazabicyclo[2.2.2]octane
DCM	dichloromethane
DITA	discontinuous isoperibolic thermal analysis
DMSO	dimethyl sulfoxide
DSC	differential scanning calorimetry
IP	intellectual property
IR	infra red spectroscopy
LAG	liquid-assisted grinding
m.p.	melting point
MeCN	acetonitrile
PSD	phase solubility diagram
SC	supramolecular construct
SMPT	solution-mediated phase transformation
SSNMR	solid state nuclear magnetic resonance
TE	thiophanate-ethyl, diethyl 4,4′-(*o*-phenylene)bis(3-thioallophanate)
TGA	thermogravimetric analysis
THF	tetrahydrofuran
TM	thiophanate-methyl, dimethyl 4,4′-(*o*-phenylene)bis(3-thioallophanate)
TPD	ternary phase diagram

CONTENTS

ABSTRACT

PREFACE

LIST OF ORIGINAL PUBLICATIONS

ABBREVIATIONS

CONTENTS

1 REVIEW OF THE LITERATURE

1.1 Introduction

In a crystalline material, molecules (~10^{14} per visible crystal[1]) are organized in an orderly repeating pattern. This repeating pattern, however, may not be the same in all crystals of a compound, resulting in polymorphs.[2] In multi-component molecular crystals, another repeating pattern has formed because molecules of another compound are included in the crystal. The different crystal forms of organic compounds are investigated in crystal engineering[3, 4] as possible routes to new functional materials, and especially in the pharmaceutical and other specialty chemical industries for better processing and increased activity of the compounds[5-8] as well as for intellectual property[9,10] reasons.

For organic molecular compounds the crystal form landscape is vast (Figure 1 and Figure 2). A compound as a single-component crystal can have polymorphs.[2] It can crystallize with solvent molecules to make hydrates or solvates.[11] It can also form other multi-component molecular crystals, *i.e.* cocrystals or salts, with compounds other than solvents. The cocrystals and salts can have hydrate or solvate forms and, in addition to this, all multi-component forms themselves can have polymorphs.

12
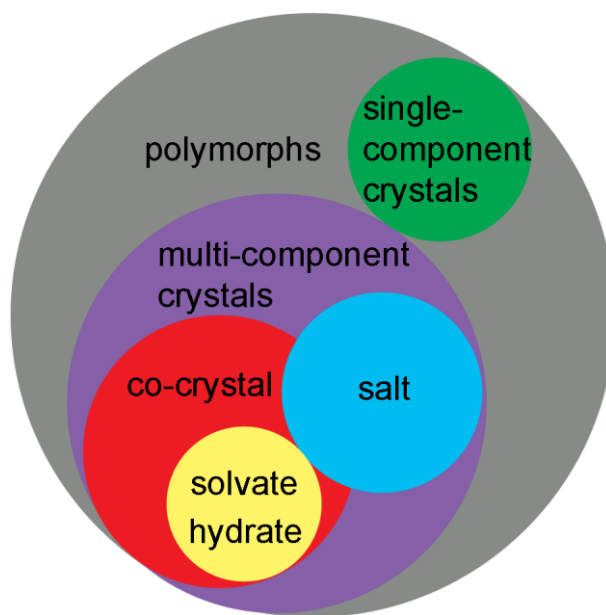
Figure 1. The crystal form landscape of molecular crystals.

As with the large amount of possible crystal forms, there are some debates on what is the correct term to describe each form and even how to correctly write the terms.[1, 12-16] In this text, the following definitions will be used: Polymorphs are different crystal forms of species that have the same composition, *i.e.* different crystalline arrangements of one compound or two or more compounds with the same ratio. Cocrystals are multi-component molecular crystals, a group that also contains solvates. Cocrystals in this text refer mainly to crystals which contain compounds that are solids at standard conditions. Solvates are crystal forms that have molecules of solvent in the crystal lattice and these include hydrates as a special case in which the solvent is water.
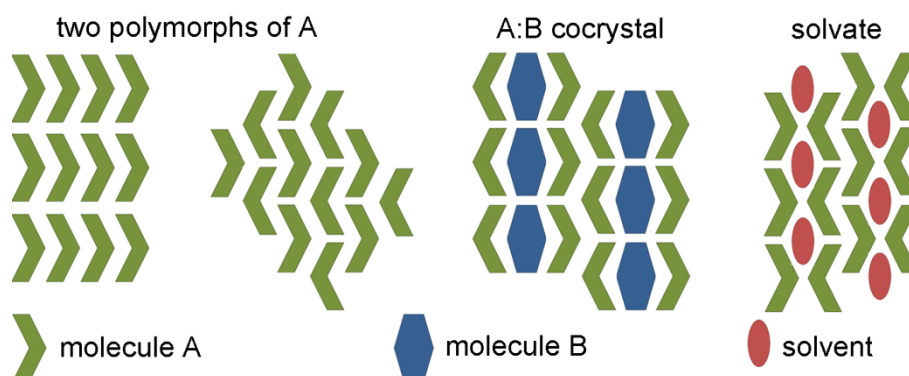
Figure 2. Some possible crystal forms of a molecule A.

There is a continuum between cocrystals and salts because the exchange of a hydrogen atom between the cocrystallizing compounds is sometimes not

complete.[17, 18] The compounds can in effect share the hydrogen, making the distinction between a salt and a cocrystal redundant. Whether two compounds form a salt or a cocrystal can also not always be predicted and this partly negates the discussion of purely neutral entities. A new class of interesting ionic cocrystals[19] has also been named in which a neutral molecule is cocrystallized with an inorganic salt. This text will mainly deal with multi-component molecular crystals between neutral molecules to distinguish cocrystals from salt forms.

Cocrystals as such are not new discoveries. According to Stahly's review[20] on cocrystals reported prior to 2000 the first organic:organic cocrystal is perhaps that between quinone and hydroquinone (Appendix) reported in 1844[21]. The full crystal structure to verify the makeup of this cocrystal, however, was not published until 1958,[22] because structure determination by single crystal X-ray diffraction was just being developed, with the first crystal structure[23] of sodium chloride published in 1913. Today the area of X-ray diffraction has developed to a point where crystal structures from single crystals can be acquired at best within a couple of hours and crystal structures from powder samples are also possible. This makes the analysis of small molecule crystalline materials almost commonplace and thus gives opportunities for the design of crystalline materials like cocrystals. The literature references for this work on the design and synthesis of cocrystals, which has also been reviewed[24-29] a number of times from the pharmaceutical perspective, have mostly been chosen from during the past decade to enlighten a picture of where cocrystal research is today.

1.2   Cocrystal design

There are cocrystals that form without any strong intermolecular interactions between the cocrystallizing compounds, but rational design of these is not possible and requires an experimental trial and error approach. Such cocrystals could be classified as clathrates, where one of the molecules is trapped within a network of the other.[30] Cocrystals which are connected via strong intermolecular interactions, however, can be designed by utilizing reliable supramolecular synthons.

1.2.1   Supramolecular synthon approach

Crystals in crystal engineering can be viewed as supermolecules consisting of superatoms, *i.e.* the assembled molecules, bound together with intramolecular interactions instead of covalent bonds. Supramolecular synthons have been defined by Desiraju[31] as "structural units within supermolecules which can be formed and/or assembled by known or conceivable synthetic operations involving intermolecular interactions". The key in designing cocrystals is

choosing a synthon, which is likely to form in a crystallization process, like a synthethic chemist chooses known reactants to make a specific covalent bond. Most often the synthons involve hydrogen bonds[32] because of their strength and directionality, but other interactions such as halogen bonding[33, 34] can also be used (Scheme 1). Aromatic π- π interactions and van der Waals forces do not yet have much use in cocrystal design, but they are not to be overlooked in experiments because they contribute to the final outcome of a crystallization.
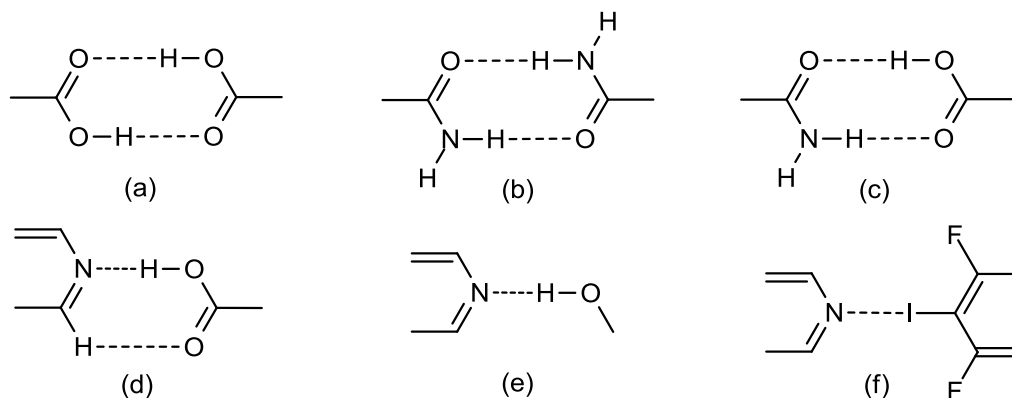
Scheme 1. Examples of common synthons: (a) acid-acid and (b) amide-amide homosynthon, (c) amide-acid, (d) pyridine-acid, (e) pyridine-hydroxyl and (f) halogen bonding heterosynthon.

The basis for designing hydrogen bonding synthons in cocrystals is in Etter's empirical hydrogen bonding rules for organic compounds:[35]

1. All good proton donors and acceptors are used in hydrogen bonding.
2. Six-membered-ring intramolecular hydrogen bonds form in preference to intermolecular hydrogen bonds.
3. The best proton donors and acceptors remaining after intramolecular hydrogen bond formation form intermolecular hydrogen bonds to one another. After this the second best donor and acceptor form a hydrogen bond and so on.

Etter[35] also gave rules for specific functional groups to give a more detailed strategy for certain types of compounds and suggested this type of work should be continued with further database studies and cocrystallization experiments to find the hierarchies of hydrogen bonds. Etter's rules for carboxylic acid cocrystals with 2-aminopyrimidine (Appendix), for example, state that both the ring nitrogen acceptors and N-H protons of 2-aminopyrimidine are used in hydrogen bonding to the acid rather than to itself, as the heterocyclic nitrogen atoms are better acceptors than the acid carbonyl and the acid O-H is a better donor than the amino group hydrogens. Twenty years later this kind of work is still ongoing. For example, Zaworotko *et al.*[36, 37] have studied the hierarchy of hydrogen bonds to the pyridine moiety by way of CSD[38] analyses and cocrystallization experiments. They deduced that the

carboxylic acid hydroxyl is comparable in strength to the alcoholic hydroxyl donor for a pyridine acceptor.[36] The pyridine-hydroxyl synthon was also found to persist even when a cyano acceptor was present.[37] These kinds of studies are still needed as pharmaceutical and other active ingredients contain a number of functionalities and competition between hydrogen bonding synthons during crystallization is inevitable in the design of cocrystals.
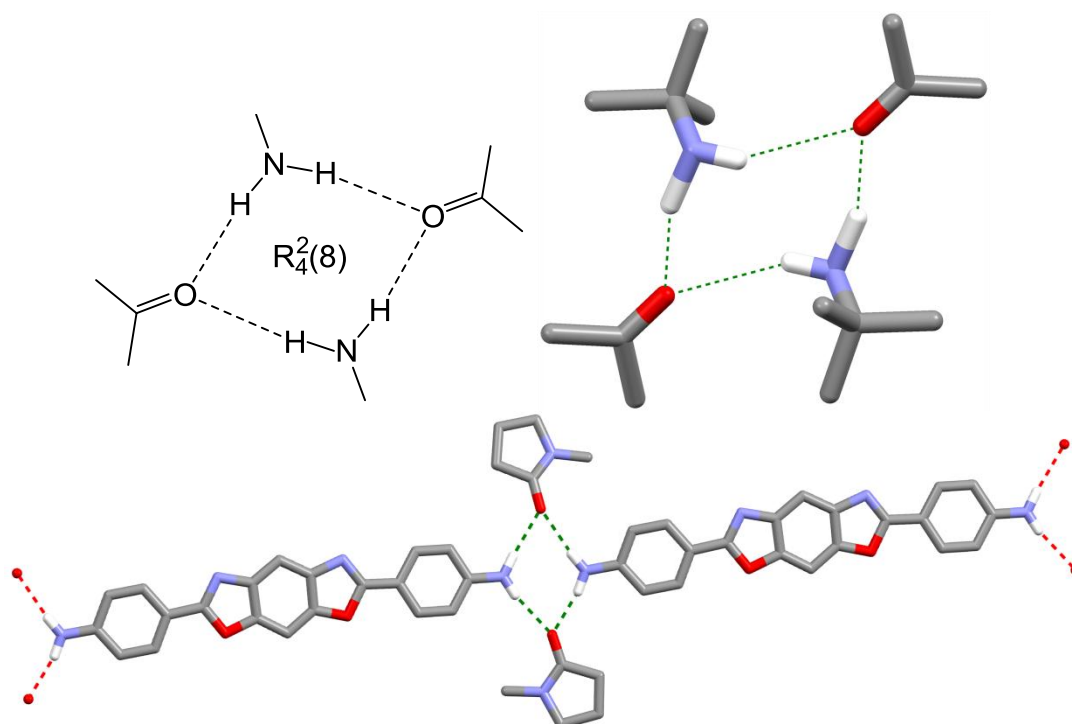
Figure 3. The planned motif of acetone and methylamine, the motif in the succesful acetone cocrystal with tert-butylamine[39] and a more complicated 2,6-bis(4-aminophenyl)benzo (1,2-d:5,4-d')dioxazole solvate with 1-methylpyrrolidin-2-one[42] showing a R_4^2 (8) hydrogen bonding motif. Non-hydrogen bonding hydrogen atoms omitted for clarity.

In addition to hierarchial studies, new synthons have to be identified and tested for robustness. Searching the CSD[38] for reoccurring hydrogen bonding motifs for specific functionalities is a good way to find new usable synthons. The database is naturally somewhat biased towards already known and utilized reliable synthons, but with 541 748 structures in January 2011 there are still chances to find synthons, that have not been systematically studied. Bernstein *et al*.[39] implemented this type of study for the $R_4^2(8)$ hydrogen bonding motif[40, 41] (ring of eight atoms with two acceptors and four donors, Figure 3 and chapter 1.4.1), which had been previously recognized, but not used as a synthon for cocrystal design. The motif was tested by implementing a database search, calculating interaction energies for a computational screen and then with proof-of-concept experiments involving very simple molecules. The most simple system of acetone and methylamine did not yield cocrystals, but a cocrystal of acetone and tert-butylamine was found with the desired synthon (Figure 3). At

least 160 more complicated cocrystal examples like the 1-methylpyrrolidin-2-one solvate[42] (Figure 3) can be found in the CSD.[38]

As with all rules, exceptions to the hydrogen bonding rules and the formation of reliable synthons are possible, because crystallization is also influenced by other weaker interactions, kinetics and close packing of molecules. Supramolecular synthon polymorphism is one example of Etter's third rule being broken. Sreekanth *et al.*[43] observed this when cocrystallizing 4-hydroxybenzoic acid and 2,3,5,6-tetramethylpyrazine by finding a polymorphic form I from acetone with an unexpected acid-acid homosynthon, but a more stable form II from acetonitrile-methanol with the expected acid-pyridine heterosynthon (Figure 4a-b). Form I was found to transform to form II at room temperature indicating it to be a possible kinetic product. Mukherjee and Desiraju[44] observed the same kind of supramolecular synthon polymorphism for the cocrystals of 4,4′-bipyridine and 4-hydroxybenzoic acid for which two cocrystal polymorphs with a 1:2 ratio, but different synthons were found (Figure 4c-d). For this system a stoichiometric variant with a 2:1 ratio was also obtained.
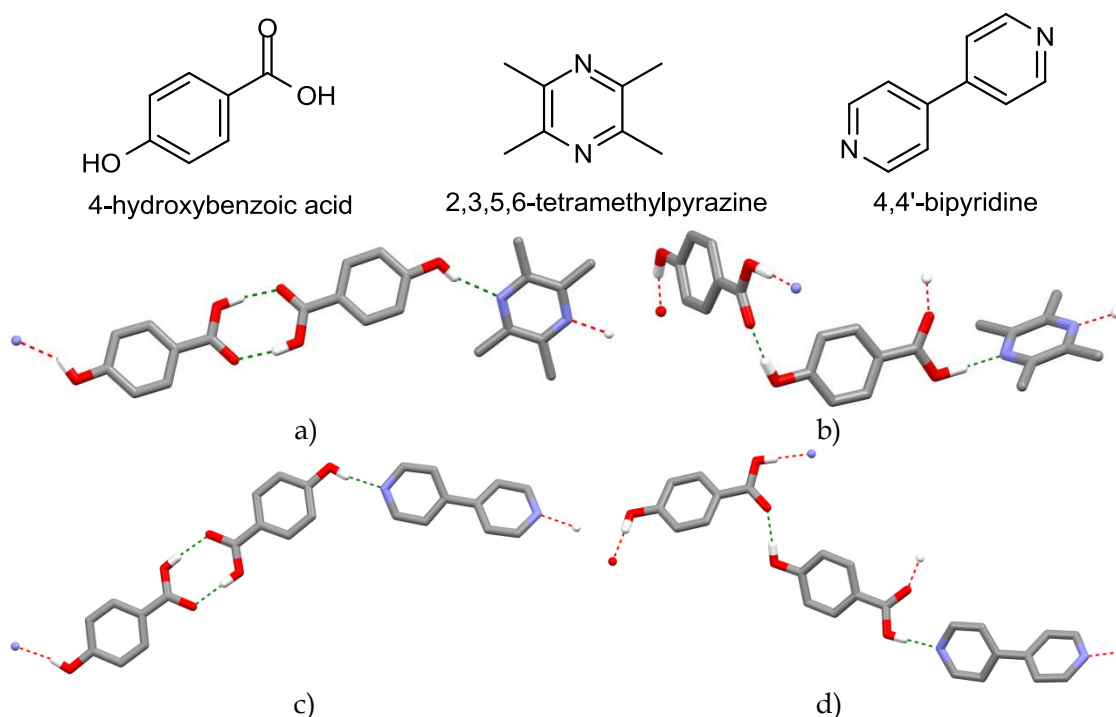
Figure 4. Supramolecular synthon polymorphism: a) Form I and b) form II of the 4-hydroxybenzoic acid - 2,3,5,6-tetramethylpyrazine cocrystal[43] and c-d) the two polymorphs of the 4-hydroxybenzoic acid - 4,4′-bipyridine cocrystal.[44] Non-hydrogen bonding hydrogen atoms omitted for clarity.

The supramolecular reaction, the crystallization, consist of molecular recognition and aggregation leading to nucleation and crystal growth. Crystallization is inherently kinetically controlled because the primary nucleation step in a supersaturated solution is ruled by kinetics.[45] As there is thus far no comprehensive way to study nucleation, the phenomenon is not fully understood and consequently not controllable. The outcome of a cocrystallization is also influenced by the close packing of molecules[46] and a loosely packed cocrystal form is likely less stable than a better packed single-component form. The outcome of such a crystallization then depends on the nucleation kinetics and the rate of solution-mediated transformation to the thermodynamically more stable form. To circumvent packing problems in cocrystal formation during experimental screening, one should pick a number of similar coformers that can make the desired synthon.

1.2.2 Synthons and cocrystals - examples

Some examples of common reliable synthons that have been used in cocrystal design and the design successes with those are presented. The examples are of active pharmaceutical ingredients (API) that are often used as model systems, and cocrystals that are more of a crystal engineering interest.

The acid-acid homosynthon (Scheme 1a) can be used in cocrystal design even though heterosynthons, *i.e.* synthons between different functional groups, are usually favored to homosynthons.[47] If two homosynthon forming molecules are different enough, a cocrystal is likely to form because the homosynthon is in effect a heterosynthon. The difference in the values of Hammett substituent constants[48], which give a quantitative measure of the electron-withdrawing and -donating potential of a functional group relative to benzoic acid, may be used to predict the formation of acid/acid cocrystals.[47, 49, 50] Combinations showing small differences in this parameter are unlikely to form cocrystals, whereas combinations with larger differences are likely to cocrystallize. When the difference is very large the compounds are likely to form salts instead of cocrystals as the pK_a values of molecules are connected to the values of the Hammett constants. Examples of two successfully designed cocrystals for which the Hammett substitution constants have large difference are the 4-cyanobenzoic acid and 3,5-dinitrobenzoic acid cocrystals of 4-aminobenzoic acid (Figure 5).[50]
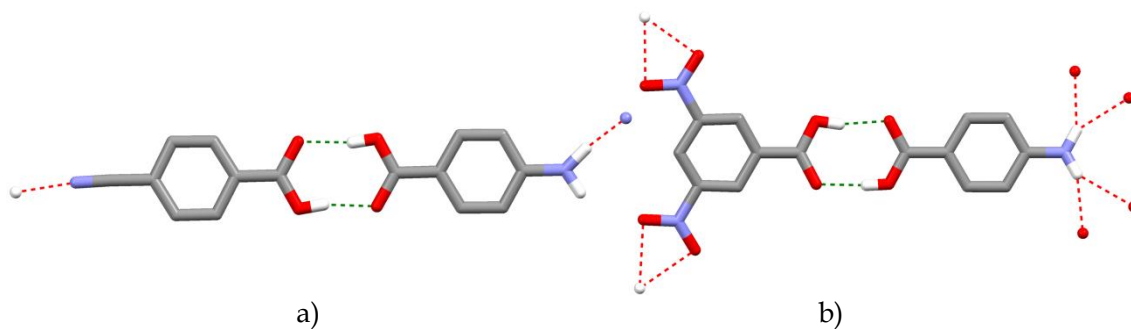
Figure 5. Cocrystals of 4-aminobenzoic acid with a) 4-cyanobenzoic acid and b) 3,5-dinitrobenzoic acid showing an acid-acid homosynthon.[50] Non-hydrogen bonding hydrogen atoms omitted for clarity.

carbamazepine   aspirin   saccharin

a)   b)
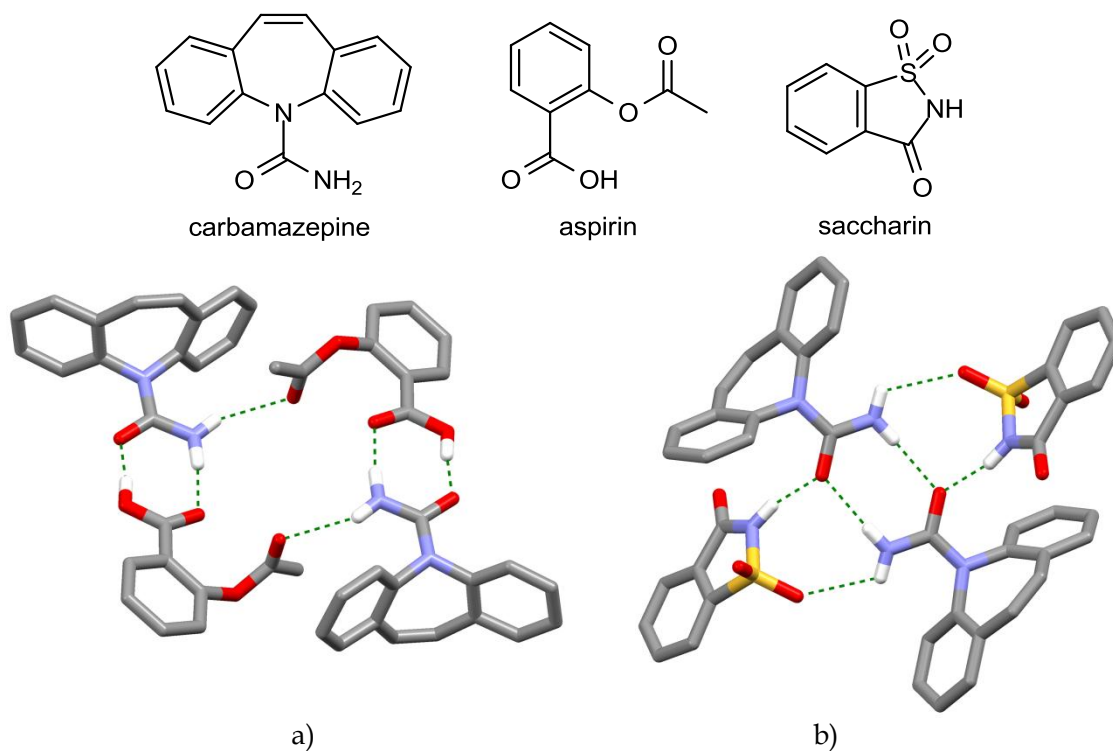
Figure 6. Carbamazepine a) aspirin cocrystal with a acid-amide heterosynthon[53] and b) saccharin cocrystal with an amide homosynthon.[54] Non-hydrogen bonding hydrogen atoms omitted for clarity.

The acid-amide heterosynthon (Scheme 1c) is very often used in cocrystal design. Carbamazepine (Figure 6) is an amide group containing active pharmaceutical ingredient (API), which has been found to crystallize as at least 50 solvates and cocrystals[51] with more constantly being found[52]. All of these forms do not utilize the acid-amide heterosynthon, but many do, like the cocrystal with aspirin[53] (Figure 6a). The cocrystal with saccharin (Figure 6b), however, utilized a different cocrystal design strategy, where the unused N-H donor left free in the amide homosynthon and the carbonyl capable of

bifurcated hydrogen bonding are used.[53] The saccharin cocrystal of carbamazepine has been found to be a viable option to the marketed polymorphic form III of carbamazepine in stability, dissolution and bioavailability studies.[7]

4,4'-bipyridine is the most often found coformer in cocrystal structures in the CDS database.[55] This is perhaps because it is a rigid molecule and a good hydrogen bond acceptor, making it ideal for cocrystal studies involving the pyridine-acid and pyridine-hydroxyl synthons (Scheme 1d-e). It can be efficiently used as a linker molecule in crystal engineering network structures. The pyridine-carboxylic acid heterosynthon has been used, for example, in crystal engineering with with di- and tricarboxylic acids.[56] The 4,4'-bipyridine cocrystal with isophthalic acid, for example, has chains of alternating bipyridine and diacid molecules as expected (Figure 7a). A 4,4'-bipyridine cocrystal with 2,2'-biphenol has similar expected chains connected with the pyridine-hydroxyl heterosynthon (Figure 7b).[57]

a)   b)
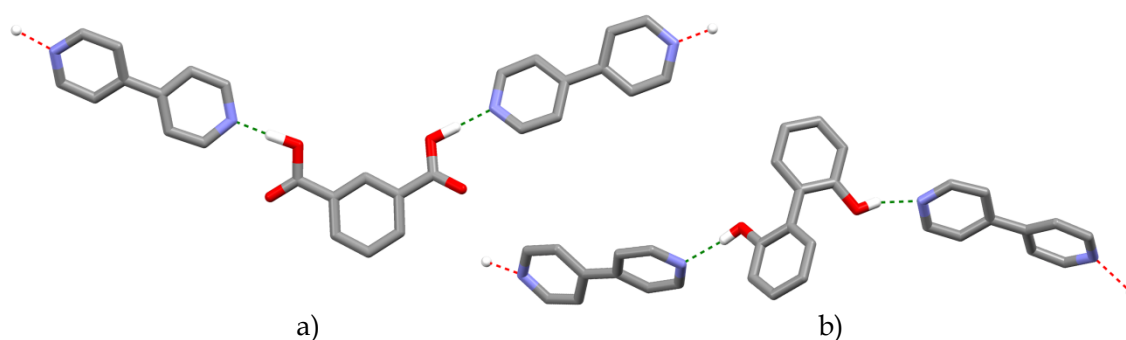
Figure 7. Chains connected with heterosynthons in the 4,4'-bipyridine cocrystals with a) isophthalic acid[56] and b) 2,2'-biphenol[57]. Non-hydrogen bonding hydrogen atoms omitted for clarity.

The carboxylic acid-pyridine heterosynthon has been found to be slightly more prevalent than the hydroxyl-pyridine heterosynthon in cocrystals where both the donor functionalities are present.[36] Depending on the number of donors and acceptors available, however, the synthons can also be found in the same structure, as in the case of 4,4'-bipyridine and 3-hydroxybenzoic acid (Figure 8a). Alternatively, the acid homosynthon can form to better allow all the donors and acceptors to participate in hydrogen bonding, like in the 1:1 cocrystal of 4-hydroxybenzoic acid and 4-phenylpyridine (Figure 8b). This further demonstrates the possibility for variable synthons even when the same functionalities are present.
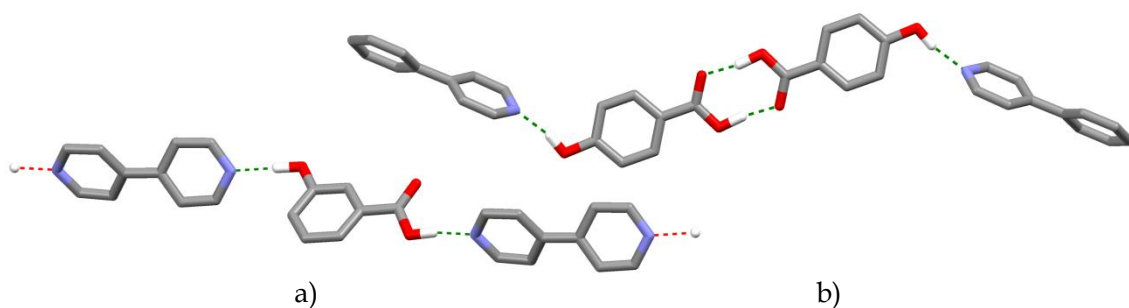
Figure 8. a) The 4,4′-bipyridine cocrystal with 3-hydroxybenzoic acid and b) the 1:1 4-phenylpyridine cocrystal with 4-hydroxybenzoic acid showing variable synthons for the same functionalities.[36] Non-hydrogen bonding hydrogen atoms omitted for clarity.

Caffeine is often used as a model pharmaceutical component for cocrystallization studies with the imidazole nitrogen of caffeine as a hydrogen bond acceptor for the carboxylic acid hydroxyl group (Figure 9) or other hydrogen bond donors.[58-64] The pharmaceutical processing problem with caffeine is that the anhydrous forms transition into a hydrate form when exposed to humidity. The caffeine cocrystal with oxalic acid (Figure 9a), however, is stable even in humid environments and could present a better dosage form for solid caffeine. [58]

caffeine   oxalic acid   1-hydroxy-2-naphthoic acid
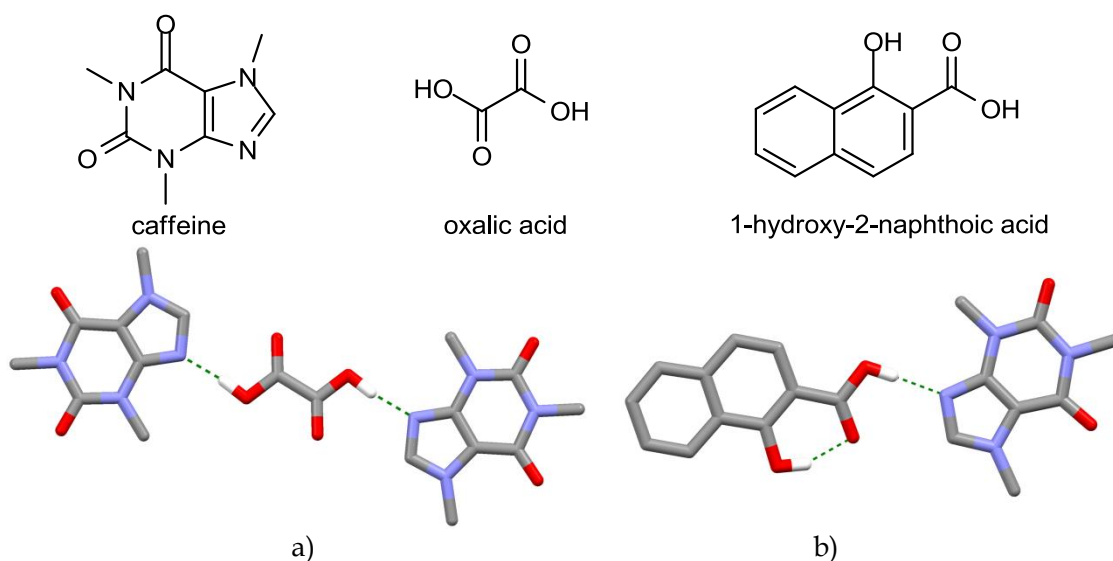
Figure 9. Examples of caffeine cocrystal with a) oxalic acid[58] and b) 1-hydroxy-2-naphthoic acid.[60] Non-hydrogen bonding hydrogen atoms omitted for clarity.

Halogen bonds (Scheme 1f) can also be used for cocrystal design. Aakeröy *et al.*[65], for example, have obtained a number of cocrystals using 1,4-diiodotetrafluorobenzene as a halogen bond donor and nitrogen heterocycles, with additional self-complementary hydrogen bonding sites, as the halogen bond acceptor. The cocrystal between 1,4-diiodotetrafluorobenzene and *N*-(pyridin-4-ylmethyl)acetamide, for example, makes an infinite ladder-like

structure (Figure 10). All the cocrystals obtained by Aakeröy *et al.*[65] were not of the expected stoichiometry with the expected synthons, but the results obtained with halogen bond synthons were similar to those usually obtained using hydrogen bond synthons.
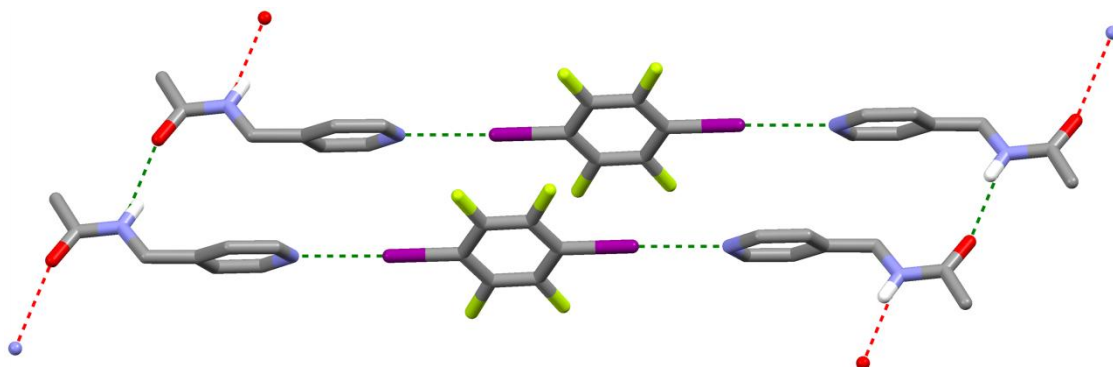
Figure 10. Ladder-like assembly in the cocrystal between 1,4-diiodotetrafluorobenzene and *N*-(pyridin-4-ylmethyl)acetamide.[65] Non-hydrogen bonding hydrogen atoms omitted for clarity.

1.2.3 Cocrystal design for active ingredients

In industrial applications one often has a compound, an active ingredient (AI), for which to find cocrystals and the steps to do this are generally the following:

1. Identify the hydrogen bond donors and acceptors of the compound.
2. Identify the synthons the compound likely forms with itself using the rules of hydrogen bonding and possible crystal structures.
3. Choose coformers which are able to form stronger hydrogen bonds with the compound than with themselves.
4. If possible, make computations to prejudge the cocrystallization capabilities of the coformers.
5. Carry out the experimental screening with the chosen coformers.
6. Analyze results and possibly choose new coformers for further experiments.

The cocrystals of itraconazole[66] (Figure 11) are an interesting example of a cocrystal screening of an API. Itraconazole is marketed as an amorphous form, which is generally not desirable for stability reasons. Cocrystal/salt screening was done with carboxylic acids (Figure 11), which could act as hydrogen bond donors making, for example, a triazole-acid heterosynthon. Six dicarboxylic acids gave cocrystals, but monoprotic acids did not. Cocrystals with fumaric acid, succinic acid, L-malic acid and (L-, D- and LD-)tartaric acid were found and the structure of the cocrystal with succinic acid was solved. In the structure two itraconazole molecules form a pocket which encapsulates the succinic acid to construct a hydrogen bonded trimer (Figure 11), which monotropic acids can not form. Additionally, malonic, glutaric, and adipic acid did not form cocrystals probably because they could not adequately fill up or fit in the cavity

of the trimer. The solubilities of the cocrystals were found to be similar to that of the amorphous phase making them good alternatives as dosage forms.
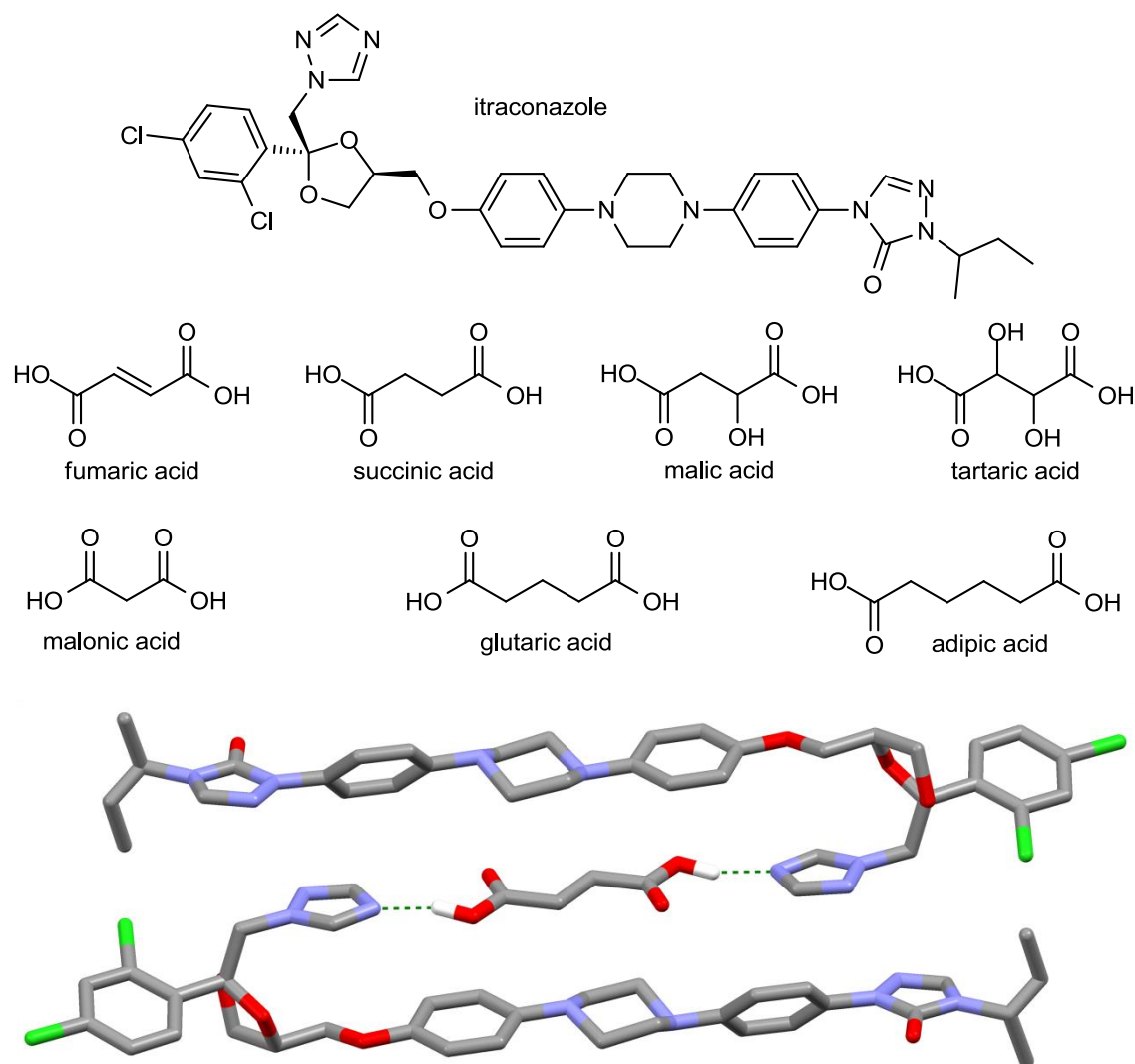
Figure 11. Molecular structure of itraconazole and the mentioned carboxylic acids. The trimer in the itraconazole-succinic acid cocrystal structure.[66] Non-hydrogen bonding hydrogen atoms omitted for clarity.

Another interesting case is a pharmaceutical active AMG 517[67-72] (Figure 12), which along with some related molecules has been found to form cocrystals with at least 14 carboxylic acids and two amides. The first cocrystal was found serendipitously in a slurry formulation and the cocrystal screening continued from there.[67] The heterosynthons formed in the cocrystals contain two hydrogen bonds between the acid/amide and a heterocyclic nitrogen acceptor next to an amide donor on AMG 517. The structures with dicarboxylic acids, like succinic acid, form a similar trimer (Figure 12a) to that in the itraconazole structure. In the case of the shorter chained malonic acid, two hydrogen bonded acid molecules take the place of the longer chained acid (Figure 12b). The

pharmaceutical properties of the cocrystals were also investigated and even the worst performing carboxylic acid cocrystals were good alternatives for further development when compared to pure crystalline AMG 517.[72]
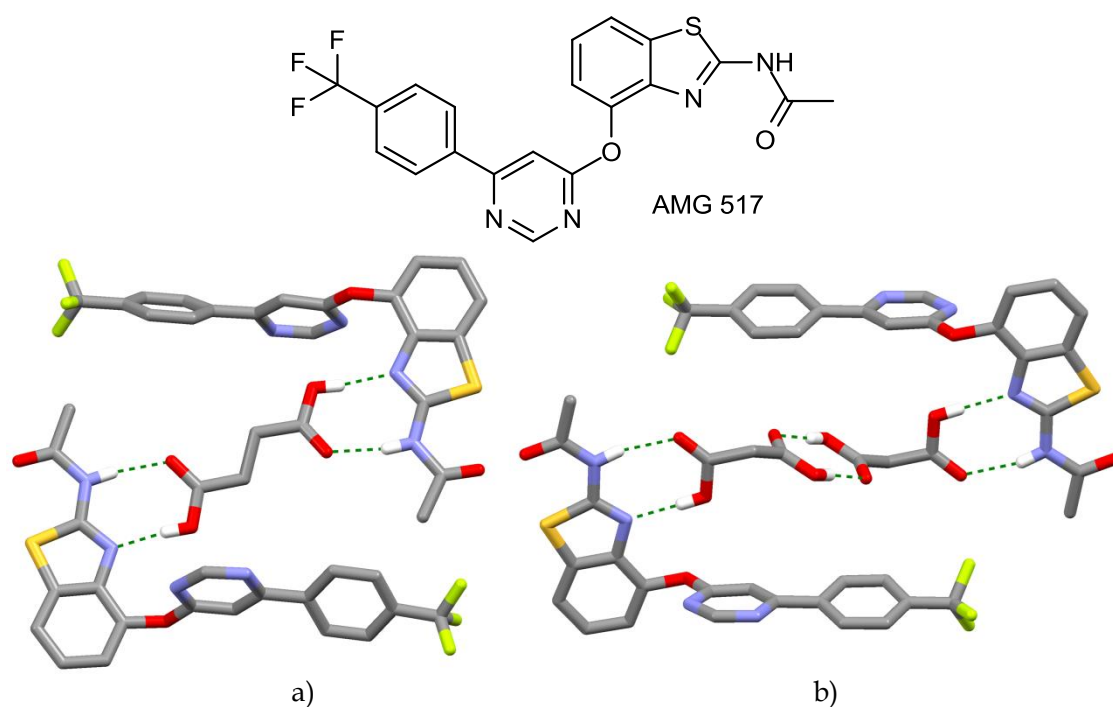
Figure 12. Molecular structure of AMG 517 and cocrystals with dicarboxylic acids. a) A trimer with succinic acid and b) a similar arrangement containing two molecules of a shorter chained malonic acid connected with an acid-acid homosynthon.[69] Non-hydrogen bonding hydrogen atoms omitted for clarity.

1.2.4   Computational approaches

Experimental screening procedures can be time-consuming and expensive, making computational pre-screening procedures desirable. A few of these methods have been recently reported and more are used by pharmaceutical and other companies involved in cocrystal screening. One method to screen for cocrystals could be crystal structure prediction[73,74], but it is still computationally very demanding and simpler approaches are needed.

The molecular complementarity in cocrystals was analyzed by Fabian[55] by way of a statistical analysis of 131 molecular descriptors, such as atom and bond counts, hydrogen bond acceptor and donor counts, size, shape, surface area and molecular electrostatic descriptors, calculated for cocrystals found in the CSD. The shapes and polarities of the cocrystal formers were found to be similar. However, no correlation was found in the size of the molecules or the relative number of hydrogen bond donors and acceptors between the molecules. The findings of this study could be used to pre-screen a list of possible coformers and a predictive computational model is apparently in development.

Mohammad *et al.*[75] reported a method to predict the formation of cocrystals using the Hansen solubility parameter[76] to evaluate the miscibility of the compounds. Compounds with a high miscibility are expected to form cocrystals. Indomethacin (Appendix) was used as a model pharmaceutical compound with a set of 33 coformers. Four coformers, of which all were among the 21 coformers that were miscible with indomethacin, were found to produce cocrystals. Two of the cocrystals were previously unreported. Mohammad *et al.* postulated that the miscibility of two compounds is required for cocrystal formation and that this could be used as a pre-screening step before experimentation.

Musumeci *et al.*[77] reported a method to virtually screen for cocrystals. In the method all the hydrogen bond donors and acceptors of the molecules are found from a molecular electrostatic potential surface and then connected in order of strength, according to Etter's hydrogen bonding rules[35]. The change in the interaction site pairing energy is then calculated. The change in energy is either zero, when all the same hydrogen bonds as in the pure compounds are formed, or larger than zero, when the hydrogen bonds change for the better. The larger the change for better, the more likely a cocrystal will form. The method does not take into account packing effects, steric constraints or cooperativity between neighbouring binding sites, but it is very fast in screening through a large list of compounds for possible coformers. It was shown that the known cocrystals of caffeine and carbamazepine were among the top hits from almost 900 molecules screened as possible coformers.

1.3 Cocrystal synthesis

Once specific compounds for cocrystallization are chosen with the help of a supramolecular synthon approach or any other method, a synthesis method for the formation of the proposed cocrystals must be chosen. The primary choices are solution crystallization, solution-mediated phase transformation, mechanochemistry and thermal methods. The cocrystal synthesis methods in this chapter are primarily described in the context of screening, but some consideration is also given to industrial scale-up and general cocrystallization mechanics, like the case of spontaneous cocrystal formation. Understanding the thermodynamics behind the methods will help in choosing a method and understanding the success or failure, even if the thermodynamics of the system are not well known, as is the case with screening. Binary and ternary phase diagrams are consequently described below.

The most used analysis methods to judge if a cocrystal has formed are X-ray diffraction of powder or single crystalline samples, infra red (IR) and Raman spectroscopy, solid state nuclear magnetic resonance (SSNMR) spectroscopy and thermal analysis with, for example, a differential scanning

calorimeter (DSC) or a thermomicroscope. A thorough description of these methods is outside the scope of this thesis.

1.3.1 Cocrystal phase diagrams

The thermodynamic outcome of a crystallization of cocrystal components (A and B) in a solvent (S) at a given temperature is depicted in a cocrystal ternary phase diagram (TPD).[78] If the ternary phase diagram of a system is known, crystallization experiments to acquire the cocrystal can be better designed and the outcomes predicted.[27, 51, 79] Ternary phase diagrams (Figure 13 for a system with a 1:1 cocrystal) are equilateral triangles with each side as a scale of the mole or weight fraction of the three chemical constituents: compound A (the active ingredient), compound B (the coformer) and the solvent (S).
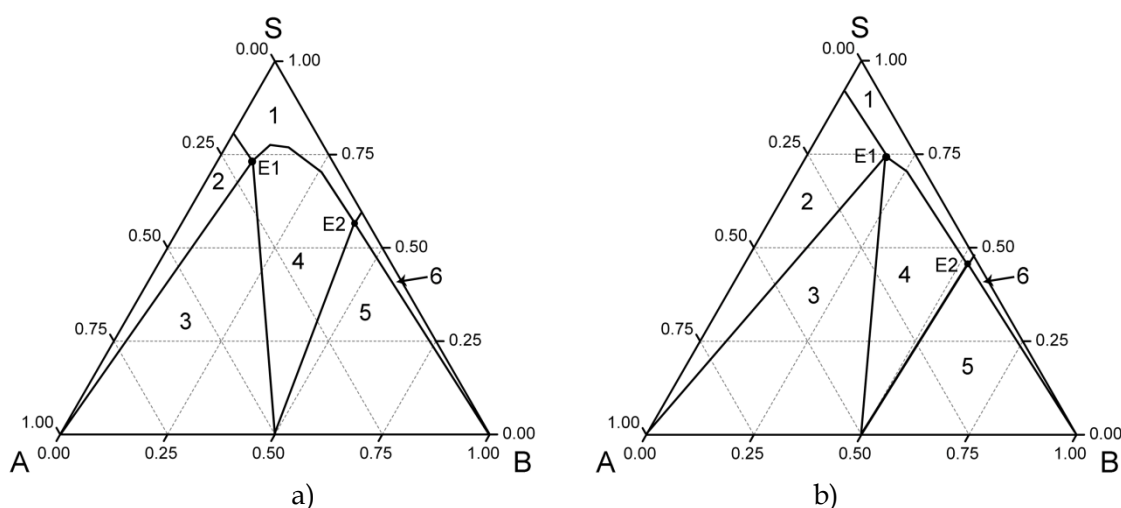
Figure 13. Ternary phase diagram of compounds A and B, which make a 1:1 cocrystal, in solvent S, a) when the solubilities of A and B vary little and b) when the solubility of A is much lower than that of B. Scales in mole fraction. Figure adapted from Rager and Hilfiker.[78]

There are six zones (1-6) in a typical TPD for a system with one cocrystal for A and B (Figure 13). In zone 1 both A and B are dissolved in the solvent and only a homogeneous liquid phase is present. In zone 2 there is solid compound A and a liquid phase. In zone 3 there is solid compound A, solid cocrystal AB and a liquid phase. In zone 4 there is solid cocrystal AB and a liquid phase. Zone 5 is like zone 3 for compound B with solid compound B, solid cocrystal AB and a liquid phase. Zone 6 is like zone 2 for compound B with solid compound B and a liquid phase. Points E1 and E2 are eutectic points where the liquid is in equilibrium with both adjacent solid phases (A and the cocrystal at point E1 and B and the cocrystal at point E2).[78] Cocrystal systems and consequently the TPDs can be complicated with polymorphs and solvate formation as well as cocrystals of different stoichiometries.[78]

Important terms for cocrystal dissolution and TPD interpretation are congruent and incongruent dissolution. For congruent dissolution the entire solid dissolves, leaving no secondary solid phase, but for incongruent dissolution a secondary solid phase crystallizes as the first solid dissolves. This is the difference for cocrystal systems in Figure 13 with a) showing congruent and b) incongruent dissolution caused by the much lower solubility of A. Starting from the bottom at a mole fraction 0.5:0.5 of A and B and adding solvent (moving straight upward in a line) for Figure 13 a) the solid cocrystal dissolves congruently with the line crossing from zone 4 to zone 1, whereas for Figure 13 b) the dissolution is incongruent with the line also crossing zone 3 and zone 2, meaning that compound A may crystallize as the cocrystal is dissolved.

Ternary phase diagrams can be determined by measuring or calculating the solubility curves of A, B and the co-crystal in the solvent S (x_A, x_B and x_{AB} in Figure 14).[78] The eutectic points E1 and E2 are the points where the solubility curves of A and B, respectively, meet up with the solubility curve of the cocrystal. Straight lines are then drawn from the eutectic points to the corresponding pure solid phases (A, B and 0.50 on the bottom of the triangle in the case of a 1:1 cocrystal). The curve from E1 to E2 is kept as the solubility curve of the cocrystal dividing zone 1 and 4. The solubility curves of A and B above E1 and E2, respectively, are also kept as the boundaries between zone 1 and zone 2/6. The sketch of the solubility curves of A, B and the cocrystal in Figure 14 then gives the TPD in Figure 13a.
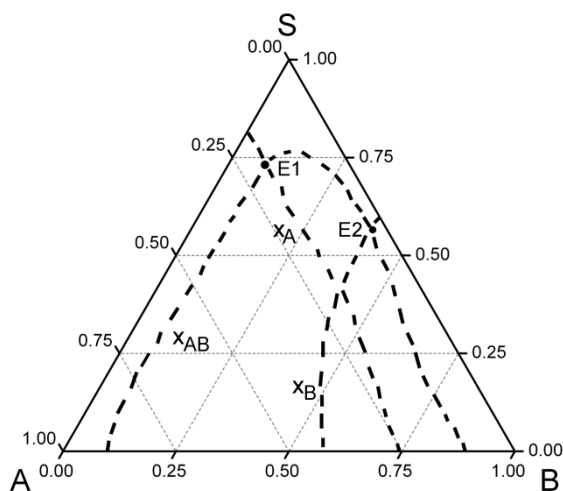
Figure 14. Solubility curves of A, B and the co-crystal in the solvent S (x_A, x_B and x_{AB}) for the determination of the phase diagram. Figure adapted from Rager and Hilfiker.[78]

The solubility of compound A is influenced by compound B in the liquid phase and this should ideally be taken into account in the solubility curves measured or calculated for the construction of a TPD. To experimentally do this, ternary mixtures of many compositions should be made, and the composition

of the liquid and the solid phases examined after equilibration to see which zone they belong to with, for example, powder X-ray diffraction and liquid chromatography.[79-82] This is a simple and good way to construct a ternary phase diagram, but also very time-consuming. In addition, a ternary phase diagram has to be determined separately for each solvent. Ainouz *et al.*[83] have, however, described a method, which can circumvent this. Experimental data from discontinuous isoperibolic thermal analysis (DITA), a calorimetric method, is used in a reference solvent to determine the first phase diagram. The phase diagrams in other solvents are then estimated by using only solubility data of A and B in that solvent and a calculated value for the slope of the cocrystal solubility curve. This reduces the amount of experiments needed and was shown to give accurate results for a trial system of an active pharmaceutical ingredient (API) with glutaric acid in three different solvents.

Guo *et al.*[80] attempted to rationalize the behavior of the cocrystal system of caffeine and maleic acid, which make two cocrystals with different stoichiometries (1:1 and 2:1), by determining a ternary phase diagram. The problem with the system was that neither cocrystal could be reliably prepared and there were reports of another polymorph of maleic acid crystallizing during cocrystallizations. The solubilities of caffeine and maleic acid are very different and the final solvent chosen was acetone in which the solubilities are most alike. However, the phase diagram still showed incongruent dissolution. The attempt in the end was somewhat unsuccessful as the 2:1 cocrystal was found to be a kinetic product which was not observed in the phase diagram, and the desired maleic acid polymorph could not be crystallized. However, the acquired phase diagram does give routes to the reproducible crystallization of the 1:1 cocrystal from acetone.

In addition to ternary phase diagrams, at least two other types of phase diagrams have been used to depict the phase behavior of cocrystallizing systems. One of these is a phase solubility diagram (PSD)[51, 84-86], which shows the solution concentrations at equilibrium with solid phases, or in other words the solubility curves of solid phases A, B and cocrystal AB as a function of solution concentration of A and B. A schematic diagram, in which the solubility dependance of A and B on the concentration of the other is taken into account, is shown in Figure 15a. In effect the PSD is another representation of the the top part of the TPD.
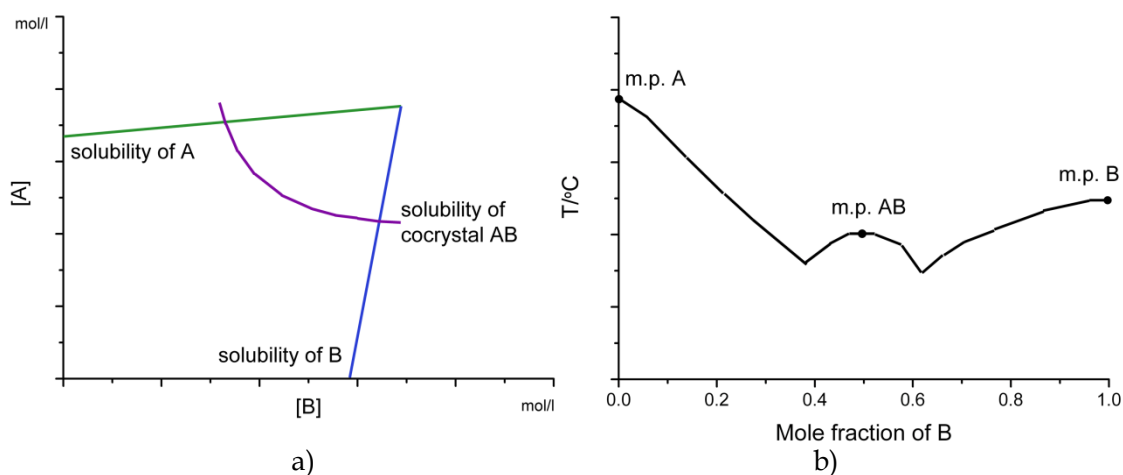
Figure 15. Schematic a) phase solubility diagram, showing the solubility dependance of A and B on the concentration of the other and the solubility of the cocrystal AB, and b) binary phase diagram.

A binary phase diagram[80, 87] (BPD) of A and B shows the thermal stability of the cocrystal system. This kind of phase diagram can be constructed from DSC or thermomicroscopic data of the pure samples and their mixtures. It is a plot of the melting points of mixtures of the two components A and B as a function of the mole (or mass) fraction of the components (Figure 15b). A BPD does not give much information for solution crystallization, but is needed in thermal screening methods, which will be discussed later.

For screening a large amount of potential cocrystal formers it is not viable to determine the phase diagrams of all the combinations. However, the trends that can be seen in phase diagrams of different systems can be used to plan experiments that are most likely to give the cocrystal. The cocrystal synthesis methods (chapter 1.3.2) are discussed in the approximate order of the amount of solvent used for the experiments and can be thought of as beginning from the top of the triangular TPD (Figure 16) with solution crystallization, reaction crystallization, solution-mediated transformation in slurries, sonochemical cocrystal formation, and liquid-assisted and neat grinding. A quantity η, the ratio of the volume of the liquid phase to the amount of solid in the experiment, has been suggested to differentiate between liquid-assisted grinding, sonication and conventional slurrying.[88] Using such a quantity could give a clearer understanding of where on the phase diagram each experiment has been done.
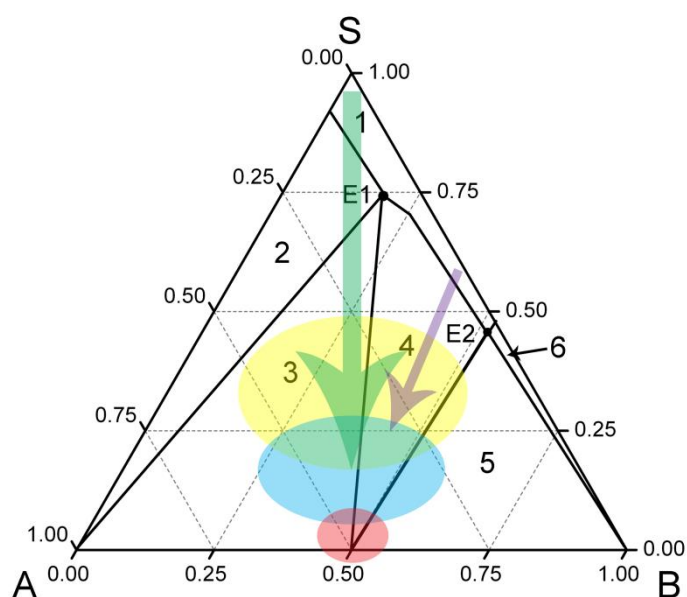
Figure 16. Green arrow showing solution crystallization from a stoichiometric solution, purple arrow showing reaction crystallization, yellow ellipse in the area of slurry crystallization, blue ellipse in the area of sonochemical cocrystal formation and red ellipse in the area of grinding in the phase diagram.

1.3.2 Solution crystallization

Solution crystallization from a number of solvents is often used for polymorph screening and because of the apparent simplicity and possibility for high-throughput applications,[89] it is also often used in cocrystal screening. Solution crystallization offers the possibility to get single crystals for structure determination, which is a significant benefit. In addition to this, solution crystallization is a valid method for industrial applications. The addition of another species, the coformer, into the crystallization system brings in added complications, which need to be taken into account for small scale screening and especially for scaling up crystallizations.

Solution crystallization experiments start from zone 1 in the ternary phase diagram (TPD, Figure 16). A simple starting point analogously to polymorph screening is stoichiometric evaporation crystallization from a number of solvents, but the matrix of many solvents and coformers makes the experimental task suitable only to high-throughput screening apparatuses. In addition, cocrystallization from stoichiometric solutions will produce the cocrystal only in cases where the solubilities are very similar with the cocrystal showing congruent dissolution. Solvents in which the solubilities are similar, should be chosen separately for all coformers and this makes experimental design more difficult.

When the two potentially cocrystallizing compounds have very different solubility, mixtures of solvents can be used. The use of mixtures can also hinder

solvate formation and therefore using complex mixtures of many solvents has been suggested.[90] For example, in cocrystallization tests of carbamazepine with 19 coformers using a mixture of nine solvents, which are known to produce carbamazepine solvates, resulted in the very stable acetic acid solvate of carbamazepine in only three cases. Using mixtures, however, can complicate the system and cause a lack of control, especially when solvents that evaporate at different rates are used in evaporation crystallization. Mixtures of many solvents can also be hard to handle in industrial scale processes, but for screening this not a big problem.

Crystallization from non-stoichiometric solutions is a strategy based on the inspection of ternary phase diagrams. The method, called reaction crystallization,[51, 91] starts with a saturated or near saturated solution of the more soluble compound B to which the less soluble compound A is added to move from zone 1 to zone 4 in the TPD. As the API is usually the less soluble compound, this strategy also reduces the amount of API needed.

Cooling crystallizations are often used in industrial applications. The problem with cooling crystallizations is that the TPD can change asymmetrically with temperature, making the prediction of the crystallization outcome difficult. The idea is to start with a mixture that is in zone 4 of the TPD and then use heat to dissolve the components. As the solution is cooled down, the thermodynamic crystallization product at the target temperature is the cocrystal, but the kinetic or thermodynamic product at a higher temperature could also be one of the pure components. During the cooling one of the pure components could consequently crystallize out. Seeding can overcome this problem and it is often used in industrial crystallizations. Seeding is also a good way to acquire single crystals of cocrystals that are otherwise not available through solution crystallization due to incongruent dissolution.[92, 93]

Supercritical fluid techniques have been used for crystallization of cocrystals of saccharin.[94, 95] The technique crystallizes the material from solution by way of an anti-solvent effect of the supercritical fluid and fast atomization of the solution by spray drying. The crystallization is thus very fast, enabling kinetic products to form. In addition to six known cocrystals of saccharin, a new, likely kinetically favored, cocrystal with theophylline (Appendix) has been found for saccharin with supercritical fluid crystallization.[95] The particle size distribution of the crystals acquired by the supercritical fluid techniques is repeatable and the particles are less aggregated than those made with grinding, showing the potential to improve the physicochemical properties of pharmaceuticals.

Pure spray drying[96] has also been suggested as a good way to get cocrystals even for incongruently dissolving systems, in which traditional stoichiometric solution crystallization does not work. The formation of the cocrystals by spray drying is likely mediated by the amorphous phase as the spray drying of pure components also often results in amorphous solids.[96]

1.3.3 Solution-mediated transformation

Solution-mediated phase transformation (SMPT) methods[61, 97, 98] are a relatively easy way to screen for cocrystals and do not necessarily require any special instrumentation. Scale up to larger quantities is also possible. Solution-mediated phase transformation, also called suspension/slurry equilibration, can, however, take time with nucleation of the cocrystal being the main kinetic barrier.[97] The mechanism behind solution-mediated transformation is based on the solvent becoming saturated with A and B and most importantly with the cocrystal, if one exists. If the cocrystal is the most stable phase in the solvent, it will eventually crystallize, dissolving more A and B until saturation can no longer be reached.

In practice, a mixture of solid A and B and the solvent, which is in zone 4 of the ternary phase diagram (Figure 16), is mixed until solution-mediated transformation results ideally only in the solid cocrystal. The simplest way is to start with a 1:1 mixture of A and B and adding only enough solvent to facilitate mixing. For screening purposes the choice of solvent is not as critical as for solution crystallizations. Even if the final result lies in zone 3 or zone 5 of the TPD with pure A or B as a solid in addition to the cocrystal, the emergence of the cocrystal can be identified. The solvent should, however, be one in which the solubilities are limited to prevent the process from going into zone 2/6 or even zone 1 of the TPD.

Polymorphs of carbamazepine cocrystals with isonicotinamide were detected by ter Horst *et al.*[98] using SMPT, and by choosing the conditions with the help of phase solubility diagrams. The kinetic barrier of crystallization allowed the presence of a metastable polymorph to be detected before it changed into the more stable form. Instead of a stoichiometric ratio of the pure components, a ratio based on the solubilities of the components was suggested for SMPT experiments, as is also indicated by the phase diagrams for incongruently dissolving systems.

High-throughput applications have also been developed for slurry screening of cocrystals. Takata *et al.*[99] used the SMPT slurry method to make cocrystals of two nonionizable pharmaceutical actives with a steroidal skeleton with just 4 mg of a 1:1 mixture of the API and coformer in 20 µl of solvent showing that a screening with SMPT slurries does not necessarily take much material. The analysis of small samples is often the bottle neck for higher throughput. The samples of Takata *et al.*[99] were manually pipetted from the crystallization vials to a stainless steel mesh that was used for filtration, and analyzed with powder X-ray diffraction on a special 48-sample aluminum plate. Kojima *et al.*[100] have developed a high-throughput slurry screening technique using a 96 well plate with *in situ* Raman microscopy as the detection method and successfully found three new cocrystals of indomethacin (Appendix),

which was used as the model API. Altogether 46 coformers were screened using only 230 mg of indomethacin.

Sonochemical cocrystal formation[101, 102] is also used for solution-mediated phase transformation methods. Because of the ultrasonic mixing, less solvent is needed for efficient mixing than when using a magnetic stirrer or rotary shaker, as is normally the case in SMPT slurries. This moves the sonochemical cocrystal formation lower in the TPD (Figure 16). Ultrasound also promotes dissolution of the pure components and nucleation in general, making the transformation faster. The amount of material used by Friscic *et al.*[88] in sonochemical cocrystallization screening was approximately 100 mg of solid mixture with 200 µl to 1200 µl of solvent. When comparing sonochemical and mechanochemical cocrystallization Friscic *et al.*[88] found that lowering the amount of solvent in a solution-mediated cocrystallization increases the propensity of cocrystal formation by increasing the potential of saturating both components in the solvent phase. This increase in efficiency by using less solvent also speaks for moving lower in the TPD triangle (Figure 16) to use mechanochemistry, *i.e.* grinding or milling.

1.3.4   Mechanochemistry

Mechanochemical preparation of cocrystals[103-105] is a relatively fast and easy screening method that requires a medium amount of material and very little or no solvent. Cocrystal can be made by grinding using just a mortar and pestle or by milling in a mechanical ball or vibratory mill (Figure 17). When a few drops of solvent is used in the grinding, the terms kneading, solvent-drop grinding and liquid-assisted grinding (LAG) are used. To make a clear distinction between the variations, dry grinding is at times referred to as neat grinding. Liquid-assisted grinding is usually faster[106] and more likely to yield the cocrystal than neat grinding. Sometimes cocrystals can be made with both liquid-assisted and neat grinding[107], but there are cocrystals like that of caffeine and citric acid[108] that cannot be obtained without the addition of solvent in the grinding. Mechanochemical cocrystallization is effective as, for example, Weyna *et al.*[109] were able to produce 25 various cocrystals acquired from solution with LAG. The opposite is often not true because of incongruent dissolution of the compounds.
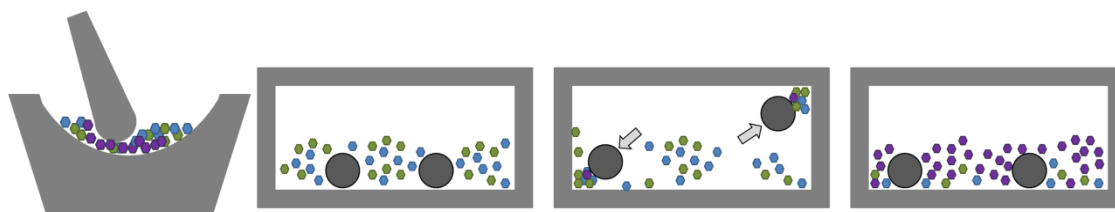
Figure 17. Schematic presentation of the preparation of cocrystals by grinding and ball-milling with the milling vessel before, during and after milling. A and B crystals blue and green and AB cocrystals purple.

The mechanism behind cocrystal formation via grinding is not completely understood.[105] The mechanism in LAG is likely solution-mediated transformation similarly to slurries and sonochemical cocrystallization.[88] Solution-mediated transformation, however, requires that the cocrystallizing compounds are soluble in the liquid used in the grinding. In cases where the compounds are not soluble, it is suggested that the liquid functions solely as a medium facilitating molecular diffusion.[105] The solvent may also act as a template for formation of a framework structure or a solvate of a cocrystal.[63, 110] The choice of the solvent may additionally promote the formation of cocrystal polymorphs.[111]

The mechanism in neat grinding is assumed to vary with the system.[105] One possible mechanism is molecular diffusion either through the gas phase, if the vapor pressures of the compounds allow this in the temperature used, or on the surface of the crystals. Diffusion is then helped by the shearing force of the grinding. Neat grinding may also be mediated by a liquid phase either through solvents included in the crystal lattice of the starting materials, when hydrates[108] or solvates are used, or through the formation of an eutectic melt of the compounds[112] that then recrystallizes. The formation of an amorphous phase in the grinding due to mechanical force may also mediate the formation of cocrystals.[113] Water, as humidity from air, can act as a plasticizer to assist in the formation of the amorphous phase, which may also be a mechanism for some liquid-assisted grinding experiments. The formation of an amorphous phase, however, can make the identification of the acquired phases difficult. In those cases time or an incentive such as heat must be used for the material to fully crystallize.

The cocrystal stoichiometry can sometimes be controlled by changing the composition of the starting material in the grinding experiment.[92, 114] An example of this are the stoichiometric variants of the caffeine/acetic acid cocrystal, which could also be classified as a solvate. A 1:2 cocrystal was acquired by grinding a 1:2 mixture and a 1:1 cocrystal by grinding a 1:1 mixture.[92] The 1:2 cocrystal was found to be stable for 6 months at ambient conditions, whereas the 1:1 cocrystal was very unstable and dissociated in a day. Stoichiometric control has also been shown for cocrystals of nicotinamide with five dicarboxylic acids.[114] All the five cocrystals have a 2:1 and a 1:1

(nicotinamide:acid) stoichiometric variant. For three of these the cocrystal stoichiometry could be changed reversibly by adding more nicotinamide or acid in the grinding. Two of the cocrystals changed only in one direction indicating that the other stoichiometric cocrystal was more stable.

Grinding can also produce polymorphs of cocrystals.[92, 93, 111] A polymorphic 1:1 cocrystal, or solvate, of caffeine with trifluoroacetic acid is an example of this.[92] Interestingly, polymorphic form I was acquired by grinding smaller batches and form II by grinding larger batches of material. Upon storage in ambient conditions form I was stable for 6 months whereas the less stable form II converted to form I in a few days. For the 2:1 cocrystals of benzoic acid with 1,4-diazabicyclo[2.2.2]octane (DABCO) and 2-aminopyridine the polymorphic form depends on the method of cocrystallization with solution crystallization producing less dense forms than grinding.[93] Interestingly, the benzoic acid cocrystal with DABCO acquired from solution transformed to the denser form when ground, whereas the benzoic acid cocrystal with 2-aminopyridine acquired from solution showed no such transformation.

As another example of polymorphic control is the 2:1 co-crystal of 4-cyanopyridine and 4,4'-biphenol, which crystallized in two polymorphic forms.[115] The two forms crystallize concomitantly from a slow evaporation of a 1:1 methanol:ethyl acetate solution whereas slow evaporation from methanol, ethyl acetate, or acetone solutions yield form I. Liquid-assisted or neat grinding always produces form II, which seems to be the more stable form because form I transforms to form II also when slurried in methanol, ethyl acetate or acetone. The formation of the two polymorphs of a caffeine cocrystal with glutaric acid that crystallized concomitantly from solution was also controlled by liquid–assisted grinding.[111] When a stoichiometric mixture was ground without solvent or with nonpolar solvents form I was produced, but with polar solvents the result was form II. The reason for this behavior is likely the stabilization of a nonpolar cleavage plane in the structure of form I which is not present in form II.

Twin-screw extrusion is a mechanochemical method that has been shown to produce cocrystals even without the use of solvents, similarly to grinding.[116] In twin-screw extrusion two parallel screws are rotated in the same or opposing directions facilitating the mixing and movement of material (Figure 18). The temperature and rate of the extrusion process can be controlled. The advantage of twin-screw extrusion in comparison to milling is that it is a continuous and scalable process making it ideal for industrial purposes.
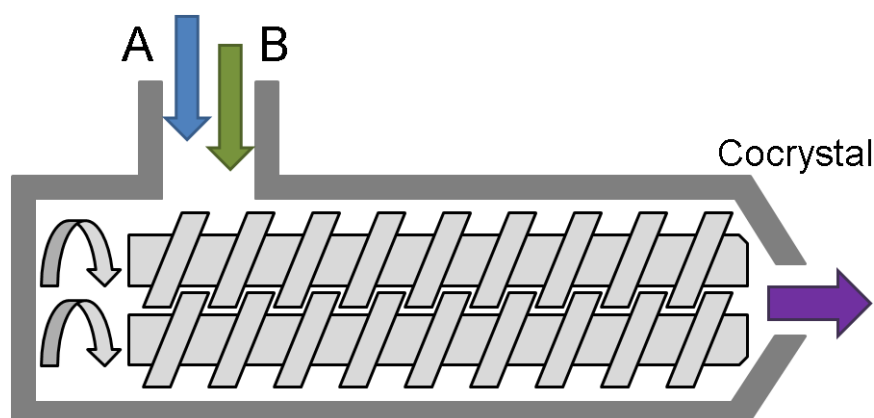
Figure 18. Schematic presentation of a twin-screw extrusion system producing a cocrystal of compounds A and B.

1.3.5 Thermal screening

Thermal screening is a good alternative screening method for compounds that are thermally stable and not volatile. Thermal screening can be done on a hot stage (*i.e.* thermo-) microscope with the mixed fusion method[117] or with a differential scanning calorimetry (DSC) instrument[118], giving either visual or energetic results to be analyzed. Thermal methods require only a small amount of material and the results are not complicated by the presence of solvents, also making the methods good from a green chemistry point of view. Seed crystals acquired from thermal methods can also be used for further crystallizations.

In the mixed fusion method[2, 117, 119] the aim is to get a sample with a zone of mixing of the two components with a concentration gradient similar to that shown in a binary phase diagram (Figure 15b). This can be done by first melting and solidifying the higher melting component on a slide, after which the lower melting component is melted on the slide so that it touches the other component, simultaneously melting part of it and creating the zone of mixing. The sample is then let solidify and visually observed while being reheated on a thermomicroscope under polarized light. If a cocrystal has formed, two eutectic melting zones can first be observed on the sides of the zone of mixing, leaving a zone of cocrystal in the middle (Figure 19a). After this the cocrystal and the two components will melt in the order of their melting points. If a cocrystal has not formed, only one eutectic melting zone is observed (Figure 19b).
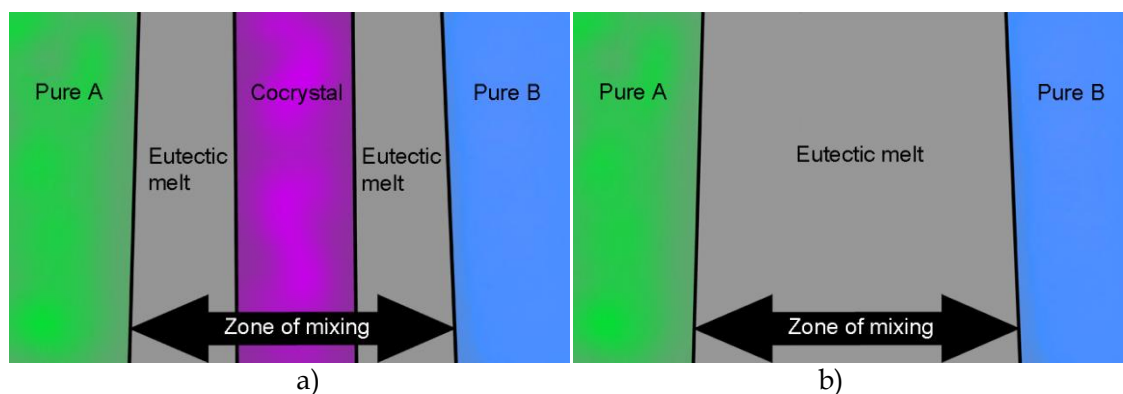
Figure 19. Schematic presentation of a samples produced with the mixed fusion method when a) a cocrystal forms and both the eutectics have melted leaving zones of A, the cocrystal and B and b) a cocrystal does not form showing only one eutectic melt.

In thermal screening with a differential scanning calorimetry (DSC) instrument, mixtures of compounds A and B are made in three molar ratios and heated in a DSC.[118] Two invariant endotherms, signifying eutectic melting followed by cocrystal melting, indicate the formation of a cocrystal. The method is fast, requires little material, no solvent and can be automated. When A or B exhibit polymorphism, however, the results can be difficult to interpret. Like other thermal methods DSC screening cannot be used for compounds that are thermally unstable.

1.3.6   Spontaneous cocrystal formation

Cocrystals have been known at times to appear serendipitously and spontaneously in mixtures of compounds.[120] The apparent spontaneity of a chemical process, however, always has a reason behind it. Vapor digestion[121] is one process that can cause the apparent spontaneity of cocrystal formation. The mechanism by which moisture generates cocrystals involves moisture uptake through deliquesence, partial or full dissolution of the components followed by nucleation and growth of the cocrystal.[122] It is thus a type of solvent-mediated transformation. The nature of the solvent absorbed can also affect the acquired cocrystal product.[121]

In spontaneous formation of cocrystals by simply mixing solid substances, cocrystals have been found to form faster at higher temperatures and relative humidities.[123] The spontaneous cocrystal formation in mixing experiments, however, was not always deliquesence-mediated as the moisture uptake was in some cases very low.[123] Pre-milling of the compounds in mixing experiments makes the transformation faster.[123] In further studies with three different size fractions of pre-milled compounds, the transformation was found to take place faster with starting crystals of a smaller size.[124] The higher surface fraction and the increase in the surface energetics due to grinding is thought to be the cause

behind this. The major contributor to spontaneous cocrystal formation is likely the particle to particle contact in the mixing.[124]

Vapor digestion and mixing solids are not good cocrystal screening methods, but it is important to consider them in the storage and processing of pharmaceutical formulations, such as tablets and powders, that can include a number of compounds. If cocrystallization were to take place, the physicochemical, and consequently, the biological properties of the formulation could change, which is not acceptable for pharmaceutical products.

1.4 Crystal structure analysis methods

The aim of this chapter is to convey what can be analyzed from a crystal structure once it is acquired by single crystal[125] or powder diffraction[126]. In addition to examining the packing visually, there are a variety of tools that can be used. The hydrogen bonding and other intermolecular interactions can be qualitatively and quantitatively examined. The packing efficiency in the crystal structures can also be calculated and similarities between structures examined. Extracting all the available information from acquired structures is important in designing the next crystal.

1.4.1 Graph-sets

A common notation for discussion of hydrogen bonding is invaluable when comparing many different structures with varying hydrogen bonding. Graph-set analysis[40, 41] facilitates this comparison and assists in finding reoccurring synthons in structures that contain complicated arrays of hydrogen bonding.

A graph-set is indicated in the form $G_d^a(r)$, where G is a pattern designator, r is the degree, a is the number of acceptors and d the number of donors. G can have four different assignments - S for self or intramolecular bonding, C for infinite chain motifs, R for ring motifs and D for discrete finite motifs of hydrogen bonds. The degree r is the number of atoms involved in the motif taking the smallest path in a ring, the repeat length of a chain or in case of a single discrete hydrogen bond 2 for the donor and acceptor atoms. The default values of one for a and d and two for r of a discrete hydrogen bond need not be shown. For example, a $S_1^1(6)$ motif is the same as S(6) and a $D_1^1(2)$ the same as D (Scheme 2). First order graph-sets (N_1) contain only one type of hydrogen bond, while second order graph-sets (N_2) contain two types of hydrogen bonds and so on. Higher order graph-set can describe the hydrogen bonding better in instances where, for example, two discrete hydrogen bonds make a ring, like the $R_2^2(8)$ of an acid and an amide, or two different finite motifs build up infinite chains in the structure (Scheme 2).
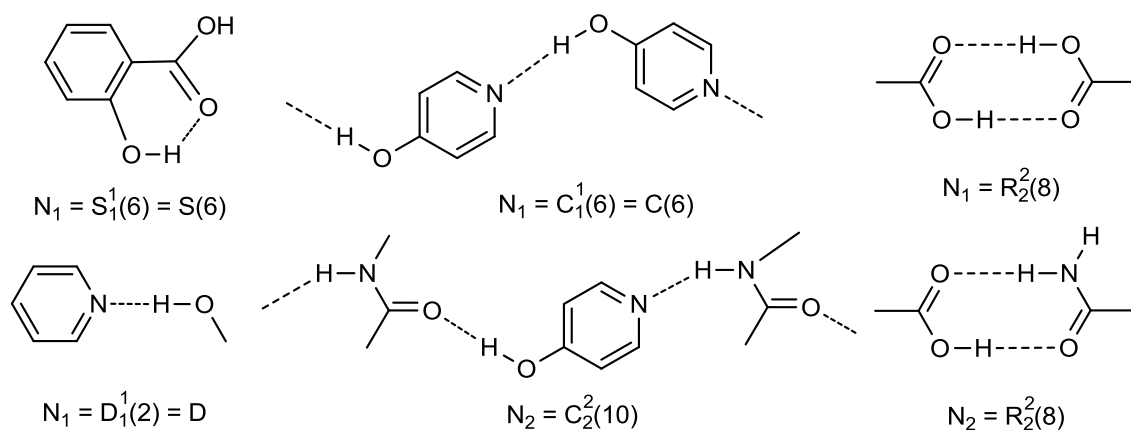
Scheme 2. Graph sets of example motifs.

1.4.2 Packing coefficient

The close packing of molecules is one of the driving forces in crystallization. The tightness of packing describes how well the molecules have achieved this and consequently how thermodynamically feasible the structure is. For polymorphs that have no strong intermolecular interactions the most densely packed form is expected to be the most stable.[127, 128] Even though this does not generally hold for crystal forms with strong intermolecular interactions, if a very loosely packed form is found, the question of another more densely packed form existing arises. The packing efficiency can most simply be assessed by calculating the packing coefficient.

The packing coefficient, introduced by Kitaigorodskii[46], is the ratio of inherent molecular volume to the total cell volume of a crystal structure. It describes the tightness of the packing of molecules in a crystal, with a bigger value meaning tighter packing. The packing coefficient is calculated with the formula $C(k) = Z * V(mol)/V(cell)$, where Z is the number of molecules in the unit cell, *V(mol)* is the molecular volume of the molecules and *V(cell)* the volume of the unit cell. The packing coefficient gives a numerical comparison between the packing tightness of different forms of a compound and unlike density does not take into account the actual molecular weights of the compounds, making possible the direct comparison of, for example, different solvates.

Price *et al.*[129] used the packing coefficient to assess the reasons behind the many solvate structures of some pharmaceutical compounds. The primary investigated compound, named Bz-423 (Appendix), typically produced either a solvate or an amorphous material in crystallizations. One unsolvated form, however, was found. According to the packing coefficients the unsolvated form is less densely packed than the seven solvates of the compound giving an explanation why solvated forms are often found. The same was tested for

structures taken from the CSD of the two polymorphs and 31 solvates of gossypol (Appendix), which readily crystallizes as unsolvated forms. For this compound all the solvated structures had packing coefficients between those of the two polymorphs, indicating that packing incentives were not a key reason for their crystallization.

1.4.3 Hirshfeld surfaces and fingerprint plots

A Hirshfeld surface[130] is a three-dimensional representation of the electron density of a molecule in a crystal. The surface envelops the space around a molecule in a crystal where the electron distribution of that molecule exceeds that of any other. This gives an effective three-dimensional map of the molecular surface in the crystal and facilitates the examination of the intermolecular interactions. On a Hirshfeld surface close contacts are red and areas with no close contacts are blue (Figure 20).
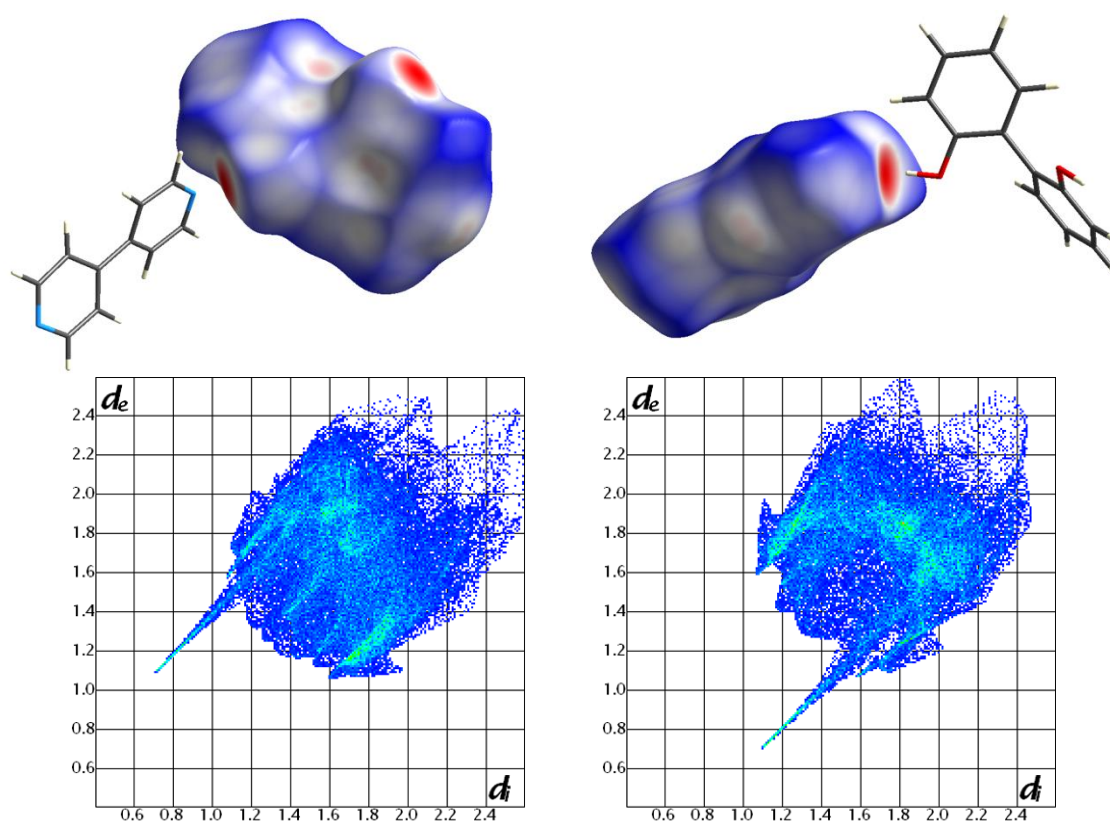
Figure 20. Example of Hirshfeld surfaces and fingerprint plots of the 2,2'-biphenyl and 4,4'-bipyridine molecules in the cocrystal.[57]

On a Hirshfeld surface intermolecular interactions can be seen in a clear graphical way with the appropriate tools, but publication of three-dimensional results is still uncommon. To overcome this problem Spackman and McKinnon have devised a two-dimensional fingerprint plot[131], which effectively

summarizes the information available on a Hirshfield surface. Fingerprint plots are unique for molecules in molecular crystals and also for symmetry inequivalent molecules within a crystal. The actual fingerprint is a plot of d_i, the distance from the nearest atom interior to the Hirshfeld surface, and d_e, the the distance from the nearest atom exterior to the Hirshfeld surface, for each point on the Hirshfeld surface. The points in the same 0.01 Å area of the plot are added up and the number of points in a given area is described by colors ranging from blue (few points), to green (moderate amount of points) to red (many points) (Figure 20).

The example Hirshfeld surfaces and fingerprint plots of these for the cocrystal of 2,2′-biphenyl and 4,4′-bipyridine in Figure 20 show the strong hydrogen bond from the phenol to the pyridine as red points on the Hirshfeld surface and as the protruding spikes in the fingerprint plots. In addition to this, the Hirshfeld surfaces show some close contacts on the aromatic parts of the molecules and C-H⋯π interactions are seen in the fingerprint plots as "wings"[131] on the sides. The scattered points in the upper right corner of the fingerprint plot are an indication of somewhat loose packing.

1.4.4 Lattice energy calculations

The lattice energy describes the total potential energy of a crystal and can be thought of as the heat of sublimation of the crystals.[132, 133] Lattice energy minimization is used for crystal structure prediction[134], but the calculation of the lattice energy of existing crystal structures can help in understanding and perhaps in predicting the properties of crystals.[135, 136] Comparison of the lattice energies of polymorphic structures can help determine the relative stability of the forms though sometimes the errors in the experimental structures and the calculations can be comparable in size to the energy differences between the forms.[136] The calculation can be done on three main levels depending on the amount of empirical data and adjustable parameters used from empirical molecular mechanics calculations[132] to semi-empirical methods[137, 138] and *ab initio* calculations[135, 139]. The lattice energy is partitioned into different energy terms, because comparison of the different energies is more revealing than the comparison of the total energy.[140] How the energies are partitioned depends on the method of calculation.

Li *et al.*[132] have used a molecular mechanics approach in lattice energy calculations. The total lattice energies were partitioned into energies of repulsive and attractive van der Waals forces, electrostatic (Coulombic) forces and hydrogen bonding.[132] The calculations were used to assess the reasons behind the crystallization of chiral drugs into homochiral or racemic crystals. Van der Waals forces were found to play an important role in this chiral discrimination, and the melting behavior and enthalpies of fusion showed correlation to the calculated van der Waals forces.

Gavezzotti uses a semi-empirical method called PIXEL[137, 138] for crystal energy calculations. In the PIXEL method molecules are represented by around 10^4 electron interaction sites, pixels, rather than nuclear positions.[141] PIXEL partitions the lattice energy into Coulombic, polarization, dispersion and repulsion energies. With PIXEL energies can also be split into molecule-molecule pairs so as to quantitatively analyze intermolecular interactions, *i.e.* the potentials and forces between molecules.[133, 140, 142] This method involves analyzing a crystal structure by means of structure determinants of a reference molecule, or in other words molecular pairs for which the distance between the centers of mass is smaller than the largest molecular dimension. The molecule to molecule Coulombic, dispersion and repulsion interaction energies of these pairs are then calculated with the PIXEL method[137, 138]. The pairs are ranked by their energies to see which structure determinants are prevalent. The prevalent interactions can then be used to identify extended hydrogen bonding or other intermolecular interaction motifs in the structure.

1.4.5 Structural similarity calculations

XPac[143] is a program described by Gelbrich and Hursthouse to assess similarity in the crystal structures of related molecules. It can be used for sets of related molecules[144] or multi-component structures[145]. The method does not identify intermolecular interactions, but finds subassemblies of molecules called "supramolecular constructs", SCs, through orientational similarities between the molecules in related structures. An analysis of the found SCs will then bring up information about strong and weak intermolecular interactions and their role in the packing of the molecules.

The procedure in XPac involves choosing a corresponding ordered set of points (COSP), *i.e.* a group of atoms from the molecules that are oriented in the same way. Clusters of molecules are then generated around a central molecule in the compared structures. Similar double subunits, *i.e.* similarly oriented pairs, formed between the central molecule and another molecule in the cluster, are then identified between the structures. The similar double subunits are then combined to triple subunits and the similarities between the structures are evaluated. The similarities are based on intermolecular, dihedral and torsion angles, but not on distances. The seed of the supramolecular construct, which describes the similar packing arrangement in the structures, is then constructed using the similar subunits of the two clusters. The seed of the SC can, for instance, consist of the central molecule and six of the fourteen molecules in the cluster of molecules around this (Figure 21). Using symmetry operations the seed can be expanded to the full SC. Supramolecular constructs can be either 0-, 1-, 2- or 3-dimensional. The 0-dimensional SC is an isolated cluster like a hydrogen bonded dimer, a 1-dimensional SC is a chain-like assembly, a 2-dimensional SC a layer assembly and a 3-dimensional SC a framework.
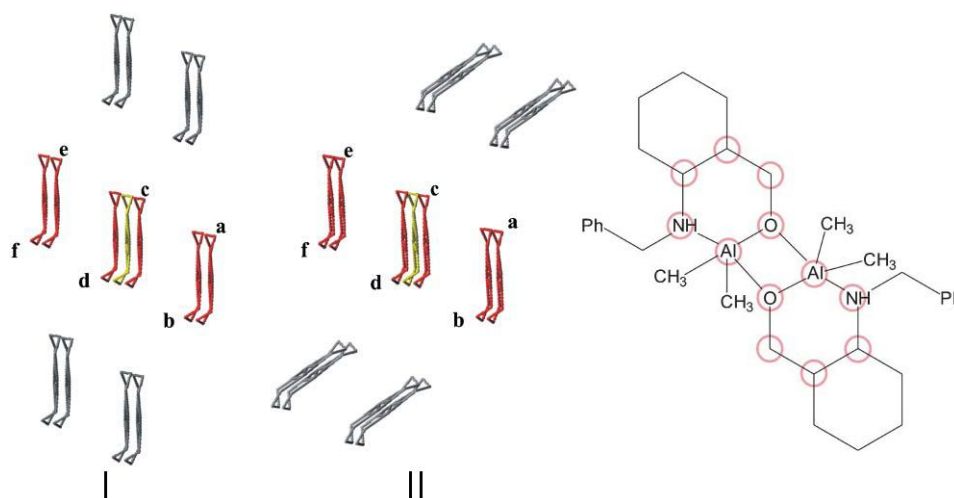
Figure 21. Clusters of molecules in polymorphs I and II of dimethylaluminium-cis(1*R*,2*S*)-benzylamino-1-cyclohexyl-methoxide showing only the atoms in the COSP (circled in the scheme). The central molecule (yellow) forms a seed of an SC with the red molecules (a-f) in the cluster.[143] (Reproduced by permission of The Royal Society of Chemistry.)

The usability of the XPac method is limited to molecules with a partially rigid backbone. The comparison of conformational polymorphs and similar flexible molecules is not possible due to the requirement for a consistent corresponding ordered set of points. Molecules with a different backbone, but with similar conformational shape can, however, be compared. The inclusion of solvents or other cocrystallizing molecules does not matter when the supramolecular constructs of the main molecules are compared.

1.5 Perspectives

The research on cocrystals is mostly done in the field of pharmaceuticals. The fruits of this race for new patentable crystal forms are, however, also useful for other chemical industries, crystal engineering and the fundamental understanding of crystalline matter. Liquid-assisted grinding seems to be winning the battle for the best experimental method for cocrystal synthesis in its versatility for experimental conditions and outcomes. As the determination of crystal structures from powder diffraction becomes more commonplace, the struggle to get single crystals for structure determination may become less acute for small molecules. Even though they will never replace the crystallization experiments, computational strategies are of an ever increasing importance in cocrystal design and in the analysis of results. Crystal structure prediction[73, 74], which has only been mentioned in this review, is also advancing as indicated by the successes of the fourth CSD blind test[146] that also included a cocrystal structure, and results of the fifth test are expected soon for a more current view of the success.

2 EXPERIMENTAL PART

2.1 Aims and background of the present work

Most of the studies on crystal forms are presently done on pharmaceutical actives because of the possibility for better dosage forms and extended intellectual property (IP) cover. Agrochemical actives are often organic molecules similar to pharmaceuticals, but the crystal forms of these have not been investigated to the same extent.

The aim of this study was to investigate the crystal forms of some agrochemical actives. The work was done mostly in collaboration with the polymorphism laboratory of BASF SE in Ludwigshafen, Germany, where the compounds were chosen among the many investigated agrochemical actives. Consequently, part of the research initially done for this thesis could not be published for IP reasons. The work done on thiophanate-methyl[I-III] (TM) and an analogous, though not industrially relevant, thiophanate-ethyl[II-IV] (TE) were exceptions. The 4-hydroxybenzoic acid cocrystals[V], on the other hand, are published in a patent.

Screening was performed by way of evaporation crystallization, solution-mediated transformation in slurries, neat and liquid-assisted grinding/milling and thermomicroscopic methods. The crystal forms obtained were studied with thermomicroscopy, TGA, DSC, IR, SSNMR, powder X-ray diffraction, and single crystal X-ray diffraction with the aim of acquiring the crystal structure. By investigating the intermolecular interactions in the single crystal structures, cocrystals could be designed.

2.2   Polymorphs and solvates of TM and TE[I,II]

Polymorph screening was carried out for two similar compounds, thiophanate-methyl (TM, dimethyl 4,4′-(*o*-phenylene)bis(3-thioallophanate)) and thiophanate-ethyl (TE, diethyl 4,4′-(*o*-phenylene)bis(3-thioallophanate)) (Scheme 3), using conventional low and medium throughput screening procedures of crystallization from a number of common solvents.
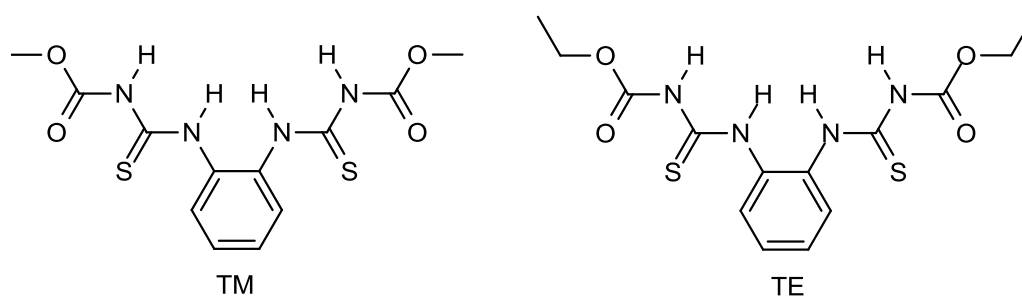
Scheme 3. Molecular structures of TM and TE.

Two polymorphs and fourteen solvates (acetonitrile/water, methanol, ethanol, acetone, dimethyl sulfoxide, cyclohexanone, dichloromethane, 1,2-dichloroethane, dioxane, pyridine, 1,2-dichlorobenzene, tetrahydrofuran, chloroform and benzene) were found for TM and crystal structures of all these solved by single crystal X-ray diffraction (Table 1).[I,II] The two polymorphs of TM show conformational and synthon polymorphism (Figure 22a-b). Form I is more stable than form II and crystallizes from acetonitrile (MeCN) and other solvents such as dimethylacetamide, methyl isobutyl ketone and 1,2-propanediol that do not form solvates. Form II was first found as a desolvation product of the solvates and a single crystal was later acquired from an MeCN:water solution, from which also the MeCN:water solvate crystallized in another experiment. Part of the hydrogen bonding pattern of the MeCN:water solvate is interestingly similar to that in TM form II (Figure 22b-c) suggesting at a cause as to why form II was successfully crystallized in these conditions.

Table 1. Crystal structure parameters of the polymorphs and solvates of TM

	TM Form I	TM Form II	TM MeCN/ water	TM DCM	TM 1,2-DCE
Formula	$C_{12}H_{14}N_4O_4S_2$	$C_{12}H_{14}N_4O_4S_2$	$3C_{12}H_{14}N_4O_4S_2$ $\cdot 2.5C_2H_3N \cdot H_2O$	$C_{12}H_{14}N_4O_4S_2$ $\cdot\ CH_2Cl_2$	$C_{12}H_{14}N_4O_4S_2$ $\cdot\ C_2H_4Cl_2$
M	342.39	342.39	1147.83	427.32	441.34
Crystal system	Monoclinic	Monoclinic	Triclinic	Triclinic	Triclinic
Space group	$P2_1/c$	$P2_1/c$	P-1	P-1	P-1
a (Å)	10.7149(5)	8.946(2)	10.641(2)	9.313(6)	9.313(2)
b (Å)	11.8405(5)	20.052(4)	13.751(3)	10.145(6)	10.150(2)
c (Å)	15.6861(6)	8.998(2)	20.181(4)	10.777(7)	10.735(2)
α (deg)	90	90	74.62(3)	83.04(4)	82.06(2)
β (deg)	132.593(2)	107.51(3)	85.49(3)	80.00(4)	79.40(2)
γ (deg)	90	90	77.97(3)	80.12(4)	79.41(2)
V (Å^3)	1465.1(2)	1539.3(5)	2784(1)	984(2)	974.7(4)
Z	4	4	2	2	2
ρcalc (g/cm3)	1.552	1.477	1.369	1.443	1.504
Meas reflns	9507	4338	12985	3274	8006
Indp reflns	1744	2653	9441	1992	2410
R_{int}	0.0572	0.0449	0.0832	0.0490	0.0450
R1 [I>2σ(I)]	0.0402	0.0424	0.0719	0.0680	0.0358
wR$_2$ [I>2σ(I)]	0.1128	0.1119	0.1748	0.1767	0.0910
GooF	1.187	1.055	1.062	1.037	1.059

	TM Methanol	TM Ethanol	TM Acetone	TM CH-one	TM DMSO
Formula	$2C_{12}H_{14}N_4O_4S_2$ $\cdot CH_3OH$	$2C_{12}H_{14}N_4O_4S_2$ $\cdot CH_3CH_2OH$	$2C_{12}H_{14}N_4O_4S_2$ $\cdot (CH_3)_2CO$	$2C_{12}H_{14}N_4O_4S_2$ $\cdot C_6H_{10}O$	$C_{12}H_{14}N_4O_4S_2$ $\cdot\ C_2H_6OS$
M	719.83	730.85	742.86	782.92	420.52
Crystal system	Triclinic	Triclinic	Triclinic	Triclinic	Monoclinic
Space group	P-1	P-1	P-1	P-1	C2/c
a (Å)	10.016(3)	9.842(2)	10.206(2)	11.277(3)	26.52(2)
b (Å)	11.430(3)	11.370(2)	11.153(2)	17.368(4)	10.321(5)
c (Å)	15.904(5)	15.988(3)	17.062(3)	19.902(5)	17.43(1)
α (deg)	101.73(1)	78.99(1)	76.69(3)	92.21(2)	90
β (deg)	90.33(1)	89.34(1)	86.07(3)	103.76(2)	94.66(3)
γ (deg)	107.692(9)	72.15(2)	72.46(3)	100.77(1)	90
V (Å^3)	1694.0(9)	1669.5(5)	1802.0(6)	3705(2)	4755(5)
Z	2	2	2	4	8
ρcalc (g/cm3)	1.405	1.454	1.369	1.404	1.175
Meas reflns	7891	9780	8844	28524	12637
Indp reflns	3543	3869	6210	9162	3184
R_{int}	0.0606	0.0660	0.1118	0.0473	0.1367
R$_1$ [I>2σ(I)]	0.0726	0.1717	0.0487	0.0411	0.0899
wR$_2$ [I>2σ(I)]	0.1975	0.4942	0.1271	0.0938	0.2145
GooF	1.104	2.166	1.022	1.038	0.988

Table 1. Continued

	TM Chloroform	TM THF	TM Dioxane	TM Pyridine	TM 1,2-DCB	TM Benzene
Formula	$C_{12}H_{14}N_4O_4S_2$ • $CHCl_3$	$C_{12}H_{14}N_4O_4S_2$ • C_4H_8O	$C_{12}H_{14}N_4O_4S_2$ • $C_4H_8O_2$	$C_{12}H_{14}N_4O_4S_2$ • C_5H_5N	$C_{12}H_{14}N_4O_4S_2$ • $C_6H_4Cl_2$	$C_{12}H_{14}N_4O_4S_2$ • C_6H_6
M	461.76	414.52	430.50	421.49	489.38	420.50
Crystal syst.	Triclinic	Triclinic	Monoclinic	Triclinic	Triclinic	Triclinic
Space group	P-1	P-1	C2/c	P-1	P-1	P-1
a (Å)	10.626(2)	10.546(2)	21.97(1)	8.244(1)	7.9951(7)	8.4106(8)
b (Å)	14.706(3)	14.470(3)	11.428(5)	10.690(2)	9.5484(9)	9.9524(9)
c (Å)	14.739(3)	14.592(2)	17.147(7)	12.493(2)	14.702(2)	12.952(2)
α (deg)	63.51(3)	65.317(8)	90	67.892(5)	81.910(4)	107.946(4)
β (deg)	77.34(3)	77.66(1)	111.24(2)	81.442(6)	84.862(4)	101.732(5)
γ (deg)	74.82(3)	76.29(1)	90	74.153(5)	73.646(4)	96.983(4)
V (Å^3)	1975.6(7)	1948.8(6)	4014(3)	979.9(2)	1064.7(2)	991.0(2)
Z	4	4	8	2	2	2
ρcalc (g/cm3)	1.552	1.4013	1.425	1.429	1.526	1.409
Meas reflns	10630	9286	7583	7870	7159	8528
Indp reflns	6828	4514	2484	2437	2645	2494
R_{int}	0.0679	0.0407	0.0475	0.0321	0.0323	0.0313
R_1 [I>2σ(I)]	0.0557	0.0526	0.0679	0.0434	0.0459	0.0373
wR_2 [I>2σ(I)]	0.1358	0.1494	0.1866	0.1082	0.1127	0.0889
GooF	1.027	1.123	1.079	1.167	1.201	1.106

a)   b)   c)
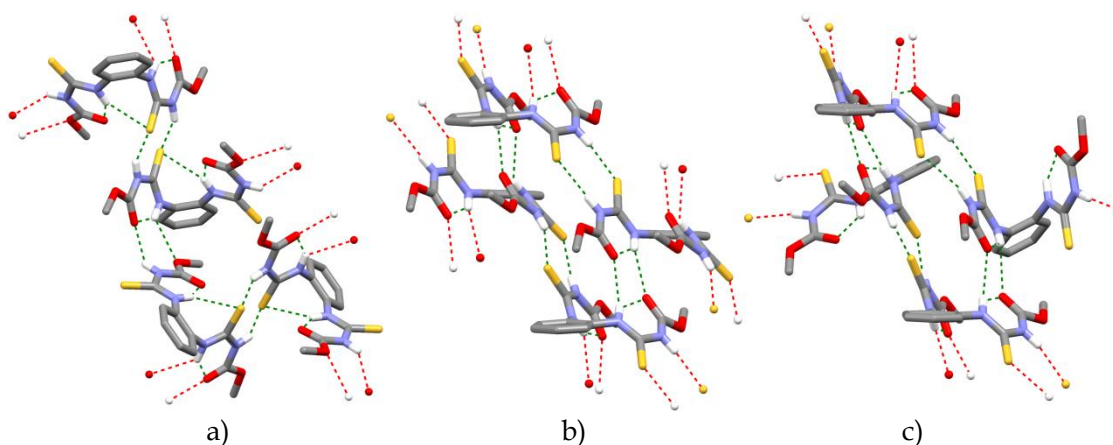
Figure 22. Hydrogen bonding in the structures of a) form I, b) form II and c) part of the MeCN:H$_2$O solvate of TM. Non-hydrogen bonding hydrogen atoms omitted for clarity.

The dichloromethane (DCM) and 1,2-dichloroethane (1,2-DCE) solvates of TM are isomorphic with the solvent molecules located in channels between chains of TM molecules. The methanol, ethanol and acetone solvates are isomorphic and the cyclohexanone (CH-one) solvate is very similar to these. In these structures the hydrogen bonding between the TM and solvent molecules builds up an arrangement where the solvent molecules are situated between two sheets of TM molecules. In the dimethyl sulfoxide (DMSO) solvate of TM one molecule of DMSO is hydrogen bonded to chains of TM molecules,

whereas another DMSO molecule is disordered in channels between the chains. The chloroform and tetrahydrofuran (THF) solvates are nearly isomorphic, but in the THF solvate chains of TM hydrogen bond to the THF molecules and in the chloroform solvate the chains are hydrogen bonded to each other. The pyridine and dioxane solvates are composed of similar hydrogen bonded chains, but the chains in the pyridine solvate arrange parallel to each other while in the dioxane solvate the chains cross. In the 1,2-dichlorobenzene (1,2-DCB) and benzene solvates the TM molecules hydrogen bond into sheets or chains, respectively, between which the solvent molecules reside.

Four polymorphs and seven solvates (isomorphic acetone, dioxane I, DCM and chloroform as well as toluene, dioxane II and pyridine) were found for TE and the crystal structures of all except one of the polymorphs solved by single crystal X-ray diffraction (Table 2).[II] TE form I is the most stable polymorph, in which the TE molecules hydrogen bond into sheets (Figure 23a). Form II, in which TE molecules are hydrogen bonded into chains that pack parallel to each other (Figure 23b), is less stable, but still similar in stability to form I as they at times crystallize concomitantly. Form III of TE, in which the TE molecules form hydrogen bonded double chains (Figure 23c), crystallized serendipitously from a solution also containing sodium acetate and is the least densely packed of the polymorphs. TE form IV is a desolvation product and single crystals have not been acquired. Refinement of the structure of form IV from powder data is currently underway.[147] The structure is monoclinic with a spacegroup of C2/c like the isomorphic solvate structures with a = 11.50 Å, b = 18.76 Å, c = 9.22 Å, β = 112.24° and V = 1846.5 Å^3. The preliminary results show the hydrogen bonding pattern to be composed of chains of TE molecules identical to that in the isomorphic solvates, from which it is acquired by desolvation.

a)   b)   c)

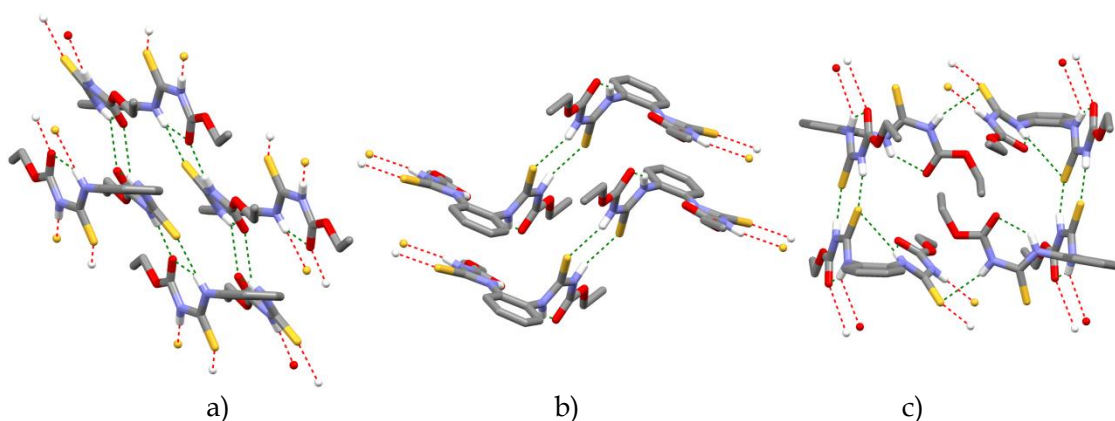**Figure 23.** Hydrogen bonding in a) form I, b) form II and c) form III of TE. Non-hydrogen bonding hydrogen atoms omitted for clarity.

In the isomorphic solvates the TE molecules hydrogen bond into chains which pack parallel and leave channels between the arms of the molecules, in which the solvent molecules reside. In the pyridine and dioxane II solvates the

hydrogen bonded unit is a pair of TE and solvent molecules, which then packs somewhat differently in the two solvates. The TE molecules in the toluene solvate also make chains, but they form spirals causing the noncentrosymmetric structure.

Table 2. Crystal structure parameters of the polymorphs and solvates of TM

	TE-form I	TE-form II	TE-form III	TE-acetone	TE-DCM
Formula	$C_{14}H_{18}N_4O_4S_2$	$C_{14}H_{18}N_4O_4S_2$	$C_{14}H_{18}N_4O_4S_2$	$C_{14}H_{18}N_4O_4S_2 \cdot C_3H_6O$	$C_{14}H_{18}N_4O_4S_2 \cdot CH_2Cl_2$
M	370.44	370.44	370.44	428.52	455.37
Crystal system	Triclinic	Monoclinic	Triclinic	Monoclinic	Monoclinic
Space group	P-1	$P2_1/c$	P-1	$C2/c$	$C2/c$
a (Å)	7.9911(1)	4.7271(1)	10.7333(5)	16.0607(2)	16.1404(3)
b (Å)	9.6750(2)	16.0239(3)	11.8079(7)	17.4629(2)	17.3754(3)
c (Å)	12.5109(3)	22.6450(4)	16.2174(12)	8.4560(1)	8.2332(2)
α (deg)	69.055(3)	90	95.293(3)	90	90
β (deg)	81.270(3)	93.750(3)	100.405(4)	111.432(3)	110.996(3)
γ (deg)	73.033(3)	90	113.044(4)	90	90
V (Å³)	862.81(3)	1711.61(6)	1829.9(2)	2207.63(5)	2155.66(8)
Z	2	4	4	4	4
ρcalc (g/cm3)	1.426	1.438	1.345	1.289	1.403
Meas. reflns.	4039	4691	8675	2547	2757
Indep. reflns.	2936	2931	6132	1878	1781
R_{int}	0.0848	0.0616	0.1113	0.0234	0.0605
R_1 [I>2σ(I)]	0.0458	0.0550	0.0603	0.0359	0.1591
wR_2 [I>2σ(I)]	0.1235	0.1120	0.1413	0.0936	0.4149
GooF	1.031	1.060	1.026	1.047	1.172

	TE-chloroform	TE-dioxane I	TE-dioxane II	TE-pyridine	TE-toluene
Chemical formula	$C_{14}H_{18}N_4O_4S_2 \cdot CHCl_3$	$C_{14}H_{18}N_4O_4S_2 \cdot C_4H_8O_2$	$C_{14}H_{18}N_4O_4S_2 \cdot C_4H_8O_2$	$C_{14}H_{18}N_4O_4S_2 \cdot C_5H_5N$	$3(C_{14}H_{18}N_4O_4S_2) \cdot 2(C_7H_8)$
Formula Mass	489.81	458.55	458.55	449.54	1295.60
Crystal system	Monoclinic	Monoclinic	Triclinic	Triclinic	Tetragonal
Space group	$C2/c$	$C2/c$	P-1	P-1	$P4_322$
a (Å)	15.5158(3)	16.8293(3)	9.2924(2)	8.8104(9)	11.7631(2)
b (Å)	18.0503(4)	17.0275(3)	11.7070(3)	11.3513(13)	11.7631(2)
c (Å)	8.5922(2)	8.2545(2)	12.1305(3)	12.500(2)	48.5257(8)
α (deg)	90	90	65.555(2)	66.635(7)	90
β (deg)	112.739(3)	111.119(3)	68.864(2)	77.989(6)	90
γ (deg)	90	90	76.329(3)	77.883(5)	90
V (Å³)	2219.34(8)	2206.54(8)	1114.61(5)	1111.1(2)	6714.5(2)
Z	4	4	2	2	4
ρcalc (g/cm3)	1.466	1.38	1.366	1.344	1.282
Meas. reflns.	2817	2410	5447	6213	11130
Indep. reflns.	1907	1647	3818	4056	5685
R_{int}	0.0476	0.0361	0.0504	0.0366	0.0399
R_1 [I>2σ(I)]	0.0755	0.0633	0.0444	0.0530	0.0434
wR_2 [I>2σ(I)]	0.1918	0.1799	0.1089	0.0985	0.0987
GooF	1.034	1.105	1.022	1.077	1.043

2.2.1 Hydrogen bonding graph-sets

The polymorphs of both TM and TE display variability in hydrogen bond motifs (Scheme 4 and Table 3). An intramolecular C=O$\cdots$H-N S(6) motif in both the arms of the molecule is always present as is expected from Etter's hydrogen bonding rules. An intramolecular S(7) motif joining the two hands of the molecule also sometimes forms. All the structures also have the intermolecular $R_2^2(8)$ motif of two C=S$\cdots$H-N hydrogen bonds from the thioamide groups. An intermolecular R_2^2 (12) motif of two C=O$\cdots$H-N bonds, which is in approximately half the structures, is the next most common. A mixed pairing of C=O$\cdots$H-N and S$\cdots$H-N bonds in a second order $R_2^2(10)$ motif is also seen in two structures (TE form I and the 1,2-DCB solvate of TM).
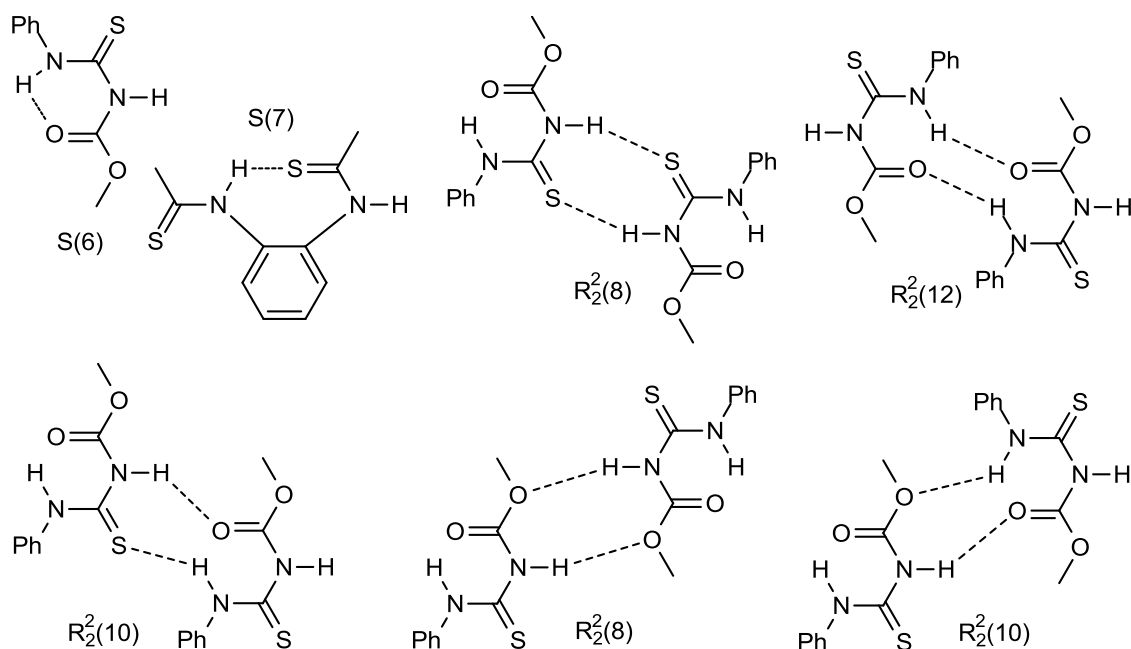
Scheme 4. Hydrogen bonding motifs in the TM and TE structures with graph set descriptors.

The alkoxy oxygen also participates in hydrogen bonding either with a $R_2^2(8)$ motif or a second order $R_2^2(10)$ motif together with the C=O in form I of TM (Figure 24a-b). The alkoxy oxygen $R_2^2(8)$ motif found in the benzene and cyclohexanone solvates of TM is further stabilized by weak hydrogen bonds from the thione to the methyl group hydrogens. The DCM and 1,2-DCE solvates of TM also have a C=O$\cdots$H-N $R_2^2(22)$ motif involved in the pairing of two TM molecules (Figure 24c).

The solvents are most often connected via a D(2) motif. In the acetone and cyclohexanone solvates a D_2^1 (3) motif is formed by two C=O$\cdots$H-N hydrogen bonds to the acetone or cyclohexanone. In the methanol and ethanol solvates of

50

TM a second order $R_4^4(12)$ motif is formed by two TM and solvent molecules (Figure 24d).

Table 3. Graph-sets found in the TM and TE polymorphs and solvates

Structure	S(6) C=O···H-N	S(7) C=S···H-N	$R_2^2(8)$ C=S···H-N pairing	$R_2^2(12)$ C=O···H-N pairing	Other	To solvent
TM form I	X	X	X		$R_2^2(10)$ mixed pairing alkoxy O···H-N, C=O···H-N	
TM form II	X		X	X		
TM MeCN H₂O	X		X	X		D(2) to water
TM DCM and 1,2-DCE	X	X	X		$R_2^2(22)$ C=O···H-N	
TM methanol and ethanol	X	X	X	X		$R_4^4(12)$ to (m)ethanol
TM acetone	X	X	X	X		$D_2^1(3)$ to acetone
TM CH-one	X	X	X	X	$R_2^2(8)$ alkoxy O···H-N pairing	$D_2^1(3)$ to CH-one
TM DMSO	X	X	X	X		D(2) to DMSO
TM chloroform	X		X	X		
TM THF	X		X	X		D(2) to THF
TM dioxane	X	X	X	X		D(2) to dioxane
TM pyridine	X		X	X		D(2) to pyridine
TM 1,2-DCB	X		X	X	$R_2^2(10)$ mixed pairing C=S···H-N, C=O···H-N	
TM benzene	X		X		$R_2^2(8)$ alkoxy O···H-N pairing	
TE form I	X		X	X	$R_2^2(10)$ mixed pairing C=S...H-N, C=O···H-N	
TE form II	X		X			
TE form III	X	X	X	X	D(2) N-H···S	
TE isostructural solvates	X		X			
TE dioxane II	X		X			D(2) to dioxane
TE pyridine	X		X			D(2) to pyridine
TE toluene	X		X			
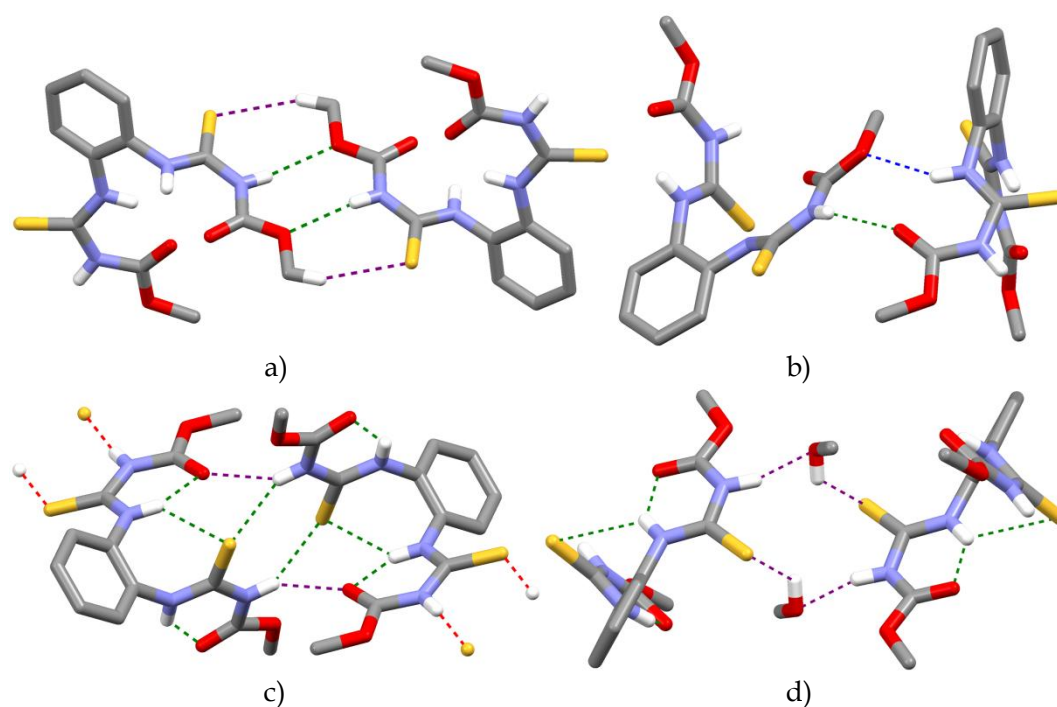
Figure 24. a) The alkoxy oxygen $R_2^2(8)$ motif supported by weak C-H$\cdots$S=C hydrogen bonds (purple) in the benzene solvate of TM, b) the alkoxy oxygen second order $R_2^2(10)$ motif with C=O in TM form I, c) the C=O$\cdots$H-N bonds (purple) of the $R_2^2(22)$ motif in the DCM solvate of TM and d) the second order $R_4^4(12)$ motif found in the methanol and ethanol solvates of TM. Non-hydrogen bonding hydrogen atoms omitted for clarity.

2.2.2 Thiophanate conformation, the thioamide ring motif and Z′

In the typical conformation of TM and TE molecules the thione sulfurs are on different sides of the benzene ring. The exceptions are the 1,2-dichlorobenzene solvate of TM and TE form I for which the sulfurs are on the same side of the ring (Figure 25a). In some structures, most clearly TE form II, TE dioxane solvate and TM benzene solvate, one of the sulfurs is roughly in the plane of the benzene ring (Figure 25b). The lowest energy conformation for TM has been calculated to be the one with the sulfurs on opposite sides.[I] With the inherent two-fold rotational symmetry of the molecule there are two inversionally related options for the lowest energy conformation. These can be identified for example as a clockwise (*cw*) conformation where the sulfurs point towards a clockwise rotation when viewed down the benzene ring and the inversion related counterclockwise (*ccw*) conformation (Figure 25c-d).

Figure 25. Conformations of TM/TE with the sulfurs on the same side of the ring (from TE form I), b) the other sulfur in plane with the ring (from TE form II) and the c) clockwise (*cw*) and d) counterclockwise (*ccw*) options (from the methanol solvate of TM). Non-hydrogen bonding hydrogen atoms omitted for clarity.

In solution the molecules can likely change conformation relatively freely, but most are expected to be in either the cw or ccw conformation. During the aggregation of molecules into crystal nuclei the conformation becomes locked at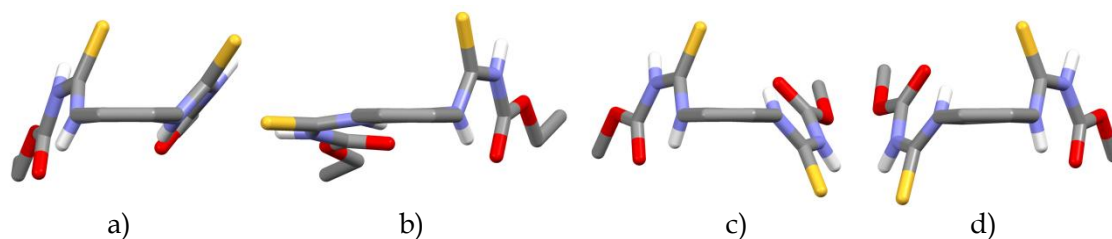 least to some extent. The thioamide $R_2^2(8)$ motif linkage is the most common in all the structures and there seems to be an interesting relationship between this, the *cw* and *ccw* conformations and the Z′, the number of TM/TE molecules in the asymmetric unit. When joining together two TM/TE molecules they can be either in the *cw* or *ccw* conformation. As they make the $R_2^2(8)$ motif the nature of the dimer formed depends on the conformation. When *cw* to *ccw* dimer is formed, the bulks of the molecules stay relatively far away from each other. When two *cw* (or two *ccw*) molecules form a dimer, however, the bulks of the molecules are quite close to each other. For chains connected with the $R_2^2(8)$ motif this results in elongated chains when *cw* and *ccw* molecules alternate and bends in the chains when there is a *cw* to *cw* (or *ccw* to *ccw*) connection (Figure 26).

In the structures where two molecules of the same *cw* or *ccw* conformation make the $R_2^2(8)$ motif Z′ is larger than one, for example in TE form III (Z′=2), the toluene solvate of TE (Z′=1.5), the MeCN/H$_2$O solvate of TM (Z′=3), the methanol, ethanol and acetone solvates of TM (Z′=2), and the cyclohexanone solvate of TM (Z′=4). High Z′ structures have been discussed in the recent literature, and a variety of causes for a high Z′ such as crystallization kinetics, frustration between competing interactions, awkward molecular shape and directional interactions that do not fit in with crystallographic symmetry have been mentioned.[148-153] The reason for the high Z′ structures in this case may be that once the $R_2^2(8)$ motif is formed, the molecules in the dimer are locked in either *cw* or *ccw*. A *cw-cw* (or *ccw-ccw*) dimer then does not fit in with crystallographic symmetry, making the crystallizing unit effectively the dimer instead of a single molecule.

The only other solvate structures with a Z′>1 are the chloroform and THF solvates of TM with a Z′=2. In these two structures the two molecules in the asymmetric unit are pseudosymmetric and the cause for the Z′ of two is likely in close packing requirements of the hydrogen bonded chains.
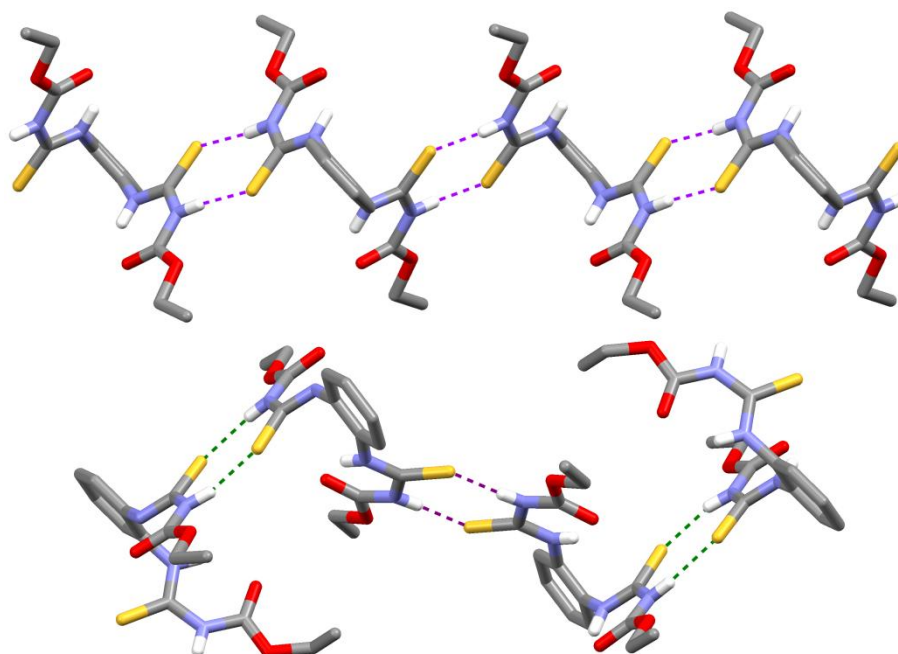
Figure 26. Straight chain of TE cw-ccw-cw-ccw molecules in the acetone solvate and bent chains of TE ccw-ccw-cw-cw molecules in form III. Non-hydrogen bonding hydrogen atoms omitted for clarity.

2.2.3 Solvates as models for cocrystals

Both TM and TE crystallize as a number of solvates. For TM especially, it was difficult to find a reasonably well dissolving solvent, which would not result in a solvate. Some of the solvates are hydrogen bonded, but some are not. The non-hydrogen bonded solvates (dichloromethane, 1,2-dichloroethane, 1,2-dichlorobenzene, chloroform, benzene and toluene) likely form because of favorable weak interactions like π-π stacking. Other than utilizing the clear solvent channels in the isomorphous solvates of TE, no other strategy for cocrystal design is evident from these structures. Interestingly, in the case of TM all the solvents that can form strong hydrogen bonds (MeCN/water, methanol, ethanol, acetone, DMSO, cyclohexanone, dioxane, pyridine, THF) are hydrogen bonded in the solvates, whereas TE crystallizes with strongly hydrogen bonding solvents (acetone and dioxane) in the cavities located between the arms of the TE molecules in the isomorphous solvates. As solvates can be considered cocrystals, the design of more cocrystals for TM and TE with a supramolecular synthon approach could be carried out using the synthons exhibited in the hydrogen bonded solvates.

Methanol and ethanol function as both hydrogen bond donors and acceptors in the solvate structures (Figure 24d). The utilization of further alcohols in cocrystal design, however, is not expected to work well because hydroxyls act as both stronger donors than the N-H, and stronger acceptors than the thione, which is primarily available for hydrogen bonding. According

to the hydrogen bonding rules the hydroxyls should then hydrogen bond to each other rather than to the TM or TE molecules. The emergence of these solvates is likely due to other favorable interactions like a weak aromatic-C-H⋯S hydrogen bond that is also seen in the similar acetone and cyclohexanone solvates.

All the other solvents primarily function only as hydrogen bond acceptors in the solvates. The hydrogen bonding to the N-H should be energetically more favorable than the $R_2^2(8)$ homosynthon of the thioamide. Cooperativity of an acceptor for the thioamide N-H and a donor for the thione could be a good approach. If the donor is better or equally good to the N-H, however, cocrystals are not expected to form because the coformer will preferably hydrogen bond with itself. Cooperative weak hydrogen bonding to the sulfinyl from the same solvent molecule is seen only in the DMSO solvate of TM with a C-H as a donor (Figure 27b).

a)   b)   c)
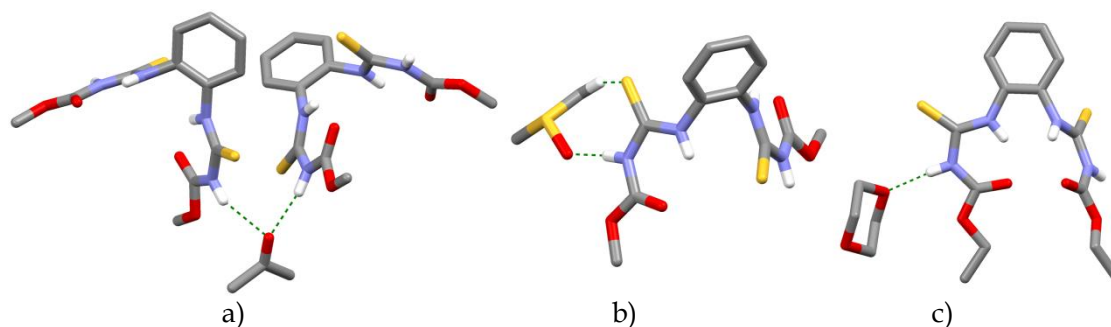
Figure 27. Hydrogen bonding synthons in the TM and TE solvates that could be used for cocrystal design. Non-hydrogen bonding hydrogen atoms omitted for clarity.

The pyridine-thioamide bond is likely the strongest hydrogen bond and has already been utilized in cocrystals.[III,IV] Coformers containing a carbonyl or sulfinyl found in CH-one, acetone and DMSO (Figure 27a-b), respectively, could be utilized as carbonyls and sulfinyls are significantly stronger acceptors than the thione group, which is most often utilized as an acceptor for the N-H donors. The ether oxygen is a weaker acceptor than carbonyl and sulfinyl and only slightly better than the thione, but it is involved in hydrogen bonding in the THF and dioxane solvates of TM and the dioxane II solvate of TE (Figure 27c), making coformers containing an ether group as a hydrogen bonding acceptor usable. The fact that in the acetone solvate and the polymorph of the dioxane solvate of TE the solvents are not hydrogen bonded brings a doubt to these approaches. The isomorphous solvate structures, however, are likely formed because the arrangement of TE molecules is very favorable. If the coformer were large enough or awkwardly shaped to not fit in the channels of solvent, a hydrogen bonded cocrystal could form.

With such an approach the emergence of solvates during polymorph screening can be thought of as an advantage that will aid in the design of

cocrystals. Screening for solvates is significantly easier as one is dealing with a two component system instead of a three component system as is usually the case when cocrystallizing two solid components. For further cocrystals of TM and TE, and possibly other thioamides, coformers containing hydrogen bond acceptors stronger than the sulfinyl and no strong donors could be used. For TE especially, molecules of a shape not able to fit in the isomorphous solvate channels should be chosen.

2.3 Cocrystal screening[III,IV,V]

2.3.1 TM and TE with compounds containing a pyridine moiety[III, IV]

Cocrystal screening was carried out for TM and TE utilizing a thioamide-pyridine heterosynthon (Scheme 5) that was found to persist in the pyridine solvates of the actives. Aakeröy *et al.*[154] state that polymorphic compounds can be good cocrystallizing agents, if they display synthon flexibility, *i.e.* variability in the hydrogen bonding patterns in the different polymorphs as some polymorphs of TM and TE. A number of commercially available molecules containing a pyridine moiety (Scheme 5) were chosen for the experiments.

Cocrystallization with 2,2′-bipyridine and biphenyl was also attempted for comparison even though the pyridine moieties of 2,2′-bipyridine are likely sterically unavailable and biphenyl contains no strong hydrogen bond acceptors. For IP reasons more experiments were carried out for TE than for TM, for which cocrystallizations with only 2,2′-bipyridine, 4,4′-bipyridine and 1,2-bis(4-pyridyl)ethane were attempted. Cocrystallization from solution, solution-mediated transformation in slurries, neat and liquid-assisted milling and thermomicroscopic methods were used in the investigations. Thermomicroscopic methods, however, were not well applicable to TM and TE because they decompose upon melting.

For both TM and TE cocrystals were found with 2,2′-bipyridine, 4,4′-bipyridine and 1,2-bis(4-pyridyl)ethane and the structures of these solved by single crystal X-ray diffraction (Table 4).[III] Additional cocrystals for TE were found with di(2-pyridyl)ketone, 2-benzoylpyridine, 3-benzoylpyridine, 4-phenylpyridine and biphenyl and crystal structures of four of them solved by single crystal X-ray diffraction (Table 4).[IV]
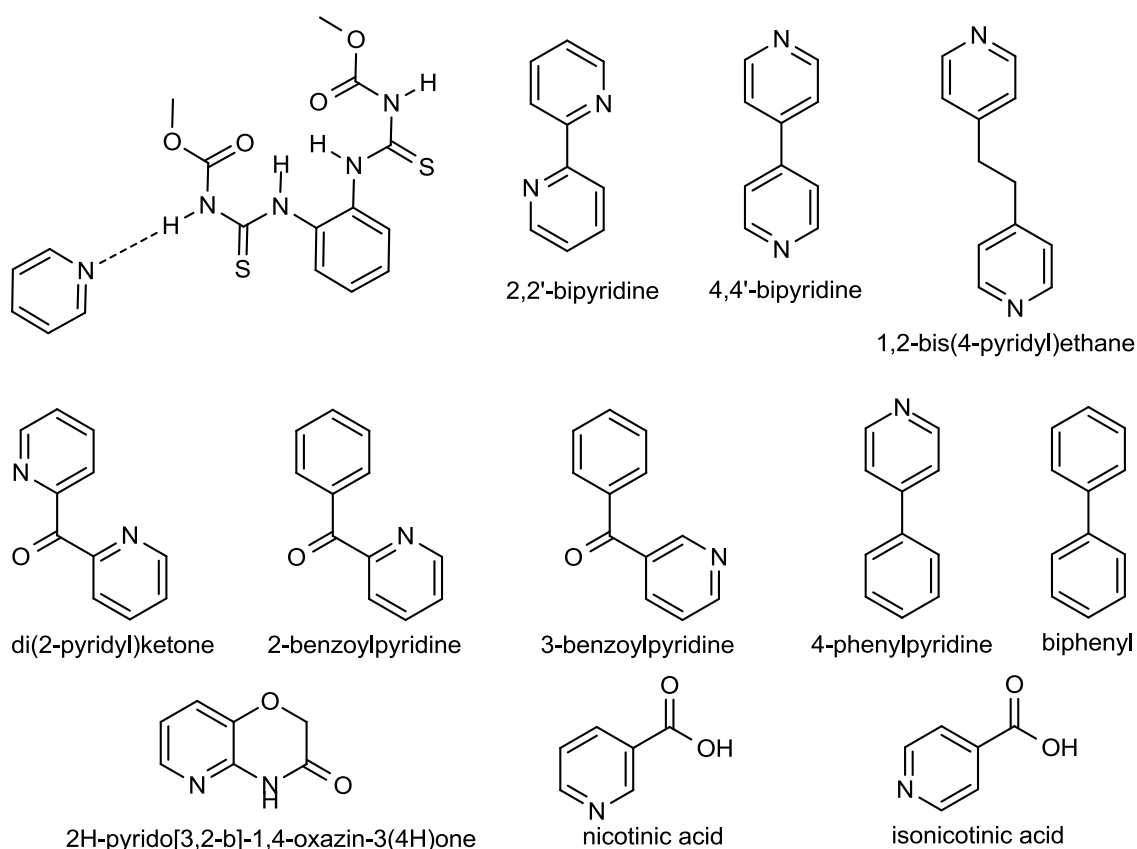
Scheme 5. The proposed pyridine⋯H-N synthon and the molecular structures of the coformers chosen for the TM and TE cocrystalllization experiments.

The expected pyridine⋯H-N synthon is found in all the cocrystals with coformers that have a sterically unhindered pyridine moiety. The thiophanate to coformer stoichiometry of the hydrogen bonded cocrystals, however, is variable with three 2:1 cocrystals (TM-4,4′-bipyridine, TM-1,2-bis(4-pyridyl)ethane and TE-1,2-bis(4-pyridyl)ethane), three 1:1 cocrystals (TE-4,4′-bipyridine, TE-di(2-pyridyl)ketone and TE-2-benzoylpyridine) and one 1:2 cocrystal (TE-3-benzoylpyridine). This variability is likely explained by the two donors available in the thiophanate molecules and the one to two pyridine acceptors available in the coformers. Consequently, stoichiometric variants of the cocrystals are likely and one milling experiment of TE with 4,4′-bipyridine did yield another powder diffraction pattern, but this was not further investigated.

Table 4. Crystal data and parameters of the TM and TE cocrystal structures.

	TM-2,2′-bipyridine	TE-2,2′-bipyridine	TM-4,4′-bipyridine	TE-4,4′-bipyridine	TM-1,2-bis(4-pyridyl)ethane
Chemical formula	$2(C_{12}H_{14}N_4O_4S_2)$ •$1.5(C_{10}H_8N_2)$ •C_2H_3N	$C_{14}H_{18}N_4O_4S_2$ •$0.5(C_{10}H_8N_2)$	$C_{12}H_{14}N_4O_4S_2$ •$0.5(C_{10}H_8N_2)$	$C_{14}H_{18}N_4O_4S_2$ •$C_{10}H_8N_2$	$2(C_{12}H_{14}N_4O_4S_2)$ •$C_{12}H_{12}N_2$
M	960.11	448.54	420.48	526.63	869.02
Crystal system	Triclinic	Monoclinic	Triclinic	Triclinic	Triclinic
Space group	P-1	$P2_1/c$	P-1	P-1	P-1
a (Å)	10.6193(3)	8.3860(7)	9.0382(2)	11.8193(4)	9.0972(2)
b (Å)	15.0562(4)	17.2950(12)	9.5723(2)	12.8098(5)	9.5762(2)
c (Å)	16.2601(4)	15.4566(11)	12.5370(3)	26.3527(10)	23.8891(3)
α (deg)	108.694(4)	90.00	100.183(3)	91.574(2)	86.224(1)
β (deg)	95.323(3)	98.93(3)	104.203(3)	95.655(2)	88.273(1)
γ (deg)	109.312(4)	90.00	101.444(3)	100.640(3)	88.214(1)
V (Å³)	2265.87(10)	2214.6(3)	1001.16(4)	3897.9(2)	2074.79(7)
Z	2	4	2	6	2
ρcalc (g/cm3)	1.407	1.345	1.395	1.346	1.391
Meas. reflns.	10805	6504	4322	18442	10604
Indep. reflns.	7733	3778	3298	13511	7144
R_{int}	0.0585	0.0975	0.1194	0.1463	0.1069
R_1 [I>2σ(I)]	0.0517	0.0713	0.0657	0.0802	0.0604
wR_2 [I>2σ(I)]	0.1257	0.1812	0.1788	0.2103	0.1459
GooF	1.032	1.039	1.069	1.071	1.043

	TE-1,2-bis(4-pyridyl)ethane	TE-di(2-pyridyl)ketone	TE-2-benzoylpyridine	TE-3-benzoylpyridine	TE-biphenyl
Chemical formula	$2(C_{14}H_{18}N_4O_4S_2)$ •$C_{12}H_{12}N_2$	$C_{14}H_{18}N_4O_4S_2$ · $C_{11}H_8N_2O$	$C_{14}H_{18}N_4O_4S_2$ · $C_{12}H_9NO$	$C_{14}H_{18}N_4O_4S_2$ · $2(C_{12}H_9NO)$	$C_{14}H_{18}N_4O_4S_2$ · $0.5(C_{12}H_{10})$
M	925.12	554.64	553.65	736.85	447.54
Crystal system	Triclinic	Monoclinic	Monoclinic	Monoclinic	Triclinic
Space group	P-1	$P2_1/c$	$P2_1/c$	$P2_1/c$	P-1
a (Å)	11.9780(10)	12.7612 (7)	12.8497 (5)	10.4541 (4)	8.8861 (1),
b (Å)	14.1211(12)	8.3916 (4)	8.5996 (3)	26.8015 (11)	10.0077 (2)
c (Å)	14.9536(12)	26.3679 (14)	26.0775 (9)	13.1925 (6)	12.7746 (3)
α (deg)	107.572(4)	90	90	90	85.098 (2)
β (deg)	106.503(5)	112.022 (3)	112.182 (2)	102.607 (2)	78.793 (1)
γ (deg)	91.062(4)	90	90	90	79.930 (1)
V (Å³)	2296.8(3)	2617.6 (2)	2668.4 (2)	3607.2 (3)	1095.65 (4)
Z	2	4	4	4	2
ρcalc (g/cm3)	1.338	1.407	1.378	1.357	1.357
Meas. reflns.	9982	6507	7725	11459	5449
Indep. reflns.	7030	4031	4631	6233	3754
R_{int}	0.1410	0.137	0.069	0.107	0.085
R_1 [I>2σ(I)]	0.0688	0.079	0.050	0.064	0.046
wR_2 [I>2σ(I)]	0.1382	0.214	0.126	0.164	0.126
GooF	1.018	1.03	1.05	1.02	1.03

In the TM/TE cocrystals with 4,4′-bipyridine and 1,2-bis(4-pyridyl)ethane the thiophanate molecules make pairs connected with the N–H⋯O=C $R_2^2(12)$ hydrogen bonding motif and two molecules of the coformer are hydrogen bonded to this pair (Figure 28a). The differences in the structures lie in the hydrogen bonding of these units into chains, either via further connections between the thiophanate molecules or the coformers. The TE cocrystals with di(2-pyridyl)ketone and 2-benzoylpyridine are isomorphic. Interestingly, these two cocrystals do not have the N–H⋯S=C $R_2^2(8)$ motif seen in all other crystal structures of TM and TE. A double chain of TE molecules is built up of C=O⋯H-N hydrogen bonding with one di(2-pyridyl)ketone/2-benzoylpyridine attached to each TE molecule (Figure 28b). The TE cocrystal with 3-benzoylpyridine is the only cocrystal where both the N-H donors that are not intramolecularly hydrogen bonded are bonded to the coformer causing the 1:2 ratio. This results in the formation of discrete units with a $D_2^2(12)$ motif (Figure 28c).
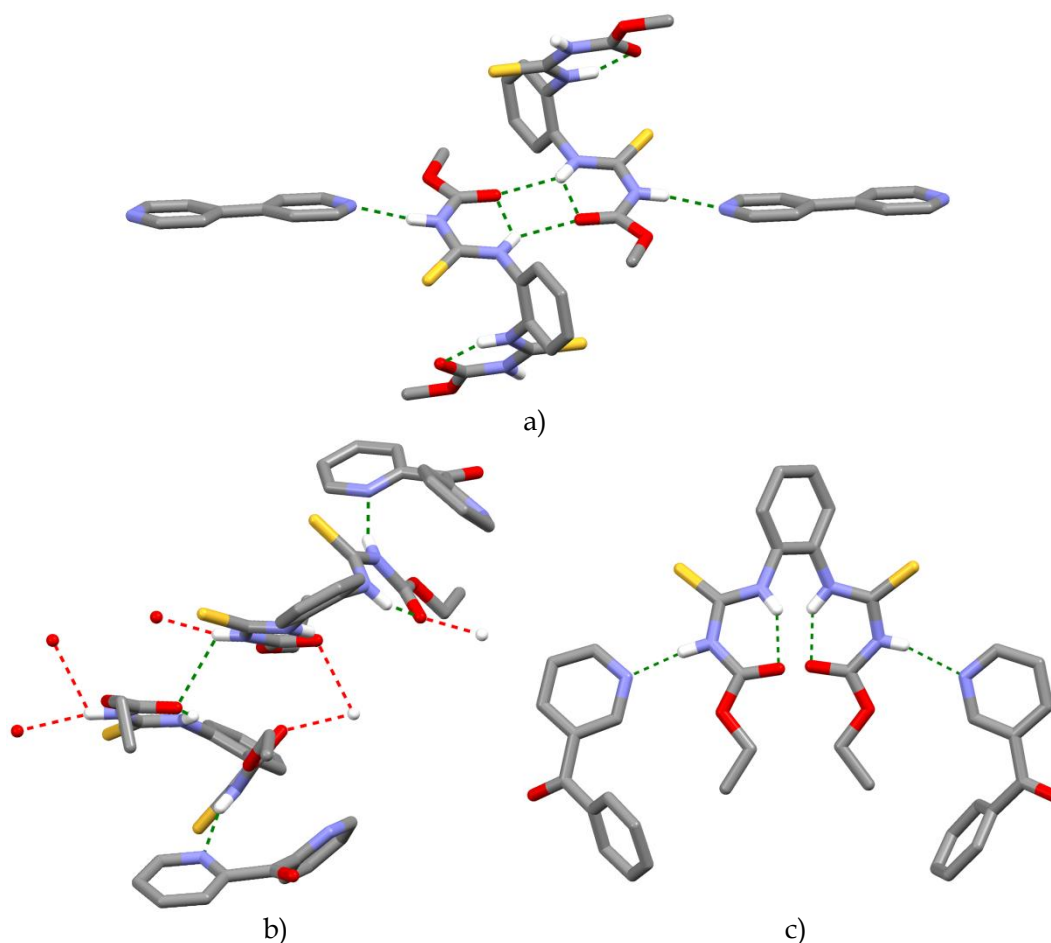
Figure 28. The basic units of the hydrogen bonded cocrystals: a) Pair formation in the TM cocrystal with 4,4-bipyridine, b) starting unit of the double chains in the TE cocrystal with di(2-pyridyl)ketone and c) discrete hydrogen bonded units in the TE cocrystal with 3-benzoylpyridine. Non-hydrogen bonding hydrogen atoms omitted for clarity.

The three non-hydrogen bonded cocrystals all make a different kind of structure. The TM cocrystal with 2,2′-bipyridine makes a clathrate-type structure where the TM molecules build a 2-dimensional framework in which one 2,2′-bipyridine molecule resides with the other 2,2′-bipyridine and the MeCN solvent molecules in between sheets made by the framework (Figure 29a). The TE cocrystal with 2,2′-bipyridine is isomorphic with the isomorphic solvates of TE, where the TE molecules build up hydrogen bonded chains with the N–H⋯S=C $R_2^2(8)$ hydrogen bonding motif and the coformer is located between the arms of the TE molecules (Figure 29b). On the other hand, the TE cocrystal with biphenyl, which has chains built with the same motif, is very similar to the benzene solvate of TM, in which the coformer is situated between the chains (Figure 29c).

a)

b)

c)
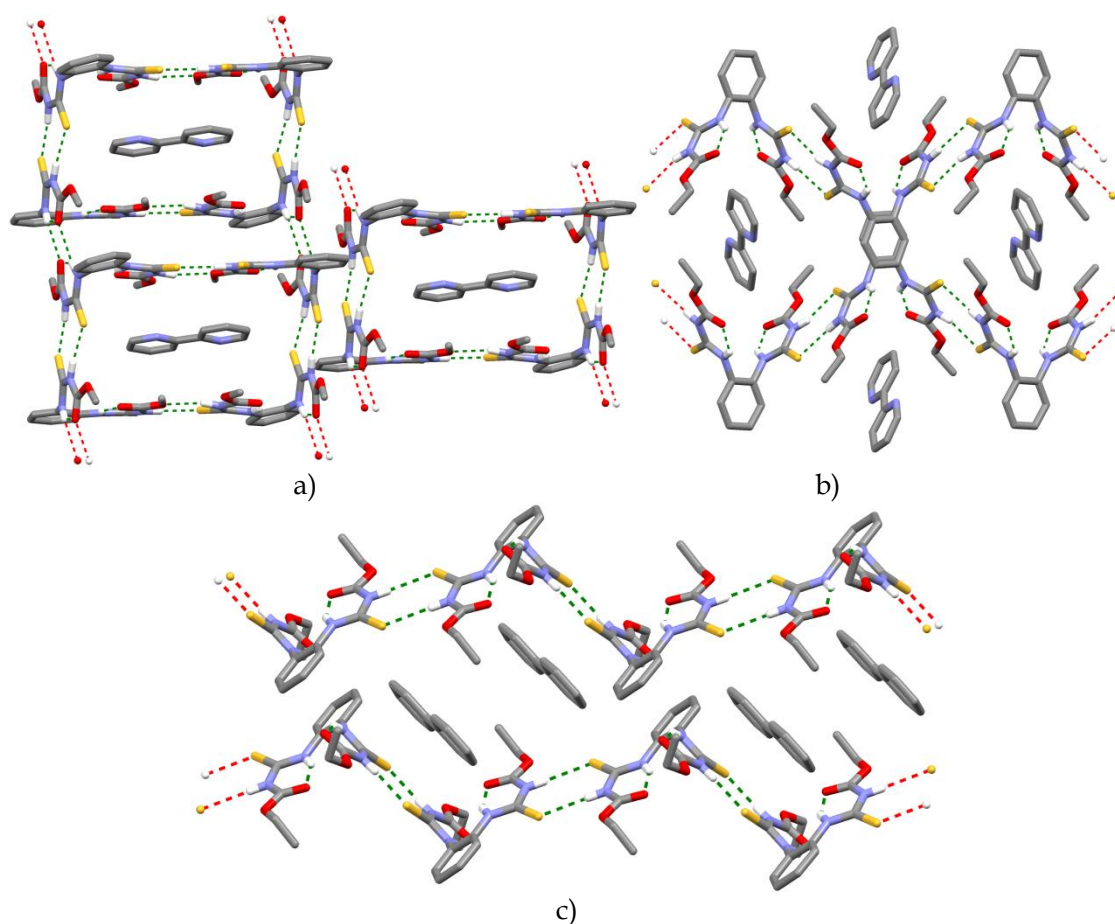
Figure 29. The basic packing of the non-hydrogen bonded cocrystals: a) clathrate framework in the TM cocrystal with 2,2′-bipyridine, and packing of chains in b) the TE cocrystal with 2,2′-bipyridine and c) the TE cocrystal with biphenyl. Non-hydrogen bonding hydrogen atoms omitted for clarity.

Cocrystals did not form with 2H-pyrido[3,2-b]-1,4-oxazin-3(4H)one and the nicotinic acids, which contain in themselves a strong hydrogen bond donor and likely form stronger hydrogen bonds with themselves. The nicotinic acids have the expected acid-pyridine hydrogen bonded synthon, which is stronger than a pyridine···H-N synthon, in their pure crystal structures.[155, 156] No crystal structure of 2H-pyrido[3,2-b]-1,4-oxazin-3(4H)one is available for comparison.

2.3.2 Agrochemical actives with 4-hydroxybenzoic acid[v]

Cocrystal screening for a number of active agrochemical ingredients (AI) was planned using a supramolecular synthon approach. The investigated AIs (pyraclostrobin, epoxiconazole, tebuconazole, boscalid, imazethapyr, imazamox and acetamiprid) (Scheme 6) contain a heterocyclic nitrogen so compounds with hydrogen bond donors capable of hydrogen bonding to the nitrogens were chosen as possible coformers.
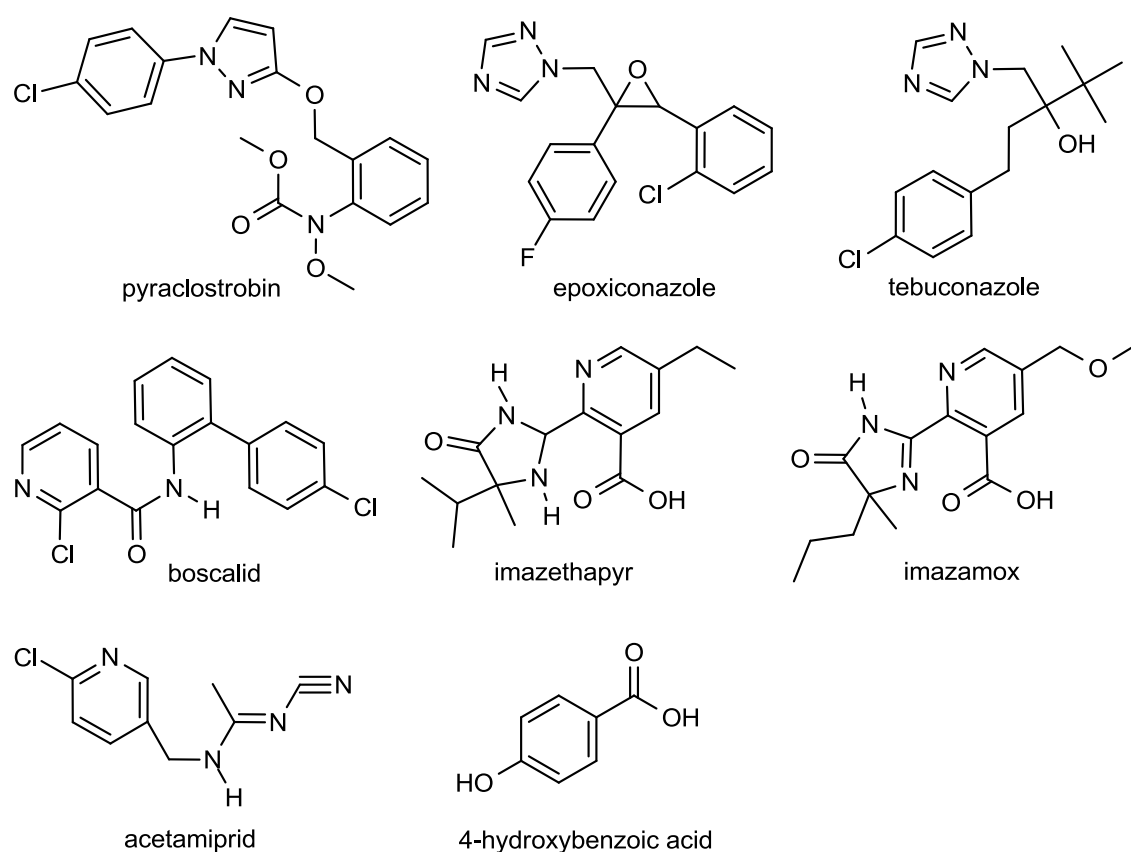
Scheme 6. Active agrochemical ingredients used in the cocrystal screening (pyraclostrobin, epoxiconazole, tebuconazole, boscalid, imazethapyr, imazamox, acetamiprid) and 4-hydroxybenzoic acid

Screening was conducted using liquid-assisted grinding (LAG) in a mechanical ball mill. Compounds were weighed in a 1:1 stoichiometric ratio and milled for 10–20 min at 20 Hz in a Retsch MM301 ball mill with a few drops of ethanol or water. The resulting powder samples were scraped from the milling vessels and a powder X-ray diffraction pattern was measured. In case of changes in the powder pattern of the sample, in comparison to the powder patterns of the pure compounds and their different crystal forms, evaporation crystallization experiments of the combinations were set up to acquire single crystals for structure determination. Cocrystals of 4-hydroxybenzoic acid with seven AIs were identified and the crystal structures of five of these solved by single crystal X-ray diffraction (Table 5). Due to IP reasons a detailed description and analysis of the crystal structures is not possible.

Table 5. Crystal structure parameters of the 4-hydroxybenzoic acid cocrystals with agrochemical actives.

	Pyraclostrobin	Epoxiconazole	Imazethapyr	Imazamox	Acetamiprid
Chemical formula	$C_{19}H_{18}ClN_3O_4$ $C_7H_6O_3$	$C_{17}H_{13}ClFN_3O$ $C_7H_6O_3$	$C_{15}H_{19}N_3O_3$ $C_7H_6O_3$	$C_{15}H_{19}N_3O_4$ $C_7H_6O_3$	$C_{10}H_{11}ClN_4$ $C_7H_6O_3$
M	525.94	467.88	427.45	443.45	360.80
Crystal system	Triclinic	Monoclinic	Monoclinic	Monoclinic	Triclinic
Space group	P-1	P2$_1$/c	P2$_1$/n	P2$_1$/n	P-1
a (Å)	8.200 (1)	18.640 (4)	6.7912 (3)	6.8988 (4)	5.9294 (3),
b (Å)	11.942 (2)	5.520 (2)	26.416 (1)	27.803 (1)	13.1194 (2)
c (Å)	13.626 (2)	23.622 (9)	12.1439 (6)	11.5194 (6)	22.4526 (11)
α (deg)	68.474 (5)	90	90	90	78.408 (2)
β (deg)	87.962 (6)	190.70 (2)	97.007 (2)	94.622 (2)	85.082 (1)
γ (deg)	80.097 (6)	90	90	90	81.015 (1)
V (Å^3)	1222.3 (2)	2111.2 (2)	2162.3 (2)	2202.4 (2)	1687.4
Z	2	4	4	4	4
ρcalc (g/cm3)	1.43	1.43	1.31	1.34	1.42
R	0.0359	0.0384	0.0657	0.1288	0.0961

The cocrystals show improved properties in comparison to the pure compounds. Melting points of the cocrystals and pure compounds were determined on a hot stage microscope under polarized light. The coformer, 4-hydroxy benzoic acid, has a melting point of 214–217 °C, which is higher than that of the agrochemical actives. All except the imazethapyr and imazamox cocrystals show an increased melting point (Table 6). For the pyraclostrobin and tebuconazole cocrystals, especially, the melting point increase is around 50 °C. A higher melting point is important in formulation processing and stability. Solubility analyses of the cocrystals were performed at room temperature by slurry equilibration experiments and analyzed by XRPD and HPLC. The imazethapyr and acetamiprid cocrystals show decreased solubility in water

with values of 480 mg/l versus 1030 mg/l for the imazethapyr cocrystal and 1890 mg/l versus 2750 mg/l for the acetamiprid cocrystal.

Table 6. Melting points (m.p.) of the pure agrochemical actives and the cocrystals

Compound	m.p. of pure compound (°C)	m.p. of cocrystal (°C)
pyraclostrobin	66	114–116
epoxiconazole	136	149–153
tebuconazole	96–104	148–149
boscalid	142–144	148–150
imazethapyr	169–173	153–159
imazamox	166	148–150
acetamiprid	99	124–127

3 SUMMARY AND CONCLUSIONS

In summary, the polymorph and cocrystal screening of two analogous fungicides, thiophanate-methyl and thiophanate-ethyl, and the cocrystal screening of seven other agrochemical actives with 4-hydroxybenzoic acid have been described. Altogether nineteen crystal structures of thiophanate-methyl including two polymorphs, fourteen solvates and three cocrystals, as well as seventeen crystal structures of thiophanate-ethyl including three polymorphs, seven solvates and seven cocrystals have been determined by single crystal X-ray diffraction. Some additional crystal forms were identified by way of powder X-ray diffraction and other methods. The large number of crystal structures enabled the identification of reliable hydrogen bond motifs that can also be used as supramolecular synthons in the design of new crystal forms. The cocrystal forms of agrochemical actives with 4-hydroxybenzoic acid, that show better properties in comparison to the pure forms, highlight the importance of cocrystallization in industrial applications.

As discussed in the review part of this thesis and supported by the results, cocrystal design with the supramolecular synthon approach is a reality. With adequate knowledge of the investigated molecules, cocrystals can reliably be designed. The applicability of the synthon approach and the understanding of intermolecular interactions can be thought of as improving with each new crystal structure deposited in the Cambridge structural database. Reliable ways to experimentally synthesize cocrystals through understanding of the factors behind the methods have also been recognized with liquid-assisted grinding in the forefront. Also with crystal structure determinations broadening from single crystals into powders and advances in structure prediction, the intermolecular interactions and packing in the crystalline products can be better investigated with a number of tools.

With constantly better understanding of the crystallization process and weak interactions the goal of crystal engineering - the design of new functional materials - is advancing. Crystal engineering is a prolific and collective

playground for structural and synthetic chemist, physicist, engineers, biologist and information technology specialists alike. This gives the chance for the continuation of the described research in any number of directions from structural studies of other agrochemical or pharmaceutical actives, or novel synthetic analogues of the thiophanates to more fundamental studies of the causes behind the crystallization of so many crystal forms. Many more cocrystals for the thiophanates could also be obtained by utilizing the synthons identified in the solvate structures.

REFERENCES

1. J. Bernstein, Polymorphism - A perspective, *Cryst. Growth Des.,* **2011,** *11,* 632-650.

2. J. Bernstein, *Polymorphism in Molecular Crystals,* Oxford University Press, United States, 2002, p. 352.

3. D. Braga, F. Grepioni, G.R. Desiraju, Crystal engineering and organometallic architecture, *Chem. Rev.,* **1998,** *98,* 1375-1406.

4. D. Braga, Crystal engineering, where from? where to? *Chem. Commun.,* **2003,** 2751-2754.

5. Ö. Almarsson, M.J. Zaworotko, Crystal engineering of the composition of pharmaceutical phases. Do pharmaceutical co-crystals represent a new path to improved medicines? *Chem. Commun.,* **2004,** *(17),* 1889-1896.

6. N. Blagden, M. de Matas, P.T. Gavan, P. York, Crystal engineering of active pharmaceutical ingredients to improve solubility and dissolution rates, *Adv. Drug Del. Rev.,* **2007,** *59,* 617-630.

7. M.B. Hickey, M.L. Peterson, L.A. Scoppettuolo, S.L. Morrisette, A. Vetter, H.R. Guzmán, J.F. Remenar, Z. Zhang, M.D. Tawa, S. Haley, M.J. Zaworotko, Ö. Almarsson, Performance comparison of a co-crystal of carbamazepine with marketed product, *Eur. J. Pharm. Biopharm.,* **2007,** *67,* 112-119.

8. D.J. Good, N. Rodríguez-Hornedo, Solubility advantage of pharmaceutical cocrystals, *Cryst. Growth Des.,* **2009,** *9,* 2252-2264.

9. W. Cabri, P. Ghetti, G. Pozzi, M. Alpegiani, Polymorphisms and patent, market, and legal battles: Cefdinir case study, *Org. Process Res. Dev.,* **2007,** *11,* 64-72.

10. A.V. Trask, An overview of pharmaceutical cocrystals as intellectual property, *Mol. Pharmaceutics,* **2007,** *4,* 301-309.

11. U.J. Griesser, The Importance of Solvates in R. Hilfiker (Ed.), *Polymorphism in the Pharmaceutical Industry,* WILEY-VCH Verlag GmbH & Co. KGaA, Weinheim, Germany, 2006, pp 211-234.

12. K.R. Seddon, Pseudopolymorph: A polemic, *Cryst. Growth Des.,* **2004,** *4,* 1087-1087.

13. G.R. Desiraju, Crystal and co-crystal. *CrystEngComm,* **2003,** *5,* 466-467.

14. J. Bernstein, ...And another comment on *Pseudo*polymorphism, *Cryst. Growth Des.,* **2005,** *5,* 1661-1662.

15. J.D. Dunitz, Crystal and co-crystal. A second opinion. *CrystEngComm,* **2003,** *5,* 506.

16. A.D. Bond, What is a co-crystal? *CrystEngComm*, **2007,** *9,* 833-834.

17. S.L. Childs, G.P. Stahly, A. Park, The salt-cocrystal continuum: The influence of crystal structure on ionization state, *Mol. Pharmaceutics,* **2007,** *4,* 323-338.

18. C.B. Aakeröy, M.E. Fasulo, J. Desper, Cocrystal or salt: Does it really matter? *Mol. Pharmaceutics,* **2007,** *4,* 317-322.

19. D. Braga, F. Grepioni, L. Maini, S. Prosperi, R. Gobetto, M.R. Chierotti, From unexpected reactions to a new family of ionic co-crystals: The case of barbituric acid with alkali bromides and caesium iodide, *Chem. Commun.,* **2010,** *46,* 7715-7717.

20. G.P. Stahly, A survey of cocrystals reported prior to 2000, *Cryst. Growth Des.,* **2009,** *9,* 4212-4229.

21. F. Wohler, Untersuchungen über des chinons, *Annalen Chem. Pharm.,* **1844,** *51,* 145-163.

22. H. Matsuda, K. Osaki, I. Nitta, Crystal structure of quinhydrone, $C_{12}H_{10}O_4$, *Bull. Chem. Soc. Jpn.,* **1958,** *31,* 611-620.

23. W.L. Bragg, The structure of some crystals as indicated by their diffraction of X-rays, *Proc. R. Soc. Lond.,* **1913,** *A89,* 248-277.

24. N. Qiao, M. Li, W. Schlindwein, N. Malek, A. Davies, G. Trappitt, Pharmaceutical cocrystals: An overview, *Int. J. Pharm.,* **2011,** *419,* 1-11.

25. N. Schultheiss, A. Newman, Pharmaceutical cocrystals and their physicochemical properties, *Cryst. Growth Des.,* **2009,** *9,* 2950-2967.

26. N. Shan, M.J. Zaworotko, The role of cocrystals in pharmaceutical science, *Drug Discov. Today,* **2008,** *13,* 440-446.

27. N. Blagden, D.J. Berry, A. Parkin, H. Javed, A. Ibrahim, P.T. Gavan, L.L. De Matos, C.C. Seaton, Current directions in co-crystal growth. *New J. Chem.,* **2008,** *32,* 1659-1672.

28. P. Vishweshwar, J.A. McMahon and M.J. Zaworotko, Crystal Engineering of Pharmaceutical Co-Crystals in E.R.T. Tiekink, J.J. Vittal (Eds.), *Frontiers in Crystal Engineering,* John Wiley & Sons Ltd, England, 2006, pp 25-49.

29. C.B. Aakeröy and N. Schultheiss, Assembly of Molecular Solids Via Non-Covalent Interactions in D. Braga, F. Grepioni (Eds.), *Making Crystals by Design,* Wiley-VCH Verlag GmbH & Co.KGaA, Germany, 2007, pp 209-240.

30. J.W. Steed and J.L. Atwood, *Supramolecular Chemistry,* 2, Wiley, United Kingdom, 2009, p. 970.

31. G.R. Desiraju, Supramolecular synthons in crystal engineering - A new organic synthesis, *Angew. Chem. Int. Ed. Eng.,* **1995,** *34,* 2311-2327.

32. G.R. Desiraju and T. Steiner, *The Weak Hydrogen Bond in Structural Chemistry and Biology,* Oxford University Press Inc., United States, 1999, p. 507.

33. P. Metrangolo, G. Resnati, Halogen bonding: A paradigm in supramolecular chemistry, *Chem. Eur. J.,* **2001,** *7,* 2511-2519.

34. K. Rissanen, Halogen bonded supramolecular complexes and networks, *CrystEngComm,* **2008,** *10,* 1107-1113.

35. M.C. Etter, Encoding and decoding hydrogen-bond patterns of organic compounds, *Acc. Chem. Res.,* **1990,** *23,* 120-126.

36. T.R. Shattock, K.K. Arora, P. Vishweshwar, M.J. Zaworotko, Hierarchy of supramolecular synthons: Persistent carboxylic acid - pyridine hydrogen bonds in cocrystals that also contain a hydroxyl moiety, *Cryst. Growth Des.,* **2008,** *8,* 4533-4545.

37. J.A. Bis, P. Vishweshwar, D. Weyna, M.J. Zaworotko, Hierarchy of supramolecular synthons: Persistent hydroxyl-pyridine hydrogen bonds in cocrystals that contain a cyano acceptor, *Mol. Pharmaceutics,* **2007,** *4,* 401-416.

38. F.H. Allen, The cambridge structural database: A quarter of a million crystal structures and rising, *Acta Cryst.,* **2002,** *B58,* 380-388.

39. J. Bernstein, J.J. Novoa, R. Boese, S.A. Cirkel, Design and preparation of co-crystals utilizing the R24(8) hydrogen-bonding motif. *Chem. Eur. J.,* **2010,** *16,* 9047-9055.

40. M.C. Etter, J.C. MacDonald, J. Bernstein, Graph-set analysis of hydrogen-bond patterns in organic crystals, *Acta Cryst.,* **1990,** *B46,* 256-262.

41. J. Bernstein, R.E. Davis, L. Shimoni, N. Chang, Patterns in hydrogen bonding: Functionality and graph set analysis in crystals, *Angew. Chem. Int. Ed. Eng.,* **1995,** *34,* 1555-1573.

42. H. Zhao, L. Sun, S.W. Ng, 2,6-bis(4-aminophenyl)benzo(1,2-d:5,4-d')dioxazole 1-methylpyrrolidin-2-one trisolvate, *Acta Cryst.,* **2005,** *E61,* o4158-o4159.

43. B.R. Sreekanth, P. Vishweshwar, K. Vyas, Supramolecular synthon polymorphism in 2:1 co-crystal of 4-hydroxybenzoic acid and 2,3,5,6-tetramethylpyrazine. *Chem. Commun.,* **2007,** 2375-2377.

44. A. Mukherjee, G.R. Desiraju, Synthon polymorphism and pseudopolymorphism in co-crystals. the 4,4'-bipyridine-4-hydroxybenzoic acid structural landscape, *Chem. Commun.,* **2011,** *47,* 4090-4092.

45. R.J. Davey, K. Allen, N. Blagden, W.I. Cross, H.F. Lieberman, M.J. Quayle, S. Righini, L. Seton, G.J.T. Tiddy, Crystal engineering - nucleation, the key step, *CrystEngComm,* **2002,** *4,* 257-264.

46. A.I. Kitaigorodskii, *Organic Chemical Crystallography,* Consultants Bureau, New York, 1961, p. 541.

47. C.C. Seaton, Creating carboxylic acid co-crystals: The application of Hammett substitution constants, *CrystEngComm,* **2011,** *13,* 6583-6592.

48. L.P. Hammett, The effect of structure upon the reactions of organic compounds. benzene derivatives, *J. Am. Chem. Soc.*, **1937,** *59,* 96-103.

49. C.C. Seaton, K. Chadwick, G. Sadiq, K. Guo, R.J. Davey, Designing Acid/Acid co-crystals through the application of hammett substituent constants, *Cryst. Growth Des.,* **2010,** *10,* 726-733.

50. K. Chadwick, G. Sadiq, R.J. Davey, C.C. Seaton, R.G. Pritchard, A. Parkin, Designing acid acid co-crystals - the use of hammett substitution constants, *Cryst. Growth Des.,* **2009,** *9,* 1278-1279.

51. S.L. Childs, N. Rodríguez-Hornedo, L.S. Reddy, A. Jayasankar, C. Maheshwari, L. McCausland, R. Shipplett, B.C. Stahly, Screening strategies based on solubility and solution composition generate pharmaceutically acceptable cocrystals of carbamazepine, *CrystEngComm,* **2008,** *10,* 856-864.

52. M. Majumder, G. Buckton, C. Rawlinson-Malone, A.C. Williams, M.J. Spillman, N. Shankland, K. Shankland, A carbamazepine-indomethacin (1 : 1) cocrystal produced by milling, *CrystEngComm,* **2011**, *13*, 6327-6328.

53. P. Vishweshwar, J.A. McMahon, M. Oliveira, M.L. Peterson, M.J. Zaworotko, The predictably elusive form II of aspirin, *J. Am. Chem. Soc.,* **2005,** *127,* 16802-16803.

54. S.G. Fleischman, S.S. Kuduva, J.A. McMahon, B. Moulton, R.D. Bailey Walsh, N. Rodríguez-Hornedo, M.J. Zaworotko, Crystal engineering of the composition of pharmaceutical phases: Multiple-component crystalline solids involving carbamazepine, *Cryst. Growth Des.,* **2003,** *3,* 909-919.

55. L. Fábián, Cambridge structural database analysis of molecular complementarity in cocrystals, *Cryst. Growth Des.,* **2009,** *9,* 1436-1443.

56. N. Shan, A.D. Bond, W. Jones, Crystal engineering using 4,4'-bipyridyl with di- and tricarboxylic acids, *Cryst. Eng.,* **2002,** *5,* 9-24.

57. E.S. Lavender, G. Ferguson, C. Glidewell, Self-assembled triple helices in the hydrogen-bonded structure of 2,2'-biphenol--4,4'-bipyridyl (1/1), *Acta Cryst.,* **1999,** *C55,* 430-432.

58. A.V. Trask, W.D.S. Motherwell, W. Jones, Pharmaceutical cocrystallization: Engineering a remedy for caffeine hydration, *Cryst. Growth Des.,* **2005,** *5,* 1013-1021.

59. D. Bučar, R.F. Henry, X. Lou, T.B. Borchardt, G.G.Z. Zhang, A "hidden" co-crystal of caffeine and adipic acid. *Chem. Commun.,* **2007,** 525-527.

60. D. Bučar, R.F. Henry, X. Lou, R.W. Duerst, T.B. Borchardt, L.R. MacGillivray, G.G.Z. Zhang, Co-crystals of caffeine and hydroxy-2-naphthoic acids: Unusual formation of the carboxylic acid dimer in the presence of a heterosynthon, *Mol. Pharmaceutics,* **2007,** *4,* 339-346.

61. D. Bučar, R. Henry, R. Duerst, X. Lou, L. MacGillivray, G. Zhang, A 1:1 cocrystal of caffeine and 2-hydroxy-1-naphthoic acid obtained *via* a slurry screening method, *J. Chem. Cryst.,* **2010,** *40,* 933-939.

62. B. Das, J.B. Baruah, Water bridged assembly and dimer formation in co-crystals of caffeine or theophylline with polycarboxylic acids, *Cryst. Growth Des.,* **2011,** *11,* 278-286.

63. T. Friščić, A.V. Trask, W.D.S. Motherwell, W. Jones, Guest-directed assembly of caffeine and succinic acid into topologically different heteromolecular host networks upon grinding, *Cryst. Growth Des.,* **2008,** *8,* 1605-1609.

64. D. Bučar, R.F. Henry, X. Lou, R.W. Duerst, L.R. MacGillivray, G.G.Z. Zhang, Cocrystals of caffeine and hydroxybenzoic acids composed of multiple supramolecular heterosynthons: Screening via solution-mediated phase transformation and structural characterization, *Cryst. Growth Des.,* **2009,** *9,* 1932-1943.

65. C.B. Aakeröy, J. Desper, M. Fasulo, I. Hussain, B. Levin, N. Schultheiss, Ten years of co-crystal synthesis; the good, the bad, and the ugly. *CrystEngComm,* **2008,** *10,* 1816-1821.

66. J.F. Remenar, S.L. Morissette, M.L. Peterson, B. Moulton, J.M. MacPhee, H.R. Guzmán, Ö. Almarsson, Crystal engineering of novel cocrystals of a triazole drug with 1,4-dicarboxylic acids, *J. Am. Chem. Soc.,* **2003,** *125,* 8456-8457.

67. A. Bak, A. Gore, E. Yanez, M. Stanton, S. Tufekcic, R. Syed, A. Akrami, M. Rose, S. Surapaneni, T. Bostick, A. King, S. Neervannan, D. Ostovic, A. Koparkar, The co-crystal approach to improve the exposure of a water-insoluble compound: AMG 517 sorbic acid co-crystal characterization and pharmacokinetics. *J. Pharm. Sci.,* **2008,** *97,* 3942-3956.

68. M.K. Stanton, A. Bak, Physicochemical properties of pharmaceutical co-crystals: A case study of ten AMG 517 co-crystals. *Cryst. Growth Des.,* **2008,** *8,* 3856-3862.

69. M.K. Stanton, S. Tufekcic, C. Morgan, A. Bak, Drug substance and former structure property relationships in 15 diverse pharmaceutical co-crystals. *Cryst. Growth Des.,* **2009,** *9,* 1344-1352.

70. M.K. Stanton, R.C. Kelly, A. Colletti, Y.-. Kiang, M. Langley, E.J. Munson, M.L. Peterson, J. Roberts, M. Wells, Improved pharmacokinetics of AMG 517 through co-crystallization part 1: Comparison of two acids with corresponding amide co-crystals. *J. Pharm. Sci.,* **2010,** *99,* 3769-3778.

71. M.L. Peterson, M.K. Stanton, R.C. Kelly, R. Staples, A. Cheng, Preparation, solid state characterization, and single crystal structure analysis of N-(4-(6-(4-(trifluoromethyl)phenyl)pyrimidin-4-yloxy)benzo[d]thiazol-2-yl)acetamide crystal forms, *CrystEngComm,* **2011,** *13,* 1170-1180.

72. M.K. Stanton, R.C. Kelly, A. Colletti, M. Langley, E.J. Munson, M.L. Peterson, J. Roberts, M. Wells, Improved pharmacokinetics of AMG 517 through co-crystallization part 2: Analysis of 12 carboxylic acid co-crystals, *J. Pharm. Sci.,* **2011,** *100,* 2734-2743.

73. N. Issa, P.G. Karamertzanis, G.W.A. Welch, S.L. Price, Can the formation of pharmaceutical cocrystals be computationally predicted? I. comparison of lattice energies, *Cryst. Growth Des.,* **2009,** *9,* 442-453.

74. P.G. Karamertzanis, A.V. Kazantsev, N. Issa, G.W.A. Welch, C.S. Adjiman, C.C. Pantelides, S.L. Price, Can the formation of pharmaceutical cocrystals be computationally predicted? 2. crystal structure prediction, *J. Chem. Theory Comput.,* **2009,** *5,* 1432-1448.

75. M.A. Mohammad, A. Alhalaweh, S.P. Velaga, Hansen solubility parameter as a tool to predict cocrystal formation, *Int. J. Pharm.,* **2011,** *407,* 63-71.

76. C.M. Hansen, The three-dimensional solubility parameter-key to paint component affinities: Solvents, plasticizers, polymers, and resins. II. dyes, emulsifiers, mutual solubility and compatibility, and pigments. III. independent calculation of the parameter components. *J. Paint Technol.,* **1967,** *39,* 505-510.

77. D. Musumeci, C.A. Hunter, R. Prohens, S. Scuderi, J.F. McCabe, Virtual cocrystal screening, *Chem. Sci.,* **2011,** *2,* 883-890.

78. T. Rager, R. Hilfiker, Stability domains of multi-component crystals in ternary phase diagrams, *Z. Phys. Chem.,* **2009,** *223,* 793-813.

79. R.A. Chiarella, R.J. Davey, M.L. Peterson, Making co-crystals-the utility of ternary phase diagrams, *Cryst. Growth Des.,* **2007,** *7,* 1223-1226.

80. K. Guo, G. Sadiq, C. Seaton, R. Davey, Q. Yin, Co-crystallization in the Caffeine/Maleic acid system: Lessons from phase equilibria, *Cryst. Growth Des.,* **2010,** *10,* 268-273.

81. K. Chadwick, R.J. Davey, G. Sadiq, W. Cross, R. Pritchard, The utility of a ternary phase diagram in the discovery of new co-crystal forms. *CrystEngComm,* **2009,** *11,* 412-414.

82. M.A. Oliveira, M.L. Peterson, R.J. Davey, Relative enthalpy of formation for co-crystals of small organic molecules, *Cryst. Growth Des.,* **2011,** *11,* 449-457.

83. A. Ainouz, J. Authelin, P. Billot, H. Lieberman, Modeling and prediction of cocrystal phase diagrams, *Int. J. Pharm.,* **2009,** *374,* 82-89.

84. S.J. Nehm, B. Rodríguez-Spong, N. Rodríguez-Hornedo, Phase solubility diagrams of cocrystals are explained by solubility product and solution complexation, *Cryst. Growth Des.,* **2006,** *6,* 592-600.

85. D.J. Good, N. Rodríguez-Hornedo, Cocrystal eutectic constants and prediction of solubility behavior, *Cryst. Growth Des.,* **2010,** *10,* 1028-1032.

86. E. Gagniere, D. Mangin, F. Puel, A. Rivoire, O. Monnier, E. Garcia, J.P. Klein, Formation of co-crystals: Kinetic and thermodynamic aspects. *J. Cryst. Growth,* **2009,** *311,* 2689-2695.

87. M. Habgood, M.A. Deij, J. Mazurek, S.L. Price, J.H. ter Horst, Carbamazepine co-crystallization with pyridine carboxamides: Rationalization by complementary phase diagrams and crystal energy landscapes, *Cryst. Growth Des.*, **2010,** *10,* 903-912.

88. T. Friščić, S.L. Childs, S.A.A. Rizvi, W. Jones, The role of solvent in mechanochemical and sonochemical cocrystal formation: A solubility-based approach for predicting cocrystallisation outcome, *CrystEngComm,* **2009,** *11,* 418-426.

89. S.L. Morissette, Ö. Almarsson, M.L. Peterson, J.F. Remenar, M.J. Read, A.V. Lemmo, S. Ellis, M.J. Cima, C.R. Gardner, High-throughput crystallization: Polymorphs, salts, co-crystals and solvates of pharmaceutical solids. *Adv. Drug Del. Rev.,* **2004,** *56,* 275-300.

90. T. Rager, R. Hilfiker, Cocrystal formation from solvent mixtures, *Cryst. Growth Des.,* **2010,** *10,* 3237-3241.

91. N. Rodríguez-Hornedo, S.J. Nehm, K.F. Seefeldt, Y. Pagan-Torres, C.J. Falkiewicz, Reaction crystallization of pharmaceutical molecular complexes, *Mol. Pharmaceutics,* **2006,** *3,* 362-367.

92. A.V. Trask, J. van de Streek, W.D.S. Motherwell, W. Jones, Achieving polymorphic and stoichiometric diversity in cocrystal formation: Importance of solid-state grinding, powder X-ray structure determination, and seeding, *Cryst. Growth Des.,* **2005,** *5,* 2233-2241.

93. S. Skovsgaard, A.D. Bond, Co-crystallisation of benzoic acid derivatives with N-containing bases in solution and by mechanical grinding: Stoichiometric variants, polymorphism and twinning. *CrystEngComm,* **2009,** *11,* 444-453.

94. L. Padrela, M.A. Rodrigues, S.P. Velaga, H.A. Matos, E.G. de Azevedo, Formation of indomethacin–saccharin cocrystals using supercritical fluid technology, *Eur. J. Pharm. Sci.,* **2009,** *38,* 9-17.

95. L. Padrela, M.A. Rodrigues, S.P. Velaga, A.C. Fernandes, H.A. Matos, E.G. de Azevedo, Screening for pharmaceutical cocrystals using the supercritical fluid enhanced atomization process, *J. Supercrit. Fluids,* **2010,** *53,* 156-164.

96. A. Alhalaweh, S.P. Velaga, Formation of cocrystals from stoichiometric solutions of incongruently saturating systems by spray drying, *Cryst. Growth Des.,* **2010,** *10,* 3302-3305.

97. G.G.Z. Zhang, R.F. Henry, T.B. Borchardt, X. Lou, Efficient co-crystal screening using solution-mediated phase transformation, *J. Pharm. Sci.,* **2007,** *96,* 990-995.

98. J.H.t. Horst, P.W. Cains, Co-crystal polymorphs from a solvent-mediated transformation, *Cryst. Growth Des.,* **2008,** *8,* 2537-2542.

99. N. Takata, K. Shiraki, R. Takano, Y. Hayashi, K. Terada, Cocrystal screening of stanolone and mestanolone using slurry crystallization, *Cryst. Growth Des.*, **2008,** *8,* 3032-3037.

100. T. Kojima, S. Tsutsumi, K. Yamamoto, Y. Ikeda, T. Moriwaki, High-throughput cocrystal slurry screening by use of in situ raman microscopy and multi-well plate, *Int. J. Pharm.*, **2010,** *399,* 52-59.

101. S. L. Childs, P. Mougin, B. Stahly, Screening for solid forms by ultrasound crystallization and cocrystallization using ultrasound, WO/2005/089375, 2005.

102. D. Bučar, L.R. MacGillivray, Preparation and reactivity of nanocrystalline cocrystals formed via sonocrystallization, *J. Am. Chem. Soc.*, **2007,** *129,* 32-33.

103. D. Braga, F. Grepioni, Solventless reactions: Reactions between or within molecular crystals. *Angew. Chem. Int. Ed.*, **2004,** *43,* 4002-4011.

104. A.V. Trask, W. Jones, Crystal engineering of organic cocrystals by the solid-state grinding approach; organic solid state reactions, *Top. Curr. Chem.*, **2005,** *254,* 41-70.

105. T. Friščić, W. Jones, Recent advances in understanding the mechanism of cocrystal formation via grinding, *Cryst. Growth Des.,* **2009,** *9,* 1621-1637.

106. N. Shan, F. Toda, W. Jones, Mechanochemistry and co-crystal formation: Effect of solvent on reaction kinetics. *Chem. Commun.*, **2002,** 2372-2373.

107. J.I. Arenas-García, D. Herrera-Ruiz, K. Mondragón-Vásquez, H. Morales-Rojas, H. Höpfl, Co-crystals of active pharmaceutical ingredients - acetazolamide, *Cryst. Growth Des.*, **2010,** *10,* 3732-3742.

108. S. Karki, T. Friščić, W. Jones, W.D.S. Motherwell, Screening for pharmaceutical cocrystal hydrates via neat and liquid-assisted grinding, *Mol. Pharmaceutics,* **2007,** *4,* 347-354.

109. D.R. Weyna, T. Shattock, P. Vishweshwar, M.J. Zaworotko, Synthesis and structural characterization of cocrystals and pharmaceutical cocrystals: Mechanochemistry vs slow evaporation from solution, *Cryst. Growth Des.,* **2009,** *9,* 1106-1123.

110. T. Friščić, A.V. Trask, W. Jones, W.D.S. Motherwell, Screening for inclusion compounds and systematic construction of three-component solids by liquid-assisted grinding, *Angew. Chem. Int. Ed.*, **2006,** *45,* 7546-7550.

111. A.V. Trask, W.D.S. Motherwell, W. Jones, Solvent-drop grinding: Green polymorph control of cocrystallisation, *Chem. Commun.*, **2004,** 890-891.

112. K. Chadwick, R.J. Davey, W. Cross, How does grinding produce co-crystals? insights from the case of benzophenone and diphenylamine, *CrystEngComm,* **2007,** *9,* 732-734.

113. A. Jayasankar, A. Somwangthanaroj, Z. Shao, N. Rodríguez-Hornedo, Cocrystal formation during cogrinding and storage is mediated by amorphous phase, *Pharm. Res.,* **2006,** *23,* 2381-2392.

114. S. Karki, T. Friščić, W. Jones, Control and interconversion of cocrystal stoichiometry in grinding: Stepwise mechanism for the formation of a hydrogen-bonded cocrystal, *CrystEngComm,* **2009,** *11,* 470-481.

115. J.A. Bis, P. Vishweshwar, R.A. Middleton, M.J. Zaworotko, Concomitant and conformational polymorphism, conformational isomorphism, and phase relationships in 4-cyanopyridine.4,4'-biphenol cocrystals. *Cryst. Growth Des.,* **2006,** *6,* 1048-1053.

116. C. Medina, D. Daurio, K. Nagapudi, F. Alvarez-Nunez, Manufacture of pharmaceutical co-crystals using twin screw extrusion: A solvent-less and scalable process. *J. Pharm. Sci.,* **2010,** *99,* 1693-1696.

117. D.J. Berry, C.C. Seaton, W. Clegg, R.W. Harrington, S.J. Coles, P.N. Horton, M.B. Hursthouse, R. Storey, W. Jones, T. Friščić, N. Blagden, Applying hot-stage microscopy to co-crystal screening: A study of nicotinamide with seven active pharmaceutical ingredients, *Cryst. Growth Des.,* **2008,** *8,* 1697-1712.

118. E. Lu, N. Rodríguez-Hornedo, R. Suryanarayanan, A rapid thermal method for cocrystal screening, *CrystEngComm,* **2008,** *10,* 665-668.

119. O. Lehmann, *Molecularphysik,* W. Engelmann, Leipzig, Germany, 1888, p. 852.

120. D. Braga, S. d'Agostino, E. Dichiarante, L. Maini, F. Grepioni, Dealing with crystal forms (the kingdom of serendip?), *Chem. Asian J.,* **2011,** *6,* 2214-2223.

121. D. Braga, S.L. Giaffreda, F. Grepioni, M.R. Chierotti, R. Gobetto, G. Palladino, M. Polito, Solvent effect in a "solvent free" reaction. *CrystEngComm,* **2007,** *9,* 879-881.

122. A. Jayasankar, D.J. Good, N. Rodríguez-Hornedo, Mechanisms by which moisture generates cocrystals, *Mol. Pharmaceutics,* **2007,** *4,* 360-372.

123. A.Y. Ibrahim, R.T. Forbes, N. Blagden, Spontaneous crystal growth of co-crystals: The contribution of particle size reduction and convection mixing of the co-formers, *CrystEngComm,* **2011,** *13,* 1141-1152.

124. C. Maheshwari, A. Jayasankar, N.A. Khan, G.E. Amidon, N. Rodríguez-Hornedo, Factors that influence the spontaneous formation of pharmaceutical cocrystals by simply mixing solid reactants, *CrystEngComm,* **2009,** *11,* 493-500.

125. W. Clegg, A.J. Blake, R.O. Gould, P. Main, *Crystal Structure Analysis Principles and Practice,* Oxford University press, Great Britain, 2001, p. 265.

126. W.I.F. David, K. Shankland, L.B. McCusker, C. Baerlocher, *Structure Determination from Powder Diffraction Data,* Oxford University press, Great Britain, 2002, p. 356.

127. A. Burger, R. Ramberger, On the polymorphism of pharmaceuticals and other molecular crystals. I, *Microchim. Acta,* **1979,** *72,* 259-271.

128. A. Burger, R. Ramberger, On the polymorphism of pharmaceuticals and other molecular crystals. II, *Microchim. Acta,* **1979,** *72,* 273-316.

129. C.P. Price, G.D. Glick, A.J. Matzger, Dissecting the behavior of a promiscuous solvate former, *Angew. Chem. Int. Ed.,* **2006,** *45,* 2062-2066.

130. M.A. Spackman, P.G. Byrom, A novel definition of a molecule in a crystal, *Chem. Phys. Lett.,* **1997,** *267,* 215-220.

131. M.A. Spackman, J.J. McKinnon, Fingerprinting intermolecular interactions in molecular crystals, *CrystEngComm,* **2002,** *4,* 378-392.

132. Z. Jane Li, W.H. Ojala, D.J.W. Grant, Molecular modeling study of chiral drug crystals: Lattice energy calculations, *J. Pharm. Sci.,* **2001,** *90,* 1523-1539.

133. A. Gavezzotti, Towards a realistic model for the quantitative evaluation of intermolecular potentials and for the rationalization of organic crystal structures. part I. philosophy, *CrystEngComm,* **2003,** *5,* 429-438.

134. S.L. Price, Computed crystal energy landscapes for understanding and predicting organic crystal structures and polymorphism, *Acc. Chem. Res.,* **2009,** *42,* 117-126.

135. T. Ikeda, K. Nagayoshi, K. Kitaura, Ab initio MO based lattice energy for molecular crystals: Packing structure of electron donor–acceptor (EDA) complex H3N–BF3, *Chem. Phys. Lett.,* **2003,** *370,* 218-226.

136. T. Beyer, S.L. Price, The errors in lattice energy minimisation studies: Sensitivity to experimental variations in the molecular structure of paracetamol, *CrystEngComm,* **2000,** *2,* 183-190.

137. A. Gavezzotti, Calculation of intermolecular interaction energies by direct numerical integration over electron densities. I. electrostatic and polarization energies in molecular crystals, *J. Phys. Chem. B,* **2002,** *106,* 4145-4154.

138. A. Gavezzotti, Calculation of intermolecular interaction energies by direct numerical integration over electron densities. 2. an improved polarization model and the evaluation of dispersion and repulsion energies, *J. Phys. Chem. B,* **2003,** *107,* 2344-2353.

139. K. Nagayoshi, K. Kitaura, S. Koseki, S. Re, K. Kobayashi, Y. Choe, S. Nagase, Calculation of packing structure of methanol solid using ab initio lattice energy at the MP2 level, *Chem. Phys. Lett.,* **2003,** *369,* 597-604.

140. A. Gavezzotti, Hierarchies of intermolecular potentials and forces: Progress towards a quantitative evaluation, *Struct. Chem.,* **2005,** *16,* 177-185.

141. A. Gavezzotti, Towards a realistic model for the quantitative evaluation of intermolecular potentials and for the rationalization of organic crystal

structures. part II. crystal energy landscapes, *CrystEngComm,* **2003,** *5,* 439-446.

142. A. Gavezzotti, Geometry and Energetics in D. Braga, F. Grepioni (Eds.), *Making Crystals by Design,* Wiley-VCH, Weinheim, Germany, 2007, pp 1-24.

143. T. Gelbrich, M.B. Hursthouse, A versatile procedure for the identification, description and quantification of structural similarity in molecular crystals, *CrystEngComm,* **2005,** *7,* 324-336.

144. M.B. Hursthouse, R. Montis, G.J. Tizzard, Intriguing relationships and associations in the crystal structures of a family of substituted aspirin molecules, *CrystEngComm,* **2010,** *12,* 953-959.

145. T. Gelbrich, M.B. Hursthouse, Systematic investigation of the relationships between 25 crystal structures containing the carbamazepine molecule or a close analogue: A case study of the XPac method, *CrystEngComm,* **2006,** *8,* 449-461.

146. G.M. Day, T.G. Cooper, A.J. Cruz-Cabeza, K.E. Hejczyk, H.L. Ammon, S.X.M. Boerrigter, J.S. Tan, R.G. Della Valle, E. Venuti, J. Jose, S.R. Gadre, G.R. Desiraju, T.S. Thakur, B.P. van Eijck, J.C. Facelli, V.E. Bazterra, M.B. Ferraro, D.W.M. Hofmann, M.A. Neumann, F.J.J. Leusen, J. Kendrick, S.L. Price, A.J. Misquitta, P.G. Karamertzanis, G.W.A. Welch, H.A. Scheraga, Y.A. Arnautova, M.U. Schmidt, J. van de Streek, A.K. Wolf, B. Schweizer, Significant progress in predicting the crystal structures of small organic molecules -- a report on the fourth blind test, *Acta Cryst.,* **2009,** *B65,* 107-125.

147. E. Nauha, M. Lahtinen, M. Nissinen, Structure refinement underway.

148. J.W. Steed, Should solid-state molecular packing have to obey the rules of crystallographic symmetry? *CrystEngComm,* **2003,** *5,* 169-179.

149. G.R. Desiraju, On the presence of multiple molecules in the crystal asymmetric unit (Z' > 1), *CrystEngComm,* **2007,** *9,* 91-92.

150. K.M. Anderson, J.W. Steed, Comment on "on the presence of multiple molecules in the crystal asymmetric unit (Z' > 1)" by Gautam R. Desiraju, CrystEngComm, 2007, 9, 91, *CrystEngComm,* **2007,** *9,* 328-330.

151. K.M. Anderson, M.R. Probert, C.N. Whiteley, A.M. Rowland, A.E. Goeta, J.W. Steed, Designing co-crystals of pharmaceutically relevant compounds that crystallize with Z' > 1. *Cryst. Growth Des.,* **2009,** *9,* 1082-1087.

152. K.M. Anderson, M.R. Probert, A.E. Goeta, J.W. Steed, Size does matter - the contribution of molecular volume, shape and flexibility to the formation of co-crystals and structures with Z' > 1, *CrystEngComm,* **2011,** *13,* 83-87.

153. J. Bernstein, J.D. Dunitz, A. Gavezzotti, Polymorphic perversity: Crystal structures with many symmetry-independent molecules in the unit cell, *Cryst. Growth Des.,* **2008,** *8,* 2011-2018.

154. C.B. Aakeröy, A.M. Beatty, B.A. Helfrich, M. Nieuwenhuyzen, Do polymorphic compounds make good cocrystallizing agents? A structural case study that demonstrates the importance of synthon flexibility. *Cryst. Growth Des.,* **2003,** *3,* 159-165.

155. F. Takusagawa, A. Shimada, Isonicotinic acid, *Acta Cryst.,* **1976,** *B32,* 1925-1927.

156. A. Kutoglu, C. Scheringer, Nicotinic acid, $C_6H_5N_2$: Refinement, *Acta Cryst.,* **1983,** *C39,* 232-234.
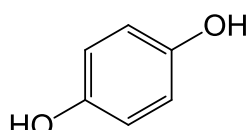
APPENDIX
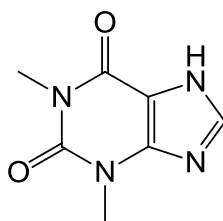
Molecular structures of compounds mentioned in the text.
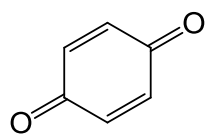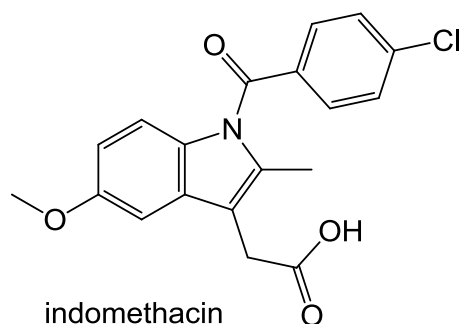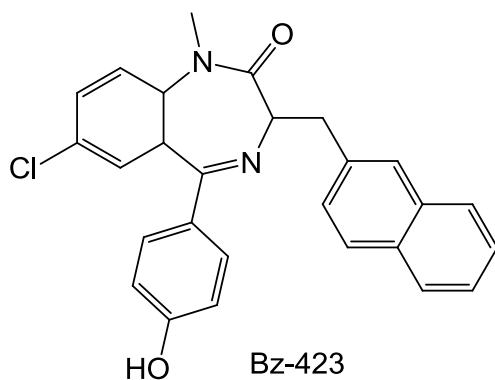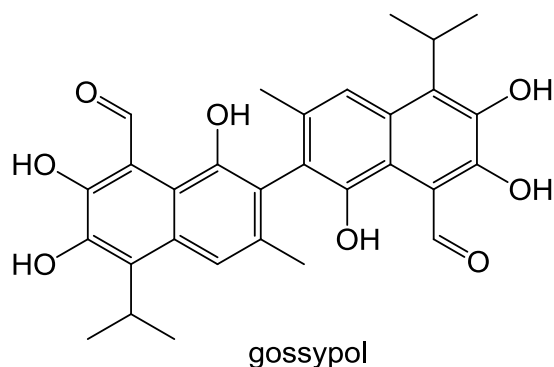

quinone
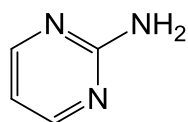
2-aminopyrimidine

hydroquinone

theophylline

indomethacin

Bz-423

gossypol

ORIGINAL PAPERS

I

Polymorphism and versatile solvate formation of thiophanate-methyl

by

E. Nauha, H. Saxell, M. Nissinen, E. Kolehmainen, A. Schäfer, & R. Schlecker, 2009

Polymorphism and versatile solvate formation of thiophanate-methyl†

Elisa Nauha,[a] Heidi Saxell,*[b] Maija Nissinen,[a] Erkki Kolehmainen,[a] Ansgar Schäfer[b] and Rainer Schlecker[b]

The polymorphism of a fungicide, thiophanate-methyl (TM), was investigated with conventional solvent screening methods. Two polymorphs, the thermodynamically most stable form I and the less stable form II, were found. TM was also found to crystallize as a plethora of different solvates which produced mostly form II upon desolvation. The structures of form I and form II and the fourteen discovered solvates were solved by single crystal X-ray diffraction. The most stable forms were further characterized by powder diffraction, thermoanalytical (TG/DTA, DSC and thermomicroscopy) and spectroscopic (IR, Raman, ¹³C CP/MAS NMR) methods.

Introduction

The growing field of crystal engineering deals with designing and synthesizing molecular solid state structures with desired properties.[1] One approach to the subject is using supramolecular synthons[2] composed of molecular fragments and the interactions between them to approximate the possible structural outcome of a crystal.

Polymorphism,[3] the ability of a compound to crystallize in more than one distinct crystal form, can be seen as a challenge in crystal engineering, but also as a means to investigate the principles of crystal formation as nature does it. In addition to polymorphs, a number of solvate forms with solvent molecules included in the crystal lattice are commonly formed with the solvent of crystallization.[4] These can further complicate the crystallization of compounds, but can also resolve some unanswered questions and be, for instance, the route to other crystal forms, not easily reached otherwise.[5] The solvent molecules in the crystal structure may either be included to decrease void space in the crystal or be, for example, hydrogen bonded to the molecules of the compound to better satisfy the possible intermolecular interactions.[6] The occurrence of polymorphs and solvates is especially high amongst molecules with flexible torsions and several low energy conformers.[7]

The literature reflects the importance of polymorphism in pharmaceutical substances.[3] The basic questions in agrochemical agents[8] are essentially the same; how many forms can be found and what are the properties and thermodynamical relationships of the forms.

We carried out a conventional solvent screening investigating the polymorphism of a pesticide active, thiophanate-methyl
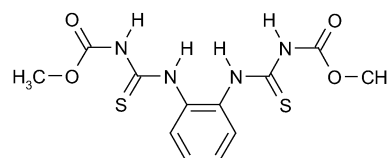
Scheme 1 The molecular structure of TM.

(TM) (Scheme 1), dimethyl 4,4′-(o-phenylene)bis(3-thio-allophanate), which is relatively flexible and capable of forming multiple hydrogen bonds as well as aromatic interactions. The motivation was to investigate whether the variation in melting points reported in the literature (135–200 °C[9]) is due to the existence of different polymorphs of TM, and on the other hand whether these forms exhibit varying hydrogen bonding arrangements. Recently, multi-component crystals, co-crystals, of TM have been reported with different agrochemical agents.[10]

TM is a fungicide and wound protectant and has been used, for example, in protecting citrus fruits against post-harvest decay in packing houses.[11] TM belongs to a group of fungicides that transform into benzimidazoles during use with TM specifically transforming into carbendazim.[11,12] Benzimidazoles work by impairing microtubule growth in fungal cells, which consequently prevents correct cell division, as microtubules are needed in forming the spindle that guides the movement of chromosomes during cell division.[13]

Experimental

Materials

TM of 99.8% purity from BASF, distilled water and solvents of analytical purity (min 99%) were used in the crystallization experiments.

Crystallizations

The used solvents included water, acetone, acetonitrile (MeCN), THF, methanol (MeOH), ethanol (EtOH), chloroform, dichloromethane (DCM), 1,2-dichloroethane (1,2-DCE), dioxane, pyridine, 1,2-dichlorobenzene (1,2-DCB), benzene, cyclohexanone, DMSO, dimethylacetamide (DMA), methyl

[a]*Department of Chemistry, Nanoscience Center, University of Jyväskylä, P.O. Box 35, FIN-40014, Finland. E-mail: maija.j.nissinen@jyu.fi; Fax: +358 14 260 4756; Tel: +358 14 260 4242*

[b]*BASF SE, GVC - A030, D-67056 Ludwigshafen, Germany. E-mail: heidi.saxell@basf.com; Fax: +49 621 60-20440; Tel: +49 621 60-49558*

† Electronic supplementary information (ESI) available: DSC and TGA/DTA curves, hydrogen bonding parameters, temperature variable CP/MAS NMR, calculated PXRDs and additional structural pictures. CCDC reference numbers 724460–724475. For ESI and crystallographic data in CIF or other electronic format see DOI: 10.1039/b905511h

isobutyl ketone and 1,2-propanediol. Amounts of 0.5 to 1.0 g of TM were dissolved in 15 to 100 ml of solvent with the help of an ultrasonic water bath (~40 °C). If the entire sample did not dissolve, solutions were filtered through a Witeg Por.2 glass filter. The solutions were allowed to evaporate at RT until crystals formed. The crystallizations from acetonitrile, DMA and methyl isobutyl ketone produced form I, while all other crystallizations produced solvates. Form II was acquired by fast crystallization from acetone under reduced pressure and a single crystal was acquired from a 1:1 mixture of acetonitrile and water. Slow cooling crystallizations produced the same results.

Thermomicroscopy

The behavior of crystals during heating was studied under polarized light with a Mettler FP82HT hot stage connected to a Mettler FP90 central processor with an Olympus BH-2 microscope. The primary heating rate used was 10 °C min^{-1} from 30 °C to melting/decomposition of the sample at around 170 °C.

TG/DTA

Thermogravimetric/differential thermal analyses were carried out with a Mettler Toledo TGA/SDTA 851 using Al_2O_3 as reference. The samples (8–22 mg) were placed in platinum sample pans for measurement with a temperature program from 30 to 605 °C at 10 °C min^{-1} and N_2 gas flow.

DSC

Differential scanning calorimetric determinations were made on a Mettler Toledo DSC 823e with TS0801RO Sample Robot and TS08006C1 Gas Control. The measurements of form I and form II were done with three different heating rates (5, 10 and 20 °C min^{-1}) from 30 to 185 °C using aluminum crucibles with pinholes.

Single crystal X-ray diffraction

X-Ray diffraction data were collected using graphite-monochromated Cu Kα radiation (λ = 1.54178 Å). The data for TM form I, the methanol, ethanol, DCM, 1,2-DCE, cyclohexanone, DMSO, THF, dioxane, pyridine, 1,2-DCB and benzene solvates were collected at 103 K on a Bruker AXS CCD Detector. The data for TM form II, the chloroform and acetone solvate and the acetonitrile solvate monohydrate were collected with a Nonius Kappa CCD diffractometer with Apex II detector at 173 K. The structures were solved with direct methods, refined, and expanded by using Fourier techniques with the SHELX-97 software package.[14] Absorption correction was performed with SADABS[15] or Denzo-SMN v0.97.638.[16] Hydrogen atoms were placed in idealized positions (C–H hydrogens) or found from the electron density map (most N–H hydrogens) and included in structure factor calculations. The N–H distances of the hydrogen bonding hydrogens were restrained to 0.91 Å to give the best fit to the X-ray data and to ensure stable refinement. The WinGX program system[17] and the Shelxtl program package[18] were used. Residual electron density in the DMSO solvate that could be assigned to severely disordered DMSO molecules was removed with the program SQUEEZE.[19] The quality of the ethanol

Table 1 Crystal data and collection parameters for form I and form II

	Form I	Form II
Formula	$C_{12}H_{14}N_4O_4S_2$	$C_{12}H_{14}N_4O_4S_2$
M	342.39	342.39
Crystal system	Monoclinic	Monoclinic
Space group	P21/c	P21/c
a/Å	10.7149(5)	8.946(2)
b/Å	11.8405(5)	20.052(4)
c/Å	15.6861(6)	8.998(2)
β/°	132.593(2)	107.51(3)
V/Å^3	1465.1(2)	1539.3(5)
Z	4	4
ρ_{calc}/g cm^{-3}	1.552	1.477
Meas. reflns	9507	4338
Indep. reflns	1744	2653
R_{int}	0.0572	0.0449
R_1 [$I > 2\sigma(I)$]	0.0402	0.0424
wR_2 [$I > 2\sigma(I)$]	0.1128	0.1119
GooF	1.187	1.055

solvate structure solution is poor and thus only preliminary data are given. The methanol in the methanol solvate is disordered over two positions and could only be refined isotropically without hydrogen atoms. The poor quality of several of the structures is due to insufficient data collection as the structures were measured for industrial purposes. Pictures of the structures were drawn with Mercury.[20] Crystal data and collection parameters of the structures are presented in Tables 1 and 2.

PXRD

Powder X-ray diffraction patterns were measured with a Siemens D5000 X-ray diffractometer with a Cu anode (λ = 1.5406 Å; 45 kV, 25 mA). The measurement temperature was 25 °C (RT) and a 2θ-angle range of 5–35° and a step resolution of 0.020° was used with a step time of 4.5 s.

^{13}C CP/MAS NMR

The ^{13}C CP/MAS NMR spectra were measured with a Bruker Avance 400 FT NMR spectrometer with a dual 4 mm CP/MAS probehead. The sample was packed in a 4 mm diameter ZrO_2 rotor, which was spun at 10 KHz rate at 296 or 373 K. Contact time for CP was 4 ms, pulse interval 4 s, time domain 2 K, which was zero filled to 8 K in frequency domain. Exponential window function with 5 Hz line broadening was used. 20 000 scans were acquired.

IR and Raman spectroscopy

The IR spectra were measured from KBr tablets on a Thermo Nicolet Nexus 470 IR spectrometer with a DTGS KBr detector. The Raman spectra were measured with a Nicolet 950 FT-Raman spectrometer.

Isothermal microcalorimetry

The dissolution energy of form I and form II was measured on a Thermometric Precision Solution Calorimeter at 25 °C with 100 ml of DMSO and 200 mg of TM.

Table 2 Crystal data and collection parameters for the solvate crystal forms of TM

	MeCN/H$_2$O[a]	DCM	1,2-DCE	Methanol[a]	Ethanol[b]	Acetone	Cyclohexanone
Formula	3C$_{12}$H$_{14}$N$_4$O$_4$S$_2$· 2.5C$_2$H$_3$N·H$_2$O	C$_{12}$H$_{14}$N$_4$O$_4$S$_2$· CH$_2$Cl$_2$	C$_{12}$H$_{14}$N$_4$O$_4$S$_2$· C$_2$H$_4$Cl$_2$	2C$_{12}$H$_{14}$N$_4$O$_4$S$_2$· CH$_3$OH	2C$_{12}$H$_{14}$N$_4$O$_4$S$_2$· CH$_3$CH$_2$OH	2C$_{12}$H$_{14}$N$_4$O$_4$S$_2$· (CH$_3$)$_2$CO	2C$_{12}$H$_{14}$N$_4$O$_4$S$_2$· C$_6$H$_{10}$O
M	1147.83	427.32	441.34	716.83	730.85	742.86	782.92
Crystal system	Triclinic	Triclinic	Triclinic	Triclinic	Triclinic	Triclinic	Triclinic
Space group	P-1	P-1	P-1	P-1	P-1	P-1	P-1
a/Å	10.641(2)	9.313(6)	9.313(2)	10.016(3)	9.842(2)	10.206(2)	11.277(3)
b/Å	13.751(3)	10.145(6)	10.150(2)	11.430(3)	11.370(2)	11.153(2)	17.368(4)
c/Å	20.181(4)	10.777(7)	10.735(2)	15.904(5)	15.988(3)	17.062(3)	19.902(5)
α/°	74.62(3)	83.04(4)	82.06(2)	101.73(1)	78.99(1)	76.69(3)	92.21(2)
β/°	85.49(3)	80.00(4)	79.40(2)	90.33(1)	89.34(1)	86.07(3)	103.76(2)
γ/°	77.97(3)	80.12(4)	79.41(2)	107.692(9)	72.15(2)	72.46(3)	100.77(1)
V/Å^3	2784(1)	984(2)	974.7(4)	1694.0(9)	1669.5(5)	1802.0(6)	3705(2)
Z	2	2	2	2	2	2	4
ρ_{calc}/g cm^{-3}	1.369	1.443	1.504	1.405	1.454	1.369	1.404
Meas. reflns	12985	3274	8006	7891	9780	8844	28524
Indep. reflns	9441	1992	2410	3543	3869	6210	9162
R_{int}	0.0832	0.0490	0.0450	0.0606	0.0660	0.1118	0.0473
R_1 [$I > 2\sigma(I)$]	0.0719	0.0680	0.0358	0.0726	0.1717	0.0487	0.0411
wR_2 [$I > 2\sigma(I)$]	0.1748	0.1767	0.0910	0.1975	0.4942	0.1271	0.0938
GooF	1.062	1.037	1.059	1.104	2.166	1.022	1.038

	DMSO[c]	Chloroform	THF	Dioxane	Pyridine	1,2-DCB	Benzene
Formula	C$_{12}$H$_{14}$N$_4$O$_4$S$_2$· (CH$_3$)$_2$SO	C$_{12}$H$_{14}$N$_4$O$_4$S$_2$· CHCl$_3$	C$_{12}$H$_{14}$N$_4$O$_4$S$_2$· C$_4$H$_8$O	C$_{12}$H$_{14}$N$_4$O$_4$S$_2$· C$_4$H$_8$O$_2$	C$_{12}$H$_{14}$N$_4$O$_4$S$_2$· C$_5$H$_5$N	C$_{12}$H$_{14}$N$_4$O$_4$S$_2$· C$_6$H$_4$Cl$_2$	C$_{12}$H$_{14}$N$_4$O$_4$S$_2$· C$_6$H$_6$
M	420.52	461.76	414.52	430.50	421.49	489.38	420.50
Crystal system	Monoclinic	Triclinic	Triclinic	Monoclinic	Triclinic	Triclinic	Triclinic
Space group	$C2/c$	P-1	P-1	$C2/c$	P-1	P-1	P-1
a/Å	26.52(2)	10.626(2)	10.546(2)	21.97(1)	8.244(1)	7.9951(7)	8.4106(8)
b/Å	10.321(5)	14.706(3)	14.470(3)	11.428(5)	10.690(2)	9.5484(9)	9.9524(9)
c/Å	17.43(1)	14.739(3)	14.592(2)	17.147(7)	12.493(2)	14.702(2)	12.952(2)
α/°	90	63.51(3)	65.317(8)	90	67.892(5)	81.910(4)	107.946(4)
β/°	94.66(3)	77.34(3)	77.66(1)	111.24(2)	81.442(6)	84.862(4)	101.732(5)
γ/°	90	74.82(3)	76.29(1)	90	74.153(5)	73.646(4)	96.983(4)
V/Å^3	4755(5)	1975.6(7)	1948.8(6)	4014(3)	979.9(2)	1064.7(2)	991.0(2)
Z	8	4	4	8	2	2	2
ρ_{calc}/g cm^{-3}	1.175	1.552	1.4013	1.425	1.429	1.526	1.409
Meas. reflns	12637	10630	9286	7583	7870	7159	8528
Indep. reflns	3184	6828	4514	2484	2437	2645	2494
R_{int}	0.1367	0.0679	0.0407	0.0475	0.0321	0.0323	0.0313
R_1 [$I > 2\sigma(I)$]	0.0899	0.0557	0.0526	0.0679	0.0434	0.0459	0.0373
wR_2 [$I > 2\sigma(I)$]	0.2145	0.1358	0.1494	0.1866	0.1082	0.1127	0.0889
GooF	0.988	1.027	1.123	1.079	1.167	1.201	1.106

[a] The H$_2$O/MeOH hydrogen atoms could not be accurately placed. [b] Preliminary data. [c] Due to the removal of a disordered DMSO molecule by Squeeze[17] the chemical formula, molecular weight and density are not accurate.

Calculation of gasphase conformers

The conformer screening was performed by a hierarchical procedure. First all possible combinations of dihedral angles were generated to define a first set of 2916 structures. For these structures molecular energies were calculated using the Dreiding force field[21] in combination with the charge equilibration method[22] (charges determined for the initial starting structure were kept fixed). All structures within the first 10 000 kcal mol^{-1} were extracted and checked for redundancies, which resulted in an intermediate set of 1716 structures. This first part was carried out with tools in the Cerius^2 program.[23] For the intermediate set of structures geometry optimizations were performed on the density functional theory level using the B-P functional[24] and TZVP basis sets[25] in the RI approximation.[26] After removal of redundant structures, 215 distinct conformers were left, which were verified as energy minima by analytical second derivatives of the energy with respect to nuclear positions. The final ranking of conformers was done based on second-order Møller–Plesset perturbation theory (MP2) energy calculations in the RI approximation[27] using TZVPP basis sets.[28] The DFT and MP2 calculations were done with the Turbomole program package.[29]

Results and discussion

Polymorphs

Two polymorphs of TM were found and characterized. Form I, of which the original commercially available sample was composed of, crystallized from acetonitrile solution (also from DMA, methyl isobutyl ketone and 1,2-propanediol solutions) and form II, or a mixture of form I and form II, was acquired mostly by desolvation of the found solvates. Pure powdered samples of form II were obtained by reduced pressure evaporation from warm acetone solutions of TM followed by heating at 80 °C in a vacuum oven for one hour. Form II was also found to crystallize from acetonitrile:water (1 : 1, v : v) solution, though not consistently. The next paragraphs describe the crystal structures of both polymorphs. The differences in the conformations of TM are discussed later in the chapter "conformations".

Crystal structure of form I

Block crystals of form I crystallized from acetonitrile solution in the monoclinic space group $P2_1/c$ with one TM molecule in the asymmetric unit (Fig. 1a). In the crystal structure one molecule of TM is hydrogen bonded with 8 hydrogen bonds in all to three adjacent molecules of TM. In addition, there are three intramolecular hydrogen bonds of which one (N–H···S=C bond) joins the two arms, i.e. the two functional groups on the benzene ring of the molecule, and the other two (N–H···O=C bonds) are within the arms (Fig. 1c).

Two types of intermolecular hydrogen bond arrangements are found in the structure (bonding parameters in ESI). The first is composed of one N–H···O=C bond and one N–H···O–C hydrogen bond and causes infinite chains of TM (the top three TM molecules in Fig. 1c). These chains are then connected by hydrogen bonds to parallel chains with a hand-in-hand arrangement that binds a pair of molecules together. This pairing arrangement (the bottom and central molecule in Fig. 1c)

consists of intra- and intermolecular bifurcated N–H···S=C and N–H···O=C hydrogen bonds. With this arrangement, every other molecule in the infinite chains is connected to one adjacent chain and every other molecule to another adjacent chain. The framework of connected chains produces infinite 2-D sheets (Fig. 1e). Aromatic and methyl groups point outward from the sheets making hydrophobic layers that facilitate the stacking of the sheets.

Crystal structure of form II

Block crystals of form II were found to crystallize from a acetonitrile : water (1 : 1) solution in the monoclinic space group $P2_1/c$ with one molecule of TM in the asymmetric unit (Fig. 1b). In this structure one TM molecule is hydrogen bonded with 8 hydrogen bonds in all to four adjacent TM molecules (Fig. 1d). There is also intramolecular N–H···O=C hydrogen bonding within the arms of the molecule.

The TM molecules are connected with two different hydrogen bonding arrangements – one with two N–H···S=C and one with two N–H···O=C hydrogen bonds. These arrangements produce infinite two dimensional sheets of TM molecules (Fig. 1f) that then stack up on each other like those in form I with hydrophobic interactions between the methyl and benzene groups.

Further characterization

The polymorphs were also characterized with PXRD, DSC, TG/DTA, thermomicroscopy, CP/MAS NMR, IR and Raman methods. In the DSCs (ESI†) of both forms decomposition started at around 165 °C with peak maxima at 174.2 and 175.9 °C for form I and form II, respectively. In the DSC of form I there is additionally a very small endothermic peak at around 115 °C, which showed up at all heating rates and is possibly explained by impurities as at that temperature there is no change observed with the thermomicroscope with which form I and form II could not be distinguished. The TG/DTA (ESI†) curves of the two polymorphs were also practically indistinguishable.

The PXRD patterns (Fig. 2a) of the two polymorphs can be clearly distinguished. PXRD patterns were thus used for form identification in further experiments. (Comparisons between experimental and calculated PXRD patterns in ESI).

Forms I and II can also be distinguished from their ^{13}C CP/MAS NMR spectra (Fig. 2b). The methyl group peaks are at 55.1 ppm for form I and 52.2 ppm for form II with a small peak at 55.0 ppm, indicating that the methyl groups are in somewhat different environments in the two forms. The peaks of the ester carbon atoms are at 153.2 and 153.1 ppm for form I and form II, respectively, and thus are in very similar environments. The benzene carbon peaks are different for the two forms and point to 3 types of environments for form I and two types of environments for form II. By comparing the chemical shifts of the corresponding C=S carbon atoms, it can be concluded that the C=S carbons with peaks at around 180 ppm are in more similar surroundings in form II than in form I since the peak separation is bigger in the spectrum of form I. From the crystal structures one can see the reason for this as in form I only one sulfur seems to be involved in hydrogen bonding and in form II both sulfurs
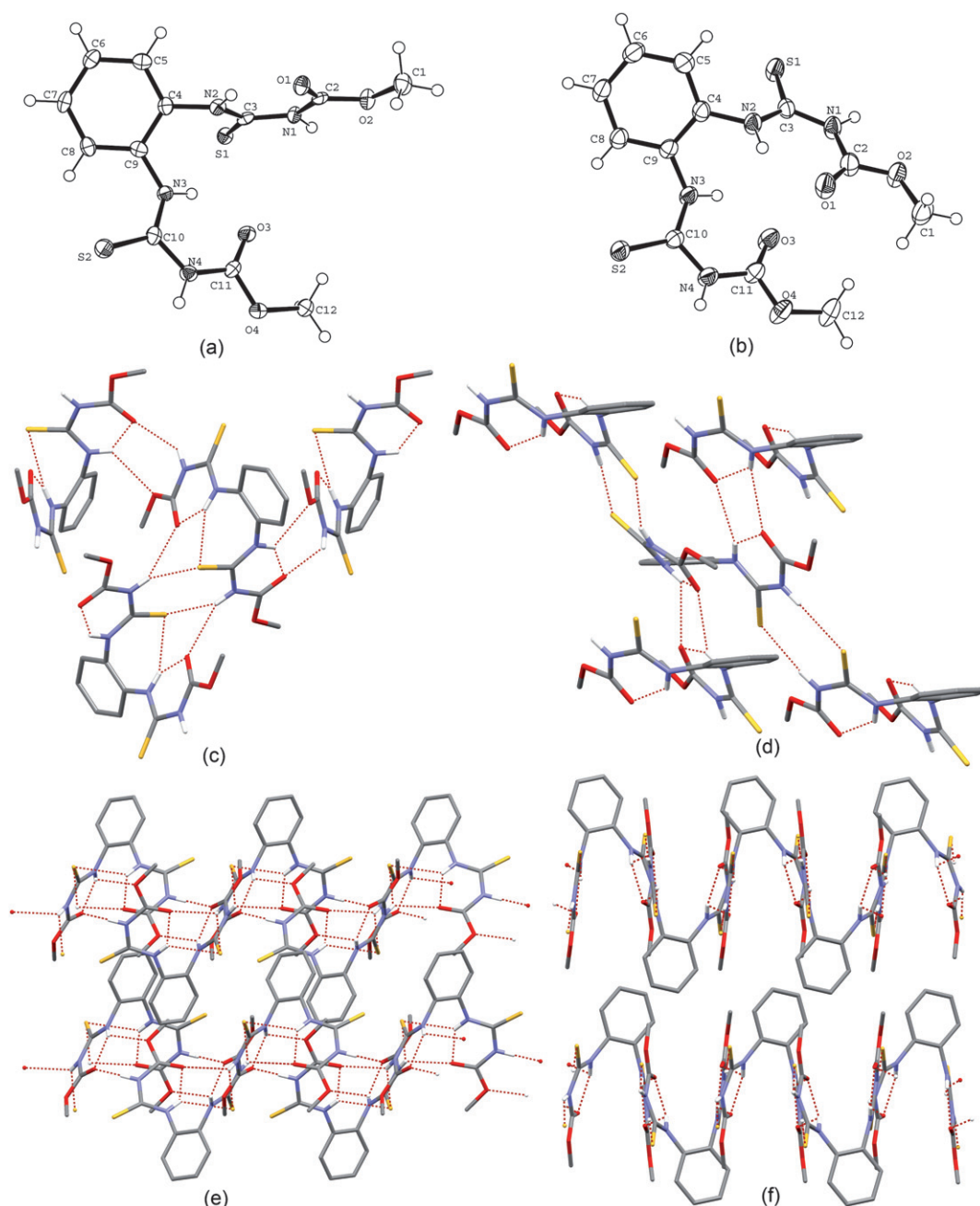
Fig. 1 ORTEP plots of (a) form I and (b) form II with the numbering of the atoms in the molecules of TM and hydrogen bonding of TM molecules in (c) form I and (d) form II, and 2-D sheets TM molecules viewed from the side in (e) form I and (f) form II. Non-hydrogen bonding hydrogens are omitted for clarity from (c)–(f).

are hydrogen bonded. Also because in form II both C=S carbon chemical shifts are deshielded in comparison to those in form I, one can conclude from the CP/MAS NMR spectrum that in form II both C=S groups are hydrogen bonded.[30]

There are differences in the IR and Raman spectra (Fig. 2c and d) of the two forms, but these were not investigated further due to PXRD being such a good method to differentiate the two forms. The IR rule[31] can be used to determine the stability order of polymorphs. The first absorption band of carbonyl oxygen atoms in the fingerprint region for form I is at 1711 cm^{-1} and for form II at 1714 cm^{-1}. The difference is small and inconsistent

with other data as it indicates form II being more stable. This difference of 3 cm^{-1} could also indicate greater involvement of the carbonyl oxygen atoms of form I in intermolecular interactions.

Transformation and stability

According to thermal analysis the relationship between the two polymorphs is monotropic, as no endothermic (or exothermic) transition is observed for either form. Temperature variable ^{13}C CP/MAS NMR (form II, RT to 100 °C) and PXRD (form I,
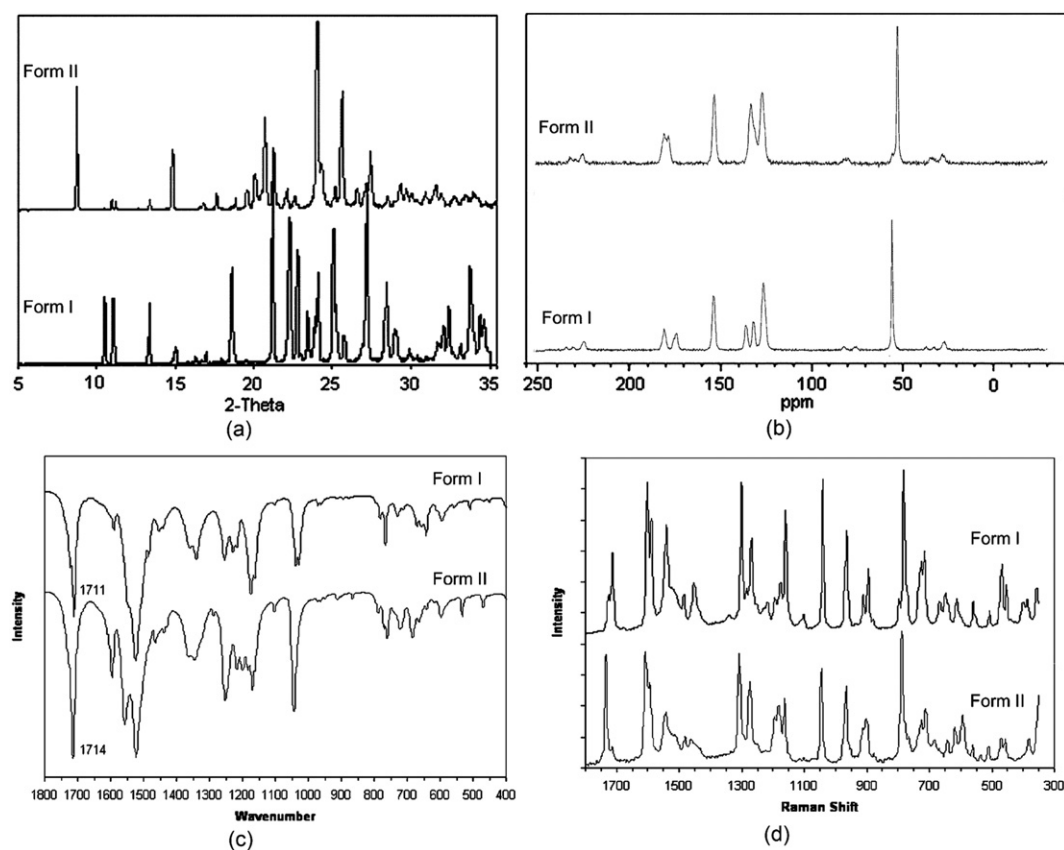
Fig. 2 (a) PXRD patterns (b) ^{13}C CP/MAS NMR spectra, (c) IR and (d) Raman spectra of forms I and II.

RT to 130 °C) analyses also indicate no transformations. However, no melting temperature could be determined and no heat-of-fusion could be measured because of the decomposition of TM and thus the heat-of-fusion rule[31] could not be used to back up our interpretation.

Form I has a calculated density of 1.51 g cm^{-3} and form II 1.46 g cm^{-3}. According to the density rule[31] the denser polymorph, in this case form I, is more stable at absolute zero. As the relationship between the polymorphs is monotropic, form I is also more stable at all temperatures. The energies of dissolution, measured by solution microcalorimetry, were −4.011 kJ mol^{-1} for form I and −6.724 kJ mol^{-1} for form II. According to the results, form I is approximately 2.7 kJ mol^{-1} lower in energy than form II. Form II also converts to form I when mixed in a suspension of water and in water-glycerol mixtures, giving further evidence of the stability of form I. The solution-mediated transformation from form I to form II occurred faster at elevated temperatures (80 °C) than at room temperature indicating form I to be more stable also at higher temperatures.

Solvates

Fourteen solvates of TM (acetonitrile/water, methanol, ethanol, acetone, DMSO, cyclohexanone, dichloromethane, 1,2-dichloroethane, dioxane, pyridine, 1,2-dichlorobenzene, THF, chloroform and benzene) were encountered during the investigations (Table 3). All but the acetonitrile solvate monohydrate crystallized quite consistently from solutions of the corresponding

solvents. Crystal structures of all the found solvates were determined. The hydrogen bonding networks and packing of the solvates is complex, as can be expected by the various hydrogen bonding possibilities and the vast amount of low energy conformers offered by TM. We do not feel that a detailed analysis is necessary here. However, we try to bring up some common features and categorize the structures where applicable.

Stability and desolvation behavior

When taken out of solution, the solvates desolvate at temperatures from room temperature (RT) to around 130 °C, as determined by thermomicroscopy (HS) and TG/DTA (Table 3). Most of the solvates also desolvate quite rapidly at room temperature when left out of solution, though the methanol and ethanol solvates seem to be rather stable and stay solvated for weeks even when out of solution. Upon desolvation (in a vacuum oven at temperatures of 80–130 °C depending on the desolvation temperature of the solvate) the tested solvates produce form II or a mixture of form I and form II, as determined with PXRD. According to the experiments, a correlation could not be recognized between the structure of the solvated or the desolvation temperature and the preferred desolvation product, even though the acetone, DCM, THF and chloroform solvates, which desolvate even at room temperature, appear to produce preferentially only form II. The reason for the emergence of mixtures may be solvent-mediated transformation occurring

Table 3 Habits, ratios of TM to solvent from TGA data, desolvation temperatures and the forms after desolvation of the found solvates

Solvate	Habit	Ratio	Desolvation T/°C		After desolvation	Solvent BP
			HS	TGA		
DCM	Blocks	1 : 1	<75	—	Form II	39.8
1,2-DCE	Blocks	1 : 1	72	73	Form II & Form I	83.5
Acetonitrile/water	Needles	1 : 1[a]	RT	—	—	82
Methanol	Plates	2 : 1	131	148	Form II & Form I	64.7
Ethanol	Plates	2 : 1	130	140	Form I & Form II	78.4
Cyclohexanone	Plates/rods	2 : 1	109	112	Form I & Form II	155.7
DMSO	Plates/blocks	1 : 1 (1 : 2)[b]	71–130	88	Form II & Form I	189
THF	Rods	1 : 1	<84	76	Form II	66
Dioxane	Blocks	1 : 1	80	111	Form II & Form I	101.1
Pyridine	Irregular blocks	1 : 1	85	125	Form II	115.2
1,2-DCB	Blocks	1 : 1	62	—	Form I & Form II	180.5
Benzene	Blocks/plates	1 : 1	58	—	—	80.1
Acetone	Plates	2 : 1	84	83	Form II	56.3
Chloroform	Needles/rods	1 : 1 (2 : 1)[c]	<60	63	Form II	61.2

[a] More precisely 3:2.5:1 (TM:MeCN:H2O). [b] The TM to DMSO ratio of 1:2 from the structure solution disagrees with the TGA result of 1:1 because of overlaps in the TGA due to the high boiling point of DMSO and the comparitatively low desolvation point of the DMSO solvate. [c] The TGA result of 2:1 disagrees with that of the structure solution most likely due to partial desolvation before analysis.

when the solvent does not leave from around the crystals as they desolvate.

Hand-in-hand pairs

The dichloromethane and 1,2-dichloroethane solvates are isomorphic and crystallize from the respective solvents by evaporation and cooling crystallization in the triclinic space group P-1 with one molecule of TM and one solvent molecule in the asymmetric unit. The TM molecules arrange in hand-in-hand pairs like the ones in form I. The pairs, however, are connected to each other with two N–H···S═C hydrogen bonds rather than the N–H···O–C hydrogen bonds that connect the pairs in form I (Fig. 3a). This arrangement of hydrogen bonds causes 1-D parallel chains of TM molecules.

The solvent molecules are situated in channels between chains of TM molecules (Fig. 3b). The distance between the closest aromatic H atoms and the Cl atoms in the DCM structure is approximately 3.07 Å, which indicates a weak interaction. The
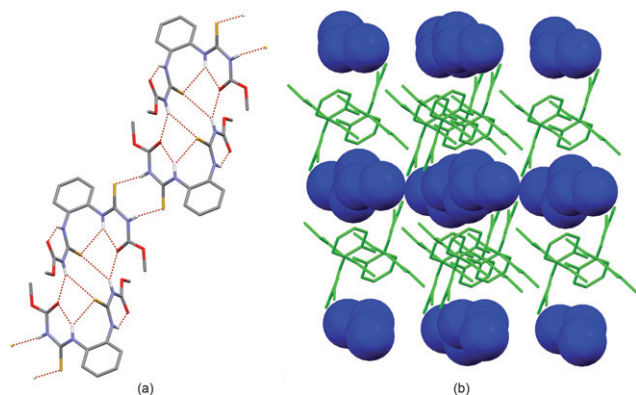
C–H hydrogen atoms of the solvent molecules in the DCM structure are also weakly hydrogen bonded to the sulfur atoms of TM with C···S distances of 3.68 and 3.93 Å and angles of 156 and 173°, respectively.

One-armed chains

The methanol, ethanol, acetone, chloroform and THF solvates crystallize in the triclinic space group P-1 with two TM molecules in the asymmetric unit. The cyclohexanone solvate also crystallizes in the space group P-1, but with four TM molecules in the asymmetric unit, whereas the DMSO solvate crystallizes in the monoclinic space group C2/c with one TM molecule in the asymmetric unit. In these solvates the main arrangement of hydrogen bonding is one where the molecules of TM arrange in chains, which include hydrogen bonds mainly to one arm of the molecules (Fig. 4 and ESI). Two types of hydrogen bond arrangements build up these chains, of which one is composed of two N–H···S═C hydrogen bonds and the other of two N–H···O═C hydrogen bonds between the molecules.
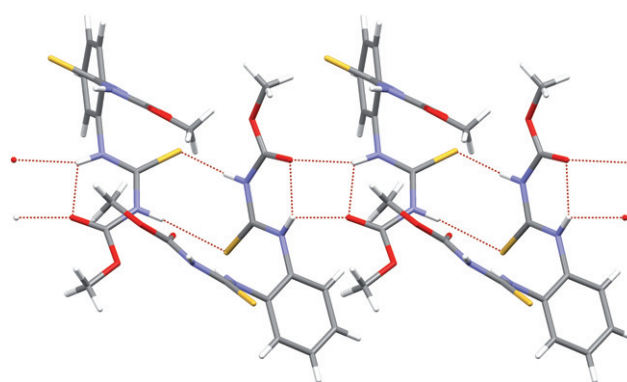

Fig. 3 (a) Hydrogen bonding of TM in the DCM and 1,2-DCE solvates (from the DCM solvate) and (b) solvent channels in the DCM solvate with the DCM molecules in space-fill style. Non H–bonding hydrogens are omitted for clarity.

Fig. 4 One-armed chain of TM molecules (from the methanol solvate) connected by N–H···S═C and N–H···O═C hydrogen bonds. Non H–bonding hydrogens are omitted for clarity.

Though the hydrogen bonding pattern of the chains is the same for all the solvates with one-armed chains, the orientation of the molecules in the chains is different due to the inclusion of different solvent molecules. The methanol, ethanol and acetone solvate structures are nearly isomorphic and the cyclohexanone solvate structure is most similar with them. The THF and DMSO solvate structures are quite different from the rest and each other. The variance in the orientation of TM molecules in the chains is most apparent in the angles of the N–H···S=C hydrogen bonds (see ESI for hydrogen bonding parameters of all the solvates†).

The arm of the TM molecules that does not build up the one-armed chains is involved in hydrogen bonding to the solvent molecules and/or in direct hydrogen bonding between adjacent chains (see ESI for pictures). In the methanol and ethanol solvates the chains are connected through two N–H···S=C hydrogen bonds between TM molecules and through hydrogen bonding to the solvent molecules, which act as both a hydrogen bond donor and acceptor. In the acetone and cyclohexanone solvate, the chains are connected with bifurcated hydrogen bonding through the solvent molecules and in the cyclohexanone solvate additionally with N–H···O–C hydrogen bonds between the TM molecules.

In the methanol, ethanol, acetone and cyclohexanone solvates the connected chains build up 2-D sheets composed of solvent molecules in between two lay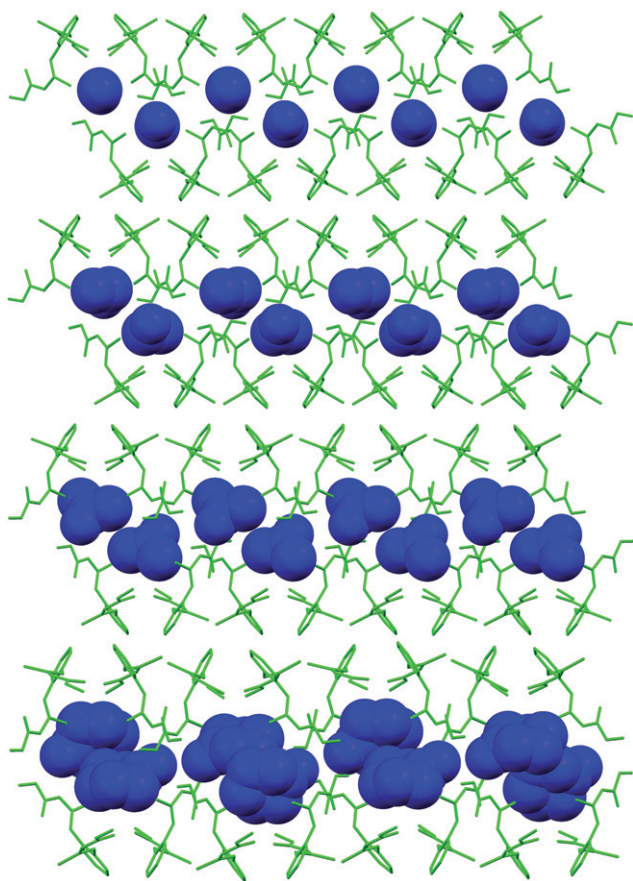ers of TM molecules (Fig. 5). These sheets then stack up on each other, being the cause for the plate-like habit of the crystals.

The THF and chloroform solvates are isomorphic with each other (Fig. 6a and b). The difference between the two is the ability of the THF molecule to form hydrogen bonds with TM and in the chloroform solvate the parallel one-armed chains are connected through hydrogen bonding via an arrangement of two N–H···S=C hydrogen bonds but in the THF solvate they are not. These two solvates have a 1 to 1 ratio of TM to solvate unlike the other solvates with the same one-armed chain hydrogen bonding arrangement of TM molecules.

In the DMSO solvate the one-armed chains, which pack parallel to each other, are not connected through hydrogen bonding. The severely disordered DMSO molecules in the DMSO solvate are placed in cavities that are lined up to form small tubular channels running through the crystal. These channels can be seen between the parallel chains when viewed from the side (Fig. 7). No hydrogen bond donors of the TM molecules point into these cavities and it is likely that the disordered DMSO molecules are merely co-crystallized to fill the empty space. The analysis of the removed electron density supports the hypothesis of having eight disordered DMSO molecules in the unit cell making the TM to solvent ratio 1 : 2.
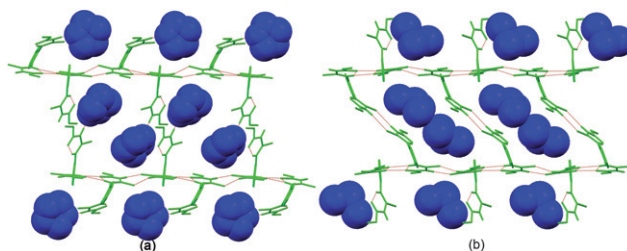

Fig. 6 Parallel packing of chains of the (a) THF solvate and the (b) chloroform solvate with solvent molecules in space-fill style. Non H–bonding hydrogens are omitted for clarity.

Fig. 5 2-D sheets in the methanol, ethanol, acetone and cyclohexanone solvates. Non H–bonding hydrogens are omitted for clarity.
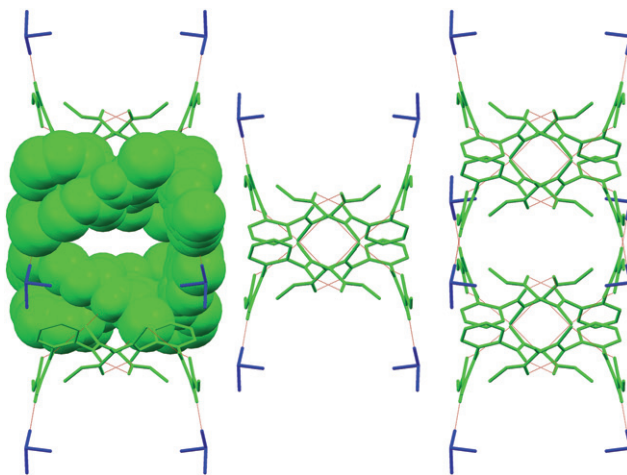

Fig. 7 DMSO solvate from one side showing the role of the ordered DMSO molecules and the channels for disordered DMSO molecules. Non H–bonding hydrogens are omitted for clarity.

Two-armed chains

The dioxane and pyridine solvates crystallize in the monoclinic space group $C2/c$ and the triclinic space group P-1, respectively, but the hydrogen bonding pattern of the TM molecules in these solvates is the same. The molecules of TM build up chains with arrangements of two N–H···S═C hydrogen bonds and two N–H···O═C hydrogen bonds involving both the arms of the molecule (Fig. 8a and b). Again as for the one-armed chains, the N–H···S═C hydrogen bonds show more variability in angles than the N–H···O═C hydrogen bonds with the hydrogen bonds in the pyridine solvate being somewhat longer than those in the dioxane solvate.

In the pyridine solvate the chains arrange parallel to each other and in the dioxane solvate they cross each other (Fig. 8c and d). In the pyridine solvate the pyridine molecules are located in channels running down the crystallographic a-axis (Fig. 8d). In the dioxane solvate there are no specific channels where the dioxane molecules reside, but they are located pairwise in cavities in the structure.

Acetonitrile solvate mono hydrate

The acetonitrile solvate mono hydrate crystallized from a 1 : 1 (v : v) acetonitrile : water solution in the triclinic space group P-1 and in addition to three TM molecules, 2 MeCN molecules and one MeCN molecule with a population density of 0.5, there is a molecule of water in the asymmetric unit. No solvate with acetonitrile without water or vice versa could be crystallized despite many attemps.

The hydrogen bonding arrangement is a combination of the arrangements in the one-armed and two-armed chains and mostly similar to that in form II with double chains composed of hydrogen bonding arrangements with two N–H···S═C or two
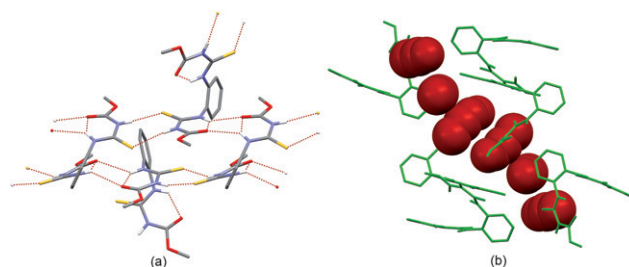
Fig. 9 (a) The hydrogen bonding arrangement and (b) the solvent channels in the MeCN solvate. Non H–bonding hydrogens are omitted for clarity.

N–H···O═C hydrogen bonds (Fig. 9a). The solvent molecules are located in channels (Fig. 9b) and hinder the formation of intact 2-D sheets like those in form II. The acetonitrile solvate mono hydrate could, in fact, be a means to the crystallization of form II as they crystallized from the same solution (different flasks).

Aromatic solvate structures

The structures of the aromatic solvates, 1,2-DCB and benzene, are considerably different from those of the other solvates and also from each other. In addition to varying hydrogen bonding (see ESI for hydrogen bonding parameters†), the conformation of the molecules of TM is also somewhat different in the structures of the 1,2-DCB and the benzene solvate.

The 1,2-dichlorobenzene solvate crystallizes in the triclinic space group P-1 with one molecule of TM and one molecule of solvent in the asymmetric unit. The arrangement of the TM molecules in the 1,2-DCB solvate resembles that in form II except there are three instead of two hydrogen bond arrangements building up the structure and the conformation of the TM molecule is different. One of the hydrogen bonding arrangements consists of two N–H···S═C hydrogen bonds, another of two N–H···O═C hydrogen bonds and the third of one N–H···S═C hydrogen bond and one N–H···O═C hydrogen bond (Fig. 10a).

The hydrogen bonding arrangements make up 2-D sheets of TM that stack up on each other, separated by the 1,2-DCB molecules (Fig. 10b). The benzene and methyl groups of TM protrude to both sides of the sheets, and aromatic interactions and weak C–H···Cl hydrogen bonds are expected between these groups and the 1,2-DCB molecules.

The hydrogen bonding in the benzene solvate structure is not similar to other structures because of N–H···O–C hydrogen bonds which are otherwise only found in form I and in the cyclohexanone solvate in combining the chains. A pair of these H···O–C hydrogen bonds and a pair of N–H···S═C hydrogen bonds build up chains of TM molecules (Fig. 11a). The distance between the sulfur, that is not hydrogen bonded to an amine hydrogen, and the methyl carbon is 3.732 Å which points toward possible weak C–H···S═C hydrogen bonding interactions. The chains pack parallel to each other with the benzene molecules in channels running through the structure (Fig. 11b).

Summary of the structures

There are interesting similarities and differences in the hydrogen bonding arrangements and the conformations of the TM
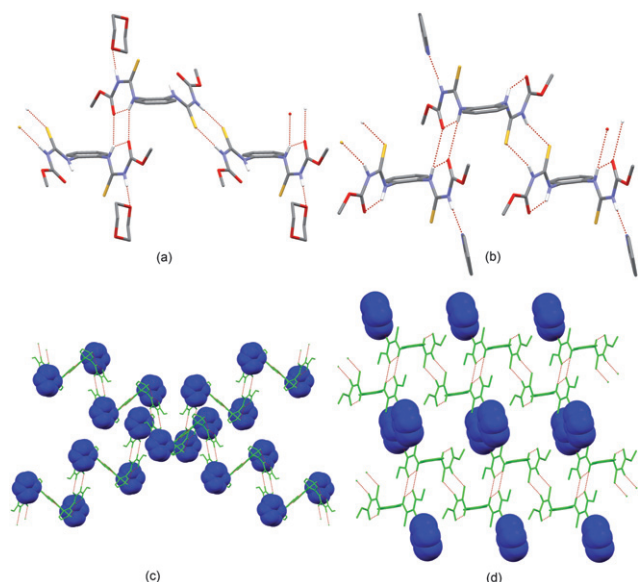

Fig. 8 Two-armed chains of TM molecules from the (a) dioxane and (b) pyridine solvates and (c) crossing chains of the dioxane solvate and (d) parallel chains of the pyridine solvate viewed down the crystallographic a-axis with solvent molecules in space-fill style. Non H–bonding hydrogens are omitted for clarity.
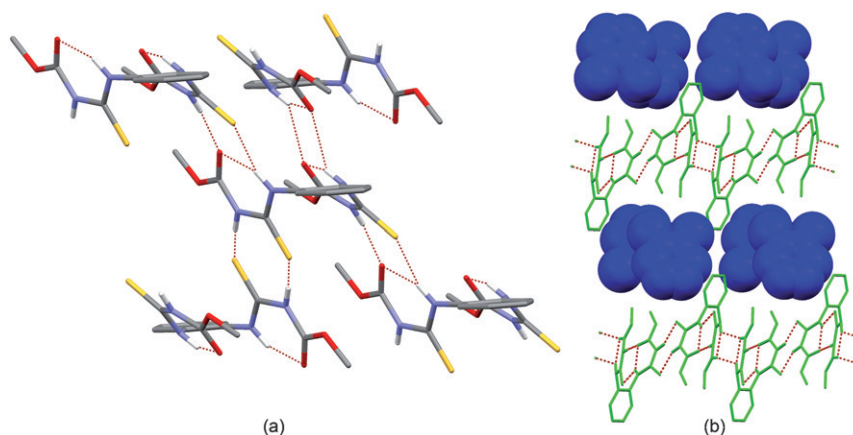
Fig. 10 (a) Hydrogen bonding in the 1,2-DCB solvate and (b) packing of the 1,2-DCB solvate sheets with 1,2-DCB molecules in space-fill style. Non H–bonding hydrogens are omitted for clarity.
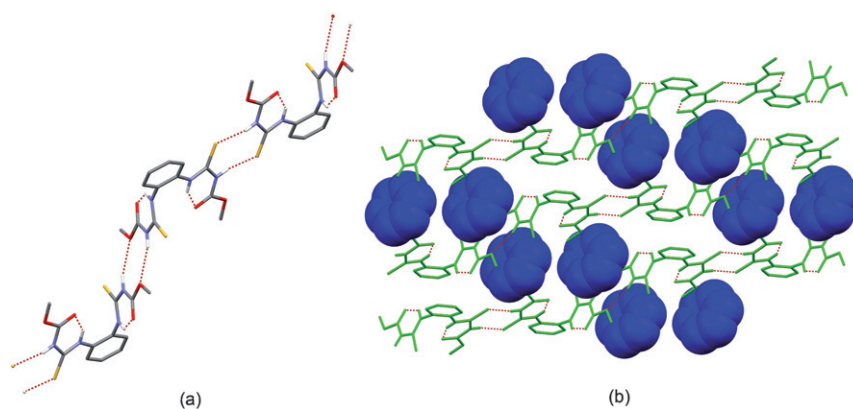

Fig. 11 (a) Chains of TM molecules and (b) the packing of the chains (with benzene molecules in space-fill style) in the benzene solvate. Non H–bonding hydrogens are omitted for clarity.

molecules in the sixteen described structures. These will be summarized here and the calculated gas phase conformers will also be looked at briefly.

Hydrogen bonding arrangements

The TM molecule has six possible hydrogen bond acceptors (two ester groups with two oxygen acceptors and two sulfur acceptors) and four amine hydrogens as possible hydrogen bond donors. This causes a number of possible intra- and intermolecular hydrogen bonding arrangements, many of which are exhibited in the described structures.

The main hydrogen bonding arrangements seem to be pairs of N–H···O=C and N–H···S=C hydrogen bonds, but the hand-in-hand pairing of TM molecules found in form I and the DCM and 1,2-DCE solvates seems to be favorable enough to bring about the formation of the weaker N–H···O–C hydrogen bond paired to a N–H···O=C hydrogen bond in the most stable form I, leaving a sulfur acceptor unused. Interestingly, in the benzene solvate pairs of N–H···O–C hydrogen bonds seem to be favored, leaving the C=O groups to hydrogen bond only intramolecularly and half the sulfur acceptors unused. Mixed pairs of one

H···O=C and one N–H···S=C hydrogen bond are found only in the 1,2-DCB solvate and form I.

Conformations

The arms of the TM molecules are fairly planar in all structures due to intramolecular N–H···O=C hydrogen bonds between N2 and O1, and N3 and O3 (the numbering of atoms is in Fig. 1).The conformations of the molecules are thus described by comparing the position of the arms of the molecules in respect to the plane of the benzene ring.

As can be seen in Fig. 12 a–d, the two polymorphs, form I (Fig. 12a) and form II (Fig. 12b), represent not only different hydrogen bonding, but also conformational polymorphism and, moreover, different conformers of TM are also observed in the solvate structures. The most remarkable difference in between form I and form II is that, unlike form II, form I has an inter-molecular N–H···S=C hydrogen bond connecting the two arms of the molecule in addition to the above mentioned N–H···O=C hydrogen bonds within the arms of the molecule. Interestingly, the acetonitrile/water solvate, with $Z' = 3$, has one of the three independent TM molecules in a confomation like that in form II and the other two more like that in form I, but not close enough
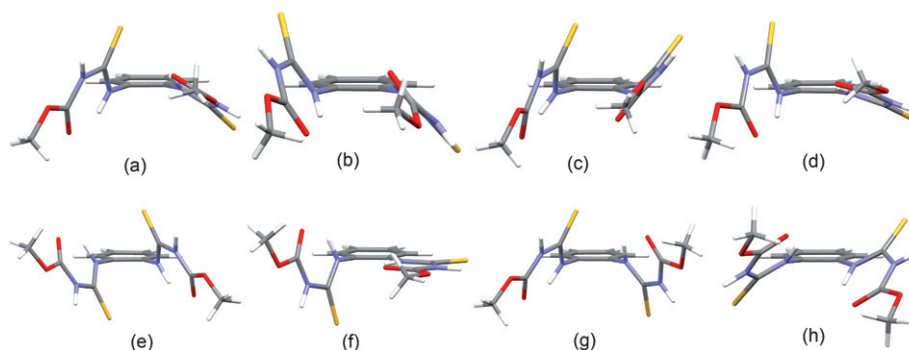
Fig. 12 Conformations of the TM molecules in (a) form I, (b) form II, (c) the 1,2-DCB and (d) benzene solvates and the four calculated gas phase conformers with the lowest energy (e) $\Delta E = 0$ kJ mol^{-1} (f) $\Delta E = 3.22$ kJ mol^{-1} (g) $\Delta E = 5.40$ kJ mol^{-1} (h) $\Delta E = 7.57$ kJ mol^{-1} viewed roughly down the plane of the benzene ring.

as to have an intermolecular N–H···S=C hydrogen bond (N–H···S=C distance approximately 3.1 Å in comparison to 2.7 Å in form I).

Calculations of the gas phase conformers of TM were done in order to get insight about the relative energies of the found conformers. Relative to the conformer with the lowest calculated energy, there are six conformers with a ΔE less than 20 kJ mol^{-1} and a total of 214 with a ΔE less than 100 kJ mol^{-1}. The six lowest energy conformers thus lie in an energy range comparative to one moderately strong hydrogen bond. The four most stable conformers (ΔE less than 8 kJ mol^{-1}, Fig.12e–h) all have the intramolecular N–H···O=C hydrogen bond that is seen in all of the crystal structures. In conformations with higher energy this bond can be changed into a N–H···O–C hydrogen bond, and in even higher energy conformers an arm of the TM molecules can be twisted into a non-planar conformation with no intra-molecular hydrogen bonding, making these higher energy conformations unlikely in crystals structures.

The conformers observed in the crystal structures have varying torsion angles between the plane of the benzene ring and the arms of the molecules with the gas-phase minimized state and direct comparison is not feasible. For example, the most stable gas phase conformer (Fig. 12e) has no good matches in the deter-mined crystal structures, though one of the TM molecules in the MeCN/H$_2$O solvate comes close. The second conformer (Fig. 12f) resembles that in the benzene solvate (Fig. 12d). The third gas-phase conformer (Fig. 12g) is quite like that in many of the solvate crystal structures and form I, but most closely resembles the TM molecules in the THF and cyclohexanone solvates. The fourth conformer (Fig. 12h) resembles most closely that in form II of TM (Fig. 12b).

The aromatic solvates have conformations of TM most unlike those in the other structures. In the benzene solvate one arm of the molecule is more in the plane of the benzene ring whereas the other arm is, conversely, less in the plane of the benzene ring than in form I. Further, the conformation of TM in the 1,2-DCB solvate (with sulfur atoms on the same side of the aromatic plane) was not found among the gas phase conformers. In this structure the planes of the arms of the TM molecules are almost parallel to each other, which is also the case in form II, and enables the formation of the similar hydrogen bonded sheet arrangements in the structures.

A lattice energy analysis and a constrained energy optimiza-tion of the observed crystal structure conformers is left out of this study as the authors do not expect that such an analysis would bring more essential information. It is, however, clear that the variability of the conformations of TM in the solved crystal structures is paralleled by a number of gas phase conformers with small energy differences and this flexibility probably accounts for the large number of solvates of TM.

Conclusions

TM was found to exists in two polymorphic forms which have very similar melting points. The original and known form I is the thermodynamically most stable form, which is monotropically related to Form II. Form II can be accessed *via* desolvation of various different solvate forms.

The discovery of a series of fourteen solvates and the structure determination of these *via* single crystal X-ray measurement is the highlight of this work. Solvent molecules capable of forming hydrogen bonds (acting either as hydrogen bond acceptors or both acceptor and donor) presented the majority, but also other, such as 1,2-dichlorobenzene and benzene were among solvate forming solvents. The isostructural methanol and ethanol solvates, with desolvation points around 140 °C, were remark-ably stable against desolvation, whereas the non-hydrogen bonded solvates desolvated already at ambient conditions.

The single crystal structures reported here represent a variety of interaction possibilities of TM varying from hydrogen bonding to aromatic and lipophilic interactions. No clear patterns in packing or formation could be drawn from the structures. It is however noteworthy that TM has a large amount of low energy conformers and several possibilities of forming hydrogen bonds. These two facts can as tradeoff, lead to new hydrogen bonding and close packing modes and can reduce the total energy difference between alternate crystal structures. The search in the CSD by van de Streek[32] shows that there are only a few compounds, many of which are not organic neutral compounds of the size of TM, with ten or more solvate structures reported. It is very likely that, similar to sulfathiazole with its over one hundred solvates,[33] several new solvates and also co-crystals with a variety of different functional groups could be found for TM.

As shown in this paper, crystallographical methods play a key role in studying polymorphism and solid state structures. However, also all the used spectroscopical methods (^{13}C CP/MAS NMR, IR and Raman) are usefull in identifying the polymorphic forms of TM from each other and can be valuable in cases where crystallographical methods are not available or can not be applied. Thermoanalytical methods are also especially helpful in determining the stability of a new modification and resolving whether it is a solvate or not.

Acknowledgements

References

1 D. Braga, G. R. Desiraju, J. S. Miller, A. G. Orpen and S. L. Price, *CrystEngComm*, 2002, **4**, 500–509; P. Erk, H. Hengelsberg, M. F. Haddow and R. Van Gelder, *CrystEngComm*, 2004, **6**, 474–483; G. R. Desiraju, *Angew. Chem., Int. Ed.*, 2007, **46**, 8342–8356.
2 G. R. Desiraju, *Angew. Chem., Int. Ed. Engl.*, 1995, **34**, 2311–2327.
3 J. Bernstein, *Polymorphism in Molecular Crystals*, Oxford University Press, United States, 2002; H. G. Brittain, *Polymorphism in Pharmaceutical Solids*, Marcel Dekker, Inc., New York, USA, 1999; U. J. Griesser, in *Polymorphism in the Pharmaceutical Industry*, ed. R. Hilfiker, WILEY-VCH Verlag GmbH & Co. KGaA, Weinheim, Germany, 2006, pp.211–234.
4 C. H. Görbitz and H.-P. Hersleth, *Acta Crystallogr., Sect. B: Struct. Sci.*, 2000, **56**, 526–534; R. Banerjee, P. M. Bhatt and G. R. Desiraju, *Cryst. Growth Des.*, 2006, **6**, 1468–1478; S. A. Barnett, D. A. Tocher and M. Vickers, *CrystEngComm*, 2006, **8**, 313–319; K. Jarring, T. Larsson, B. Stensland and I. Ymén, *J. Pharm. Sci.*, 2006, **95**, 1144–1161; T. Hosokawa, S. Datta, A. R. Sheth, N. R. Brooks, V. G. Young and D. J. W. Grant, *Cryst. Growth Des.*, 2004, **4**, 1195.
5 D. D. Wirth and G. A. Stephenson, *Org. Process Res. Dev.*, 1997, **1**, 55–60; J. Bauer, J. Morley, S. Spanton, F. J. J. Leusen, R. Henry, S. Hollis, W. Heitmann, A. Mannino, J. Quick and W. Dziki, *J. Pharm. Sci.*, 2006, **95**, 917–928.
6 C. H. Price, G. D. Glick and A. J. Matzger, *Angew. Chem., Int. Ed.*, 2006, **45**, 2062–2066.
7 A. Nangia, *Acc. Chem. Res.*, 2008, **41**(5), 595–604.
8 U. J. Griesser, D. Weigand, J. M. Rollinger, M. Haddow and E. Gstrein, *J. Therm. Anal. Calorim.*, 2004, **77**, 511–522; D. Chopra,

9 *GB Pat., 1 307 250*, 1970; *GB Pat., 1 313 966*, 1970; *US Pat., 3 852 278*, 1973.
10 WO *2008/096005*.
11 J. Dekker and S. G. Georgopoulos, *Fungicide Resistance in Crop Protection*, Centre for Agricultural Publishing and Documentation, Wageningen, Netherlands, 1982.
12 C. S. Tomlin, *The e-Pesticide Manual*, Version 3.2 13, British Crop Production Council (BCPC), Great Britain, 2005.
13 G. K. Dixon, L. G. Copping and D. W. Hollomon, *Antifungal Agents Discovery and Mode of Action*, BIOS Scientific Publishers Ltd, Oxford, UK, 1995.
14 G. M. Sheldrick, *Acta Crystallogr., Sect. A: Fundam. Crystallogr.*, 2007, **64**, 112–122.
15 R. H. Blessing, *Acta Crystallogr., Sect. A: Fundam. Crystallogr.*, 1995, **51**, 33.
16 Z. Otwinowski, D. Borek, W. Majewski and W. Minor, *Acta Crystallogr., Sect. A: Fundam. Crystallogr.*, 2003, **59**, 228–234.
17 L. J. Farrugia and WinGX, *J. Appl. Crystallogr.*, 1999, **32**, 837–838.
18 SHELXTL Version 6.14., *Bruker Analytical X-ray Solutions*, 2000, Madison, Wisconsin, USA.
19 P. van der Sluis and A. L. Spek, *Acta Crystallogr., Sect. A: Fundam. Crystallogr.*, 1990, **46**, 194–201.
20 C. F. Macrae, P. R. Edgington, P. McCabe, E. Pidcock, G. P. Shields, R. Taylor, M. Towler and J. van de Streek, Mercury 1.4.1, *J. Appl. Crystallogr.*, 2006, **39**, 453–457.
21 S. L. Mayo, B. D. Olafson and W. A. Goddard III, *J. Phys. Chem.*, 1990, **94**, 8897.
22 A. K. Rappe and W. A. Goddard III, *J. Phys. Chem.*, 1991, **95**, 3358.
23 Cerius² V4.6, Accelrys Inc., 2001, San Diego.
24 A. D. Becke, *Phys. Rev. A: At., Mol., Opt. Phys.*, 1988, **38**, 3098; J. P. Perdew, *Phys. Rev. B: Condens. Matter Mater. Phys.*, 1986, **33**, 8822; J. P. Perdew, *Phys. Rev. B: Condens. Matter Mater. Phys.*, 1986, **34**, 7406(E).
25 A. Schäfer, C. Huber and R. Ahlrichs, *J. Chem. Phys.*, 1994, **100**, 5829.
26 K. Eichkorn, F. Weigend, O. Treutler and R. Ahlrichs, *Theor. Chim. Acta*, 1997, **97**, 119.
27 F. Weigend and M. Häser, *Theor. Chim. Acta*, 1997, **97**, 331.
28 TZVPP is the acronym used in the Turbomole basis set library and denotes a valence triple-zeta basis set (TZV, see ref. 23) augmented with Dunning's correlation consistent polarization functions T. H. Dunning, Jr., *J. Chem. Phys.*, 1989, **90**, 1007; D. E. Woon and T. H. Dunning, Jr., *J. Chem. Phys.*, 1993, **98**, 1358.
29 *Turbomole* V5.10, University of Karlsruhe 2008, http://www.turbomole.com.
30 K. Masuda and F. Horii, *Macromolecules*, 1998, **31**, 5810–5817.
31 A. Burger and R. Ramberger, *Microchim. Acta*, 1979, **72**, 259–271; A. Burger and R. Ramberger, *Microchim. Acta*, 1979, **72**, 273–316.
32 J. van de Streek, *CrystEngComm*, 2007, **9**, 350–352.
33 A. L. Bingham, D. S. Hughes, M. B. Hursthouse, R. W. Lancaster, S. Tavener and T. L. Threlfall, *Chem. Commun.*, 2001, 603–604.

T. P. Mohan, K. Sundaraja Rao and T. N. Guru Row, *CrystEngComm*, 2005, **7**, 374–379.

II

**Comparison of the polymorphs and solvates of two analogous
fungicides - a case study of the applicability of a supramolecular
synthon approach in crystal engineering**

by

E. Nauha, A. Ojala, H. Saxell & M. Nissinen, 2011

CrystEngComm

PAPER

Comparison of the polymorphs and solvates of two analogous fungicides—a case study of the applicability of a supramolecular synthon approach in crystal engineering†

Elisa Nauha,[a] Antti Ojala,[b] Maija Nissinen*[a] and Heidi Saxell[b]
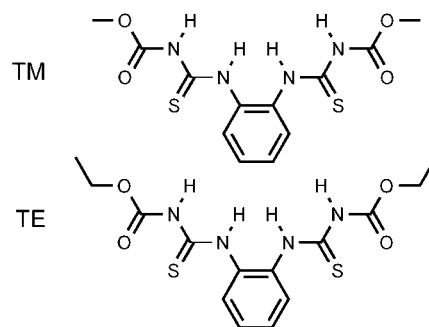
The polymorphism and solvate formation of thiophanate-ethyl (TE), a fungicidal active, were investigated by solvent crystallization and compared to a close analogue, thiophanate-methyl (TM). Four polymorphs and seven solvates of TE were found and structurally compared with the previously found two polymorphs and fourteen solvates of TM by analyzing the hydrogen bonding patterns and using fingerprint plots, packing coefficients and lattice energies. TE and TM have the same functional groups that can build identical supramolecular synthons. Despite the strong similarities, the polymorphs and solvates of the two actives show significant differences in hydrogen bonding and packing. The results demonstrate the challenges in using a supramolecular synthon approach, and promote the importance in finding methods to also make use of packing effects and lipophilic interactions in crystal engineering.

In a crystallization process, the molecules arrange in an energetically favorable way. The energetic incentive of favorable intermolecular interactions, the strongest of which are hydrogen bonds for neutral molecules, and reduction in void space, negotiate for the best arrangement of molecules in the crystal. For most organic molecules, there are several ways to arrange, causing polymorphs to appear.[1] In a solvent based polymorph screening, it is typical to also find solvates that are often more stable than the polymorphs of a compound in the solvate forming solvent.[2] The crystallization outcome then depends on the kinetics of crystallization and the presence of other contributing additives, either the solvent or other species, in the crystallization medium.

The aim in modern crystal engineering is the targeted discovery of multicomponent crystals, *i.e.* cocrystals. As solvates can be considered to belong to a subgroup of cocrystals, the study of solvate formation can give an insight for designing cocrystals. Suitable cocrystals can enable the tuning of the crucial physical and chemical parameters such as the solubility, vapour pressure, crystal habit *etc.*, of an active ingredient in pharmaceutical, agrochemical or other areas.[3] The prevailing model for cocrystal engineering is using a supramolecular synthon approach, where supramolecular synthons, which consist of intermolecular interactions (especially hydrogen bonds), are viewed as bonds for the construction of supermolecules, *i.e.* crystals.[4]

Crystal structures give the most definite understanding of the crystal packing and intramolecular interactions, and help give strategies for crystal engineering. The conformation of the molecule, hydrogen bonding and other intermolecular interactions as well as the packing can be assessed with the help of a number of tools. The packing coefficients,[5] fingerprint plots[6] and lattice energies[7] can be calculated to ensure all relevant features, such as intermolecular interactions and packing density, are noted when assessing the structure visually. The use of graph set symbols[8] for hydrogen bonding facilitates the easy comparison of hydrogen bonding in similar structures.

[a]*University of Jyväskylä, Department of Chemistry, Nanoscience Center, PO Box 35, FIN-40014, Finland. E-mail: maija.nissinen@jyu.fi; Fax: +35814 2604756; Tel: +35814 2604242*
[b]*BASF SE, GVC/C—A030, 67056 Ludwigshafen, Germany. E-mail: heidi. saxell@basf.com; Fax: +49621 6020440; Tel: +49621 6049558*

Scheme 1 Molecular structures of thiophanate-methyl (TM) and thiophanate-ethyl (TE).

We have previously investigated thoroughly the polymorphism and solvate formation,[9] as well as cocrystal formation,[10] of the fungicidal active thiophanate-methyl (TM, dimethyl 4,4′-(o-phenylene)bis(3-thioallophanate), Scheme 1). According to our findings, TM has two conformational polymorphs and at least fourteen solvates. TM is an excellent example of a small molecule with possibilities to serve as a versatile supramolecular building block that has conformational flexibility and is able to form host–guest frameworks. To get an understanding of the applicability of a supramolecular synthon approach, we investigated the polymorphism of a close analogue of TM that differs only by two CH_2 groups. Thiophanate-ethyl (TE, diethyl 4,4′-(o-phenylene)bis(3-thioallophanate), Scheme 1) is a fungicide that has been withdrawn from the European market[11] because of safety issues and the availability of an efficient alternative, mainly TM, which is identical in fungicidal function and from a supramolecular synthon perspective. This paper reports the four found polymorphs of TE, as well as the analysis of the achieved single crystal structures of three polymorphs and seven solvates, as comparison with the previously reported TM structures.

Experimental

Materials

TE of 99% purity from Chem Service, distilled water and solvents of analytical purity (min 99%) were used in the crystallization experiments. To save the material TE was reused without purification.

Crystallizations

Approximately 20 mg samples of TE were dissolved in 5 ml of solvent (acetonitrile, 1 : 1 acetonitrile : water, acetone, ethanol, methanol, DCM, chloroform, pyridine, dioxane and toluene : methanol). The solution was transferred to a clean test tube, which was covered with parafilm with a few holes. The solvent was left to evaporate at room temperature.

PXRD

For powder X-ray diffraction analysis the original TE was hand grinded, pressed to a zero background silicon plate and measured on a PANalytical X'Pert Pro system in reflection mode with CuKα1-radiation. A 2θ-angle range of 5–40° and a step time of 60 s were used with step resolution of 0.0167°. Figures were drawn with X'Pert HighScore Plus.[12]

Single crystal X-ray diffraction

The X-ray diffraction data were collected on a Nonius Kappa CCD-diffractometer with an Apex II detector at 173 K, using graphite-monochromated CuKα radiation ($\lambda = 1.54178$ Å), or in the case of the pyridine solvate graphite-monochromated MoKα radiation ($\lambda = 0.71073$ Å). Absorption correction was performed with Denzo-SMN 1997.[13] The structures were solved by direct methods, refined, and expanded by Fourier techniques with the SHELX-97 software package.[14] All non-hydrogen atoms, except for the disordered toluene molecule, were refined anisotropically.

Hydrogen atoms were placed in idealized positions or found from the electron density map (hydrogen bonding N–H hydrogens), and included in structure factor calculations. The N–H hydrogen atoms found in the electron density map were restrained to a distance of 0.91 Å to give the best fit to the X-ray data and to ensure stable refinement. Pictures of the structures were drawn with Mercury.[15] Crystal data and collection parameters are presented in Tables 1 and 2.

In the dioxane I, DCM and chloroform solvates the solvent molecules are disordered over a symmetry axis in two positions. There are voids of 42 Å³ in the toluene solvate structure that are surrounded by the ethyl groups of TE and the toluene molecules making the inclusion of water unlikely due to hydrophobic surroundings. The toluene molecule is in a general position, but disordered over two positions that are coplanar and at a 180° angle relative to each other. In form III there are voids of around 45 Å³ between the arms of one of the symmetry unequivalent molecules with no significant residual electron density.

Lattice energy calculations

The lattice energies (E_{latt}) of the polymorphs of TE and TM were calculated using the Cerius² program package.[16] All computations were performed with the default settings of the program and following the previously published procedure.[7] Atomic charges were assigned by a QEq method and cross-checked with AM1 which yielded essentially similar results. The E_{latt} values were calculated with a Dreiding II force field for the energetically optimized structures. During structure optimization the molecules were treated as rigid objects and only the unit cell dimensions were allowed to change. The optimized unit cells diverged less than 3% of the original values.

The approximated modeling yielded generally similar energetic values for the polymorphs in a meaningful energy window. However, due to the inaccurate nature of the method (e.g. lack of polarizability), the absolute values are not reliable and only the relative energies should be judged. Precise E_{latt} calculations

Table 1 Crystal data and collection parameters of the polymorphs of TE

	TE-form I	TE-form II	TE-form III
Chemical formula	$C_{14}H_{18}N_4O_4S_2$	$C_{14}H_{18}N_4O_4S_2$	$C_{14}H_{18}N_4O_4S_2$
Formula mass	370.44	370.44	370.44
Crystal system	Triclinic	Monoclinic	Triclinic
a/Å	7.9911(1)	4.7271(1)	10.7333(5)
b/Å	9.6750(2)	16.0239(3)	11.8079(7)
c/Å	12.5109(3)	22.6450(4)	16.2174(12)
α/°	69.055(3)	90.00	95.293(3)
β/°	81.270(3)	93.750(3)	100.405(4)
γ/°	73.033(3)	90.00	113.044(4)
V/Å³	862.81(3)	1711.61(6)	1829.9(2)
Temperature/K	173(2)	173(2)	173(2)
Space group	$P\bar{1}$	$P2(1)/c$	$P\bar{1}$
Z	2	4	4
Meas. reflns	4039	4691	8675
Indep. reflns	2936	2931	6132
R_{int}	0.0848	0.0616	0.1113
R_1($I > 2\sigma(I)$)	0.0458	0.0550	0.0603
wR(F^2) ($I > 2\sigma(I)$)	0.1235	0.1120	0.1413
R_1 (all data)	0.0520	0.0898	0.0963
wR(F^2) (all data)	0.1299	0.1283	0.1633
GOF on F^2	1.031	1.060	1.026

Table 2 Crystal data and collection parameters of the solvates of TE

	TE–acetone	TE–DCM	TE–chloroform	TE–dioxane I[a]	TE–dioxane II	TE–pyridine	TE–toluene[b]
Chemical formula	$C_{14}H_{18}N_4O_4S_2 \cdot C_3H_6O$	$C_{14}H_{18}N_4O_4S_2 \cdot CH_2Cl_2$	$C_{14}H_{18}N_4O_4S_2 \cdot CHCl_3$	$C_{14}H_{18}N_4O_4S_2 \cdot C_4H_8O_2$	$C_{14}H_{18}N_4O_4S_2 \cdot C_4H_8O_2$	$C_{14}H_{18}N_4O_4S_2 \cdot C_5H_5N$	$3(C_{14}H_{18}N_4O_4S_2) \cdot 2(C_7H_8)$
Formula mass	428.52	455.37	489.81	458.55	458.55	449.54	1295.60
Crystal system	Monoclinic	Monoclinic	Monoclinic	Monoclinic	Triclinic	Triclinic	Tetragonal
a/Å	16.0607(2)	16.1404(3)	15.5158(3)	16.8293(3)	9.2924(2)	8.8104(9)	11.7631(2)
b/Å	17.4629(2)	17.3754(3)	18.0503(4)	17.0275(3)	11.7070(3)	11.3513(13)	11.7631(2)
c/Å	8.4560(1)	8.2332(2)	8.5922(2)	8.2545(2)	12.1305(3)	12.500(2)	48.5257(8)
α/°	90.00	90.00	90.00	90.00	65.555(2)	66.635(7)	90.00
β/°	111.432(3)	110.996(3)	112.739(3)	111.119(3)	68.864(2)	77.989(6)	90.00
γ/°	90.00	90.00	90.00	90.00	76.329(3)	77.883(5)	90.00
V/Å³	2207.63(5)	2155.66(8)	2219.34(8)	2206.54(8)	1114.61(5)	1111.1(2)	6714.5(2)
Temperature/K	173(2)	173(2)	173(2)	173(2)	173(2)	173(2)	173(2)
Space group	$C2/c$	$C2/c$	$C2/c$	$C2/c$	$P\bar{1}$	$P1$	$P4(3)22$
Z	4	4	4	4	2	2	4
Meas. reflns	2547	2757	2817	2410	5447	6213	11 130
Indep. reflns	1878	1781	1907	1647	3818	4056	5685
R_{int}	0.0234	0.0605	0.0476	0.0361	0.0504	0.0366	0.0399
$R_1(I > 2\sigma(I))$	0.0359	0.1591	0.0755	0.0633	0.0444	0.0530	0.0434
$wR(F^2)$ ($I > 2\sigma(I)$)	0.0936	0.4149	0.1918	0.1799	0.1089	0.0985	0.0987
R_1 (all data)	0.0393	0.1739	0.0893	0.0704	0.0575	0.0757	0.0631
$wR(F^2)$ (all data)	0.0967	0.4220	0.2058	0.1870	0.1175	0.1096	0.1084
GOF on F^2	1.047	1.172	1.034	1.105	1.022	1.077	1.043

[a] Low data completeness (83%) and new crystallizations produced TE–dioxane II. [b] Contains one TE in a general position and half a TE on a twofold axis.

would need expansive DFT calculations and/or extensive calibration of the force fields to reach the accuracy that is needed to judge the total energies which often diverge 1–2 kcal mol^{-1} between the polymorphs.[17]

Results and discussion

Four polymorphs and seven solvates of thiophanate-ethyl were found during the solvent screening experiments. The polymorphs were named in order of discovery as forms I–IV. Samples crystallized from acetonitrile and methanol produced crystals of TE form I and a sample crystallized from ethanol produced crystals of form II. Samples crystallized from 1 : 1 acetonitrile : water concomitantly produced crystals of form I and form II. Form III was crystallized from a methanol solution that also contained sodium acetate. The pyridine, toluene, acetone, dioxane, DCM and chloroform samples produced solvate crystals. Two polymorphic solvates (dioxane I and II) were crystallized from dioxane in the course of trying to get better crystals of the first one. The fourth polymorph of TE was identified by powder diffraction, but no single crystal structure was obtained. Form IV appears upon desolvation of the isomorphous solvates (acetone, dioxane I, DCM and chloroform).

TE form I

In TE form I as in all the structures of TE there is an intramolecular N–H⋯O=C hydrogen bond in a S(6) motif in both the arms of the molecule that restricts the conformation of the arms. The molecules of TE in form I are connected to each other by three kinds of hydrogen bonding motifs, of which one consists of two N–H⋯S hydrogen bonds R2,2(8), another of two N–H⋯O=C hydrogen bonds R2,2(12) and the third of one N–H⋯S hydrogen bond and one N–H⋯O=C hydrogen bond R2,2(10) (Fig. 1). The TE molecules thus connect into two-dimensional sheets that stack upon each other. The benzene and ethyl groups of TE protrude from both sides of the sheets, and there are face-to-face π–π stacking interactions, with ring distances of approximately 3.5 Å, between the sheets.

TE form II

The TE molecules in form II build up hydrogen bonded chains with the same R2,2(8) motif consisting of two N–H⋯S hydrogen bonds as in form I (Fig. 1). Unlike in form I there are only intramolecular N–H⋯O=C hydrogen bonds. The chains arrange parallel to each other guided by π–π stacking interactions between the benzene rings and dipole–dipole interactions between the carbonyls in adjacent chains. The parallel chains make up sheet-like structures that stack upon each other in a manner similar to that in form I with benzene and ethyl groups of TE protruding from both sides of the sheets.

TE form III

Unlike in forms I and II, the Z′ of form III is 2. The molecules build hydrogen bonded chains of the two symmetrically unequivalent molecules (A and B) connected with two N–H⋯S hydrogen bonds in the binary level R2,2(8) arrangement and with two N–H⋯C=O hydrogen bonds in a binary level R2,2(12)

arrangement (Fig. 1). This chain involves only one arm of the molecules. Two chains are connected to each other via N–H⋯S hydrogen bonds on the other arms of the molecules with a R2,2 (8) arrangement and a D1,1(2) motif. There are also intramolecular N–H⋯S hydrogen bonds in a S(7) motif.

Solution NMR evidence suggests that there is some interaction between the N–H hydrogens and the acetate present in the crystallization, which could have influenced the aggregation of TE molecules initiating the crystallization of this form. The Z′ of 2 and the presence of small voids suggest that this could be a case of crystallization "on the way".[18]

TE form IV

Form IV was found to be a desolvation product of the isomorphous solvates and can be identified from the PXRD pattern. The original sample from ChemService was found to be a combination of form I and form IV (PXRD in Fig. 2). This can be most clearly seen in the peaks caused by form IV at 9.5, 16.3 and 23.7°2θ.

The unit cell of this polymorph was determined from the powder pattern using X'Pert HighScore Plus and the most likely candidate is a monoclinic cell with a possible space group of C2/c with a = 11.50, b = 18.76, c = 9.22, β = 112.24° and V = 1846.5 Å³. A structure in this cell can easily be imagined from the isomorphous solvate structures by removing the solvent and moving the TE molecules to fill the formed voids. Efforts to solve the structure from powder data are currently underway.

Packing efficiency of the polymorphs

The fingerprint plots in Fig. 1 show a graphical representation of the packing in forms I to III. The packing coefficients (Fig. 3) of the structures were also determined[19] in order to get a numerical estimate of the packing efficiency. According to the results, form II packs the most tightly with form I in second place. The packing coefficient and the hydrogen bonding seem to explain the similar stability of forms I and II since form I has more and stronger intermolecular hydrogen bonds than form II, but form II packs more tightly. Form III, on the other hand, packs very loosely and is expected to be less stable even though there is a lot of hydrogen bonding.

The packing coefficients were calculated also for the previously reported polymorphs of TM. TM form I is clearly more densely packed than form II. This can also be seen in the fingerprint plots (Fig. 4). From the fingerprint plots one can also say that the N–H⋯S hydrogen bonds in form II are shorter, indicating a stronger nature. The stronger N–H⋯O hydrogen bonds are, however, somewhat shorter for form I.

Experimental observations on the stability

Thermal methods to determine the stabilities of the forms could not be used because TE decomposes on melting or when heated for prolonged periods. Very few experiments were done to find out the stability order of the polymorphs, because the forms could not be reproduced in large quantities. The occasional concomitant crystallization suggests that form I and form II are quite similar in stability, but attempts to crystallize form II in larger amounts resulted only in form I. The kinetics of the
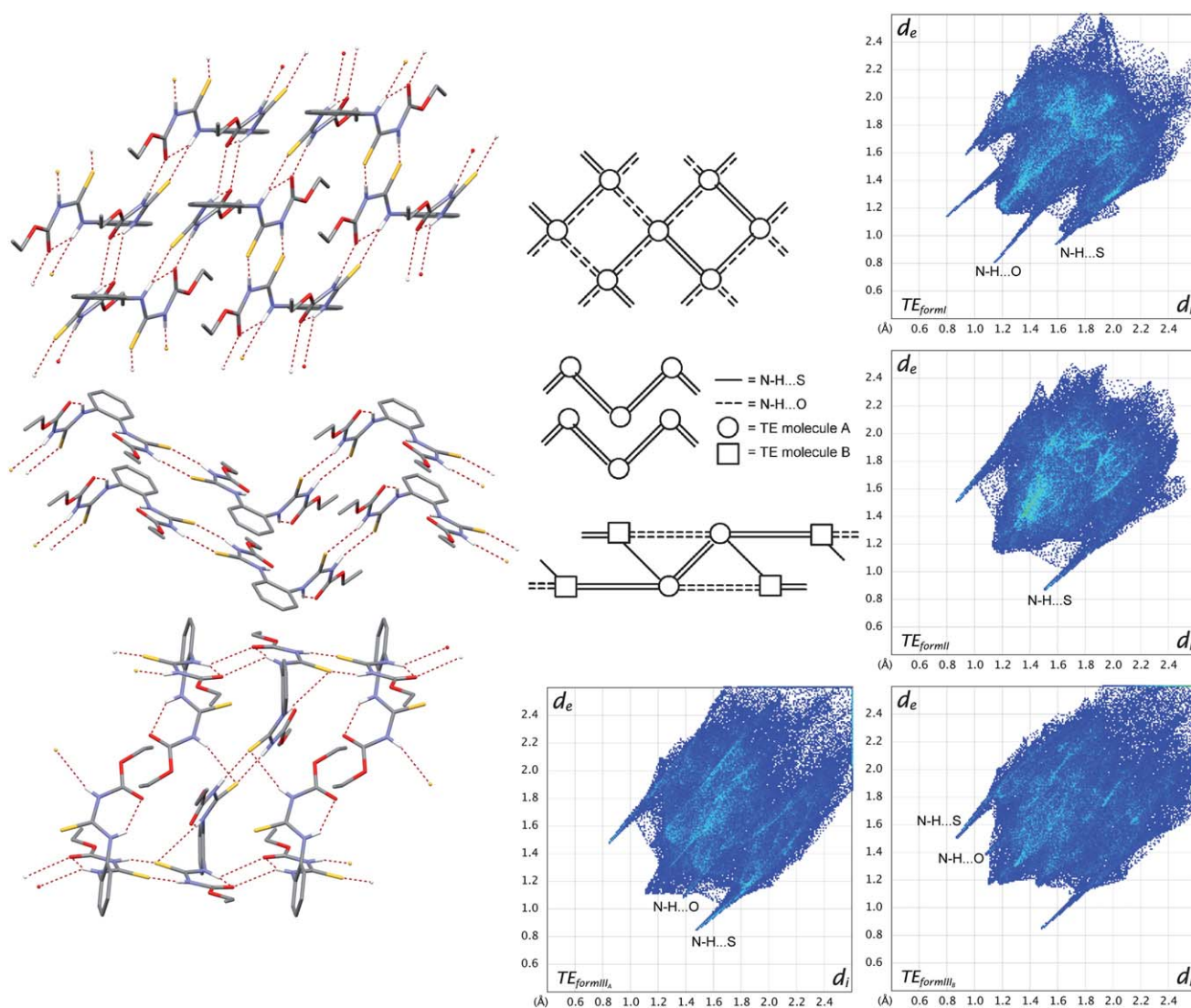
Fig. 1 Hydrogen bonding in the sheets of TE form I (top), in the chains of TE form II (middle) and the double chains of TE form III (bottom) with non-hydrogen bonding hydrogen atoms removed for clarity The simplified diagrams of the hydrogen bonding and the fingerprint plots of forms I–III.
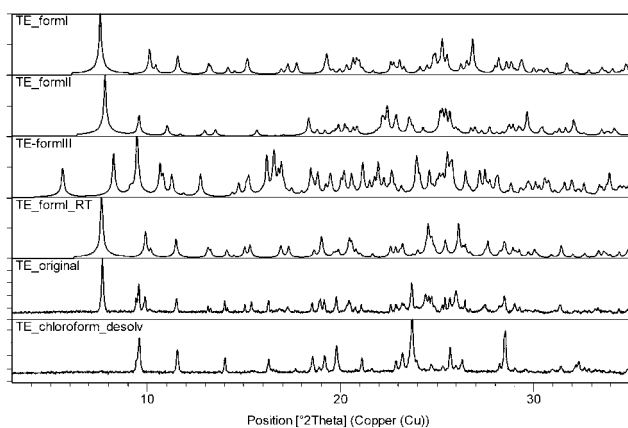

Fig. 2 From top to bottom calculated PXRD patterns of TE form I–III at 173 K and form I at RT, the PXRD pattern of the original TE sample and of form IV from desolvation of the chloroform solvate.
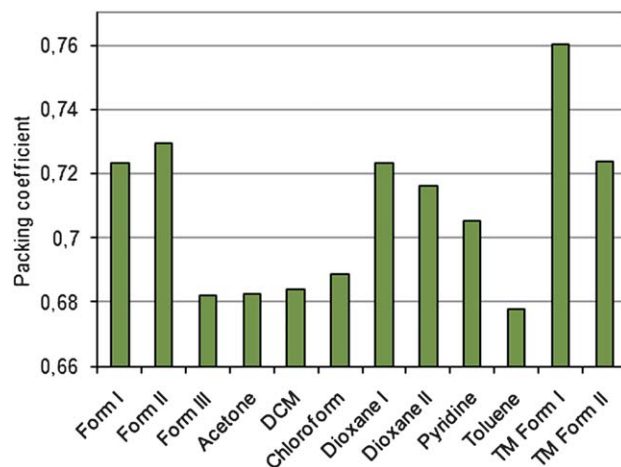

Fig. 3 Packing coefficients of the single crystal structures of TE and the polymorphs of TM.

crystallizations are likely the cause of this behavior. When the original sample, a mixture of form I and form IV, was slurried in MeCN–water mixtures, it changed to pure form I.

Lattice energies of the polymorphs

The lattice energies (E_{latt}) of the polymorphs (Table 3) were calculated to get understanding of the energies governing the packing of the forms.

The computed E_{latt} of different TE polymorphs are inside 3 kcal mol^{-1} and indicate a stability order of I > II > III which is supported by the available experimental observations. The van der Waals energy (E_{vdw}) component, which describes the non-bonding attractive and repulsive interactions, is typically most accurately modeled by the force field calculations. This is considerably larger, indicating denser packing, for form II compared to forms I and III, which is in-line with the crys-tallographical densities of the polymorphs. Also the fingerprint plots (Fig. 1) show average shorter intermolecular distances for form II. The calculated coulombic energies (E_C), which describe the electrostatic interactions in the crystal, show a discrepancy in that the energy value for TE form II is positive, indicating an unfavorable interaction. The cause for this is likely the short intra- and intermolecular C=O···O=C distances which are in the range of 3.05 to 3.11 Å. The E_C calculations, however, are problematic due to inaccurate determination of the electronic charges and should be judged with some caution.[20] Calculated hydrogen bond energies (E_H)[21] gave similar energies for forms I and II, but clearly lower for form III. The result is somewhat surprising as the fingerprint plots indicate that form I has some substantially stronger intermolecular hydrogen bonds than the two other polymorphs. However, the high E_H term of form II can be explained by the intramolecular N–H···O=C bonds which are most linear and shortest in form II.
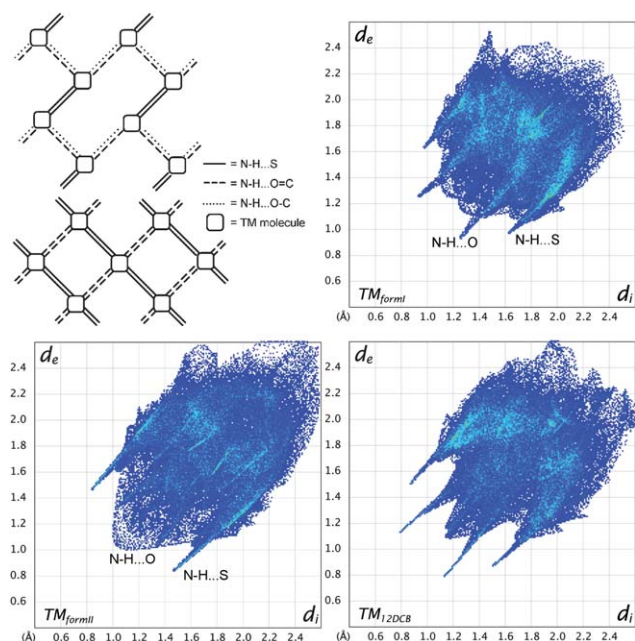
Table 3 Lattice energies of the polymorphs of TE and TM in kcal mol^{-1}

Polymorph	E_{vdw}	E_C	E_H	E_{latt}
TE form I	−33.96	−1.89	−6.08	−41.94
TE form II	−38.38	4.09	−6.02	−40.31
TE form III	−31.81	−3.90	−3.41	−39.11
TM form I	−33.99	−8.54	−3.18	−45.71
TM form II	−29.79	−1.20	−6.13	−37.11

The energy calculations of TM polymorphs gave significantly higher E_{vdw} for form I as also indicated by the packing coefficient and the fingerprint plot in Fig. 4, but also indicate stronger total hydrogen bonding (E_H) in the crystals of form II. In any case, the total E_{latt} shows that form I is clearly the more stable of the two polymorphs, though, the relatively high E_C of form I might be overestimated and thus exaggerate the total energy difference.

Structural comparison to TM

A hydrogen bonding diagram and fingerprint plots of TM forms I and II were drawn for comparison (Fig. 4). The polymorphs of TE and TM do not have matching hydrogen bonding arrange-ments. TE form I and TM form II are very similar at a quick glance but the hydrogen bonds are different. The structure of the hydrogen bonded sheets in TE form I is, however, identical to that of TM in the 1,2-dichlorobenzene solvate[9] (fingerprint plot in Fig. 4). In the TM solvate the solvent molecules are located between the sheets that are consequently further away from each other than in the TE polymorph. The extra methyl groups of TE possibly enable closer packing of the sheets without the need for guests. A conformation where the sulfur atoms are on the same side of the benzene ring is interestingly only seen in these two structures of all the 26 solved structures for TM[9] and TE.

The conformation of the TE molecule in form II is most like that of the TM molecule in the benzene solvate.[9] The other arm of the molecule, however, is not as planar as in TE form II and consequently the intramolecular C=O···O=C distance that in TE form II is 3.11 Å is now 3.66 Å. The hydrogen bonding pattern is somewhat different in these two structures with the TM solvate having chains of TM connected with the common R2,2(8) motif as well as a R2,2(8) ether O pairing motif.

The hydrogen bonded chains of TE and packing in form III is most similar to that in the very stable ethanol and methanol solvates of TM, which also have a Z' of 2. The D1,1(2) motif and the unused C=S acceptor in one of the TE molecules in form III are replaced in the TM solvents by hydrogen bonds to the solvent molecules.

The same hydrogen bonding motifs are consistently found in the structures of TE and TM. The N–H···S R2,2(8) motif is very prevalent in forming chains as well as pairs of molecules. The R2,2(12) C=O···H–N motif, that is seen for TE only in form I and form III, is much more common for structures of TM where 12 out of 16 structures have this motif. Mixed pairing of hydrogen bonds to sulfur and oxygen is shown in only a couple of structures like the R2,2(10) motif in TE form I. Some forms of TM also use the ether O for hydrogen bonding, but this is not seen in the structures of TE.

Fig. 4 Hydrogen bonding diagram and fingerprint plots of TM form I, form II and the 1,2-dichlorobenzene solvate.

TE solvates

Structures of four isomorphous solvates (acetone, dioxane I, DCM and chloroform), a toluene solvate, a dioxane solvate polymorph and a pyridine solvate of TE were acquired.

In all the solvates the hydrogen bonding consists of N–H⋯S hydrogen bonds in the R2,2(8) motif with no intermolecular N–H⋯O=C bonds. In the isomorphous solvates the R2,2(8) motifs connect into chains (Fig. 5a) that pack parallel to each other with π–π stacking interactions to neighboring parallel chains with ring distances of approximately 3.4 Å. The solvent molecules are located between the arms of the TE molecules in channels running through the structure in the direction of the crystallographic c-axis (Fig. 5b).

In the pyridine and dioxane II solvates the N–H⋯N or N–H⋯O D(2) motifs to the solvent, respectively, block the formation of chains of TE molecules leaving only hydrogen bonded pairs of TE molecules (Fig. 6a and b) connected with the R2,2(8) motif.

In the toluene solvate the R2,2(8) motifs connect into spiraling chains, causing the chirality of the structure (Fig. 7). The parallel spirals intertwine making up stacks of benzene rings running through the structure. The disordered toluene molecules are located in channels running in the same direction as the elongation of the spirals.

According to the packing coefficients (Fig. 3) the hydrogen bonded pyridine and dioxane solvates pack more tightly than the isomorphous and toluene solvates, the only exception being dioxane I, where the dioxane molecule more effectively fills the space available for it in the solvent channels. The isomorphous and toluene solvate crystals are very unstable when out of solution, desolvating in seconds per minute, whereas the hydrogen bonded solvates, especially pyridine, are stable for hours.
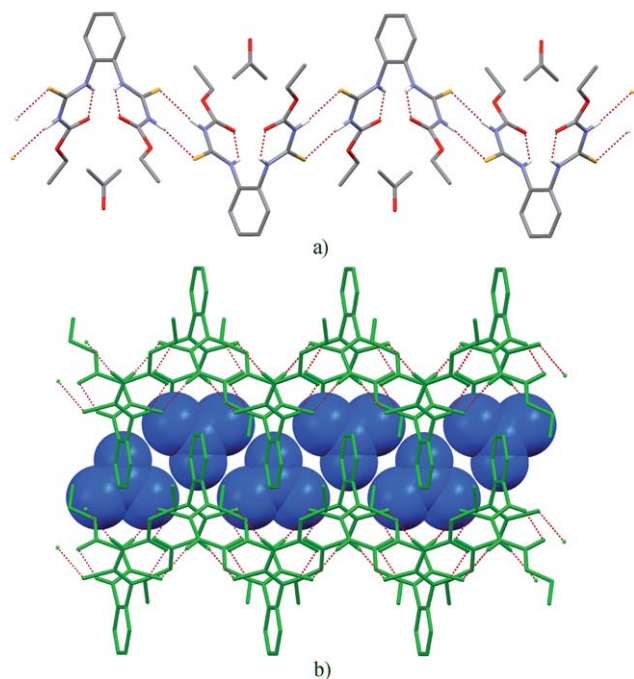
Comparison to TM solvates. Both TE and TM have a large amount of solvates (Table 4), though neither has been found to have a pure hydrate. Even though TM and TE are very similar it is difficult to find clearly similarly hydrogen bonded structures between them. The closest analogues are the pyridine solvates, in which the pyridines are N–H⋯N hydrogen bonded to the thiophanates.

Interestingly, no methanol and ethanol solvates of TE were found, whereas in the case of TM these solvates crystallize easily and are very stable. The methanol and ethanol solvates of TM are isomorphous with each other and also very similar in hydrogen bonding to the acetone and cyclohexanone solvates. Likely, the formation of similar solvates of TE is hindered by packing problems regarding the larger size and more lipophilic nature of TE. The same kind of hydrogen bonding is, however, exhibited by TE form III, which has voids in the structure and likely if the correct solvent and crystallization conditions could be found, a solvate with similar hydrogen bonding could crystallize.

TE, unlike TM, is able to make evident solvent channels that run in between the two arms of the molecule. In addition to acetone, dioxane, dichloromethane and chloroform other solvent molecules of similar size (molecular volume of around 55 to 90 Å³, see Table 4) are suspected to fit in these channels and also form isomorphous solvates. Ethanol is perhaps too small, but propanol could be ideal and 1,2-dichloroethane and DMSO possible solvate formers. The molecular volume of pyridine (∼80 Å³) is also such that it could fit in the solvent channels. The strong hydrogen bonding interactions between the solvent and the TE molecules, however, seem to determine the structure of the solvate in this case. Toluene is likely too large or unsuitably shaped to fit in the solvent channels and thus makes another type of structure.
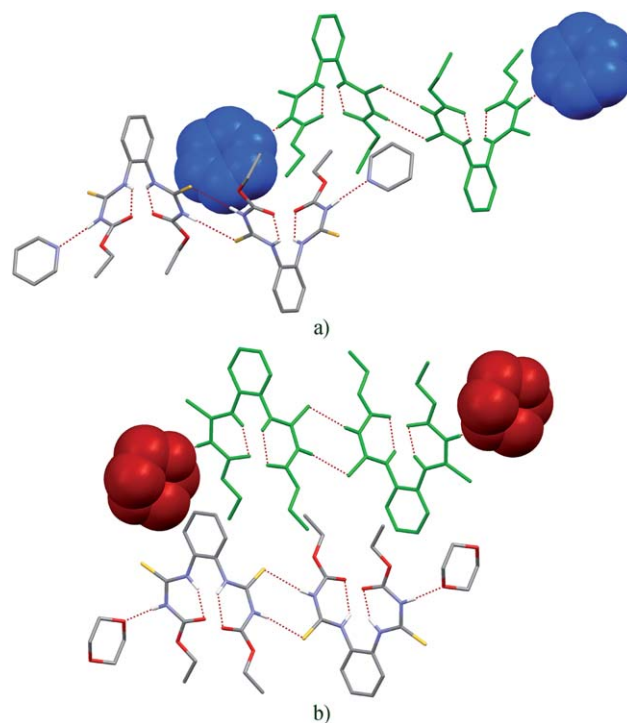

Fig. 5 (a) Hydrogen bonded chains of TE acetone solvate and (b) the channels of acetone in the structure with non-hydrogen bonding hydrogen atoms removed for clarity.

Fig. 6 Two hydrogen bonded double pairs of (a) the TE–pyridine solvate and (b) the TE–dioxane solvate with non-hydrogen bonding hydrogen atoms removed for clarity.
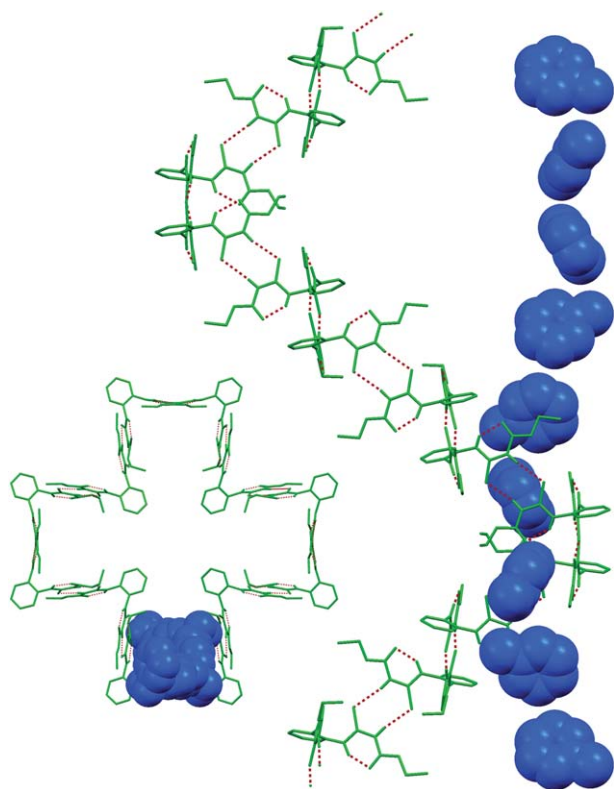
Fig. 7 One spiral in the toluene solvate from the side and top with toluene molecules in space fill style and non-hydrogen bonding hydrogen atoms and disorder removed for clarity.

Table 4 Molecular volumes[a] of some common solvents and whether TM or TE solvates have been found with these

Solvent	Molecular volume	TM solvate	TE solvate
Water	18.02	–[b]	—
Methanol	37.21	Yes	—
Acetonitrile	46.06	Yes[b]	—
Ethanol	54.16	Yes	—
DCM	56.51	Yes	Yes
Acetone	64.74	Yes	Yes
Chloroform	70.07	Yes	Yes
1/2-Propanol	70.82/70.60	*	*
DMSO	71.43	Yes	–
1,2-Dichloroethane	73.31	Yes	–
THF	77.99	Yes	*
Pyridine	79.89	Yes	Yes
Benzene	87.04	Yes	*
Dioxane	86.97	Yes	Yes 2
Dimethylacetamide	94.09	–	*
Toluene	100.61	–	Yes
Cyclohexanone	104.79	Yes	*
1,2-Dichlorobenzene	111.12	Yes	*

[a] Volumes from molinspiration.com. [b] A MeCN/H$_2$O combination solvate, – none found or * not tested.

Conclusions

Four polymorphs and seven solvates of thiophanate-ethyl were found and the crystal structures of all except polymorph IV solved. Thiophanate-ethyl and thiophanate-methyl are examples of when the applicability of a supramolecular synthon approach

alone is limited. The behavior of TE is quite similar to that of thiophanate-methyl in that both willingly form solvates and polymorphs, but with varying combinations of hydrogen bonding motifs and conformations of molecules. The N–H⋯O=C bond is the strongest possible hydrogen bond for TM and TE so one would expect it to show up more frequently than the weaker N–H⋯S=C hydrogen bond. This, however, is not the case, especially for TE. Moreover, the solvate structures of the two actives vary greatly giving no general strategies for the design of cocrystals.

The challenge is that even though there are clearly a few best hydrogen bonding motifs, the conformational possibilities enable these to be used in a variety of combinations, which cannot be predicted. Another reason is the possibility for other weaker and not so directional, but combinatorially strong interactions like π–π-stacking and lipophilic effects. These can outweigh the propensity for certain kinds of hydrogen bonding synthons between molecules, like in the isomorphous solvates of TE. The reduction in void space is another factor since the energetic advantages in a certain kind of packing of molecules are difficult to predict.

We expect a supramolecular synthon approach to be most applicable with conformationally rigid molecules that have a limited number of clear hydrogen bonding possibilities. Another case where a supramolecular approach could be used successfully, even with more complicated systems, would involve using reoccurring hydrogen bonds, like the hydrogen bond from TE/TM to the pyridine nitrogen. A further strategy for cocrystal design with TE could be in fitting small cocrystallizing molecules in the channels of the isomorphous solvates.

Notes and references

1 J. Bernstein, *Polymorphism in Molecular Crystals*, Oxford University Press, United States, 2002; H. G. Brittain, *Polymorphism in Pharmaceutical Solids*, Marcel Dekker, Inc., New York, USA, 1999.

2 U. J. Griesser, in *Polymorphism in the Pharmaceutical Industry*, ed. R. Hilfiker, WILEY-VCH Verlag GmbH & Co. KGaA, Weinheim, Germany, 2006, pp. 211–234.

3 O. Almarsson and M. J. Zaworotko, *Chem. Commun.*, 2004, 1889–1896, DOI: 10.1039/b402150a; N. Blagden, M. de Matas, P. T. Gavan and P. York, *Adv. Drug Delivery Rev.*, 2007, **59**, 617–630, DOI: 10.1039/b402150a; P. Vishweshwar, J. A. McMahon, J. A. Bis and M. J. Zaworotko, *J. Pharm. Sci.*, 2006, **95**, 499–516, DOI: 10.1039/b402150a.

4 G. R. Desiraju, *Angew. Chem., Int. Ed. Engl.*, 1995, **34**, 2311–2327; A. Nangia and G. R. Desiraju, *Acta Crystallogr., Sect. A: Found. Crystallogr.*, 1998, **54**, 934–944, DOI: 10.1107/S0108767398008551; C. B. Aakeröy and D. J. Salmon, *CrystEngComm*, 2005, **7**, 439–448, DOI: 10.1039/b505883j; G. R. Desiraju, *Angew. Chem., Int. Ed.*, 2007, **46**, 8342–8356, DOI: 10.1107/S0108767398008551.

5 A. I. Kitaĭgorodskiĭ, *Organic Chemical Crystallography*, Consultants Bureau, New York, 1961.

6 M. A. Spackman and J. J. McKinnon, *CrystEngComm*, 2002, **4**(66), 378–392.

7 Z. J. Li, W. H. Ojala and D. J. W. Grant, *J. Pharm. Sci.*, 2001, **90**, 1523–1539.

8 M. C. Etter and J. C. MacDonald, *Acta Crystallogr., Sect. B: Struct. Sci.*, 1990, **46**, 256–262; J. Bernstein, R. E. Davis, L. Shimoni and N.-L. Chung, *Angew. Chem., Int. Ed. Engl.*, 1995, **34**, 1555–1573.

9 E. Nauha, H. Saxell, M. Nissinen, E. Kolehmainen, A. Schäfer and R. Schlecker, *CrystEngComm*, 2009, **11**, 2536–2547, DOI: 10.1039/b905511h.

10 R. Israels, H. E. Saxell, M. Bratz, M. Kuhns and P. Erk, *Pat.*, WO/2008/096005, 08. 02. 2008

11 Eu Commission, *Off. J. Eur. Communities*, 23. 11. 2002, **L319**, 3–11.

12 PANalytical B.V., 2006, 2.2b.

13 Z. Otwinowski, D. Borek, W. Majewski and W. Minor, *Acta Crystallogr., Sect. A: Found. Crystallogr.*, 2003, **59**, 228–234, DOI: 10.1107/S0108767303005488.

14 G. M. Sheldrick, *Acta Crystallogr., Sect. A: Found. Crystallogr.*, 2008, **64**, 112–122, DOI: 10.1107/S0108767307043930.

15 C. F. Macrae, P. R. Edgington, P. McCabe, E. Pidcock, G. P. Shields, R. Taylor, M. Towler and J. van de Streek, *J. Appl. Crystallogr.*, 2006, **39**, 453–457, DOI: 10.1107/S002188980600731X.

16 *Crystal Packer Program in Cerius2 Program Package, 4.6, Accelrys*, 2001.

17 M. A. Neumann and M.-A. Perrin, *J. Phys. Chem. B*, 2005, **109**, 15531–15541; M. A. Neumann, *J. Phys. Chem. B*, 2008, **112**, 9810–9829.

18 J. W. Steed, *CrystEngComm*, 2003, **5**, 169–179; G. R. Desiraju, *CrystEngComm*, 2007, **9**, 91–92; K. M. Anderson and J. W. Steed, *CrystEngComm*, 2007, **9**, 328–330.

19 The packing coefficient describes the tightness of the packing of molecules in a crystal, with a bigger value meaning tighter packing, and is calculated with the formula $C(k) = Z*V(mol)/V(cell)$, where Z is the number of molecules in the unit cell, $V(mol)$ is the molecular volume of the molecules and $V(cell)$ is the volume of the unit cell. For these calculations the disorder of the solvent was not taken into consideration.

20 S. Brodersen, S. Wilke, F. J. J. Leusen and G. Engel, *Phys. Chem. Chem. Phys.*, 2003, **5**, 4923–4931.

21 The E_H is computed in Cerius2 by 12–10 potential with an angular term: $E_H = (C_{ij}/r_{ij}^{12}) - (D_{ij}/r_{ij}^{10}) \cos^4 \theta$, where θ is the angle between the donor, hydrogen and acceptor and C and D are empirical parameters. Accurate determination of the hydrogen bond energy is, however, problematic for several reasons of which one is the power of 10 in the attractive term which makes the function sensitive for the separation of the hydrogen and acceptor atom as the energy drops rapidly with the increasing distance. The function is also sensitive for the bonding angle due to the power of 4 in the cosine θ term.

III

Packing incentives and a reliable N-H···N-pyridine synthon in co-crystallization of bipyridines with two agrochemical actives

by

E. Nauha, E. Kolehmainen & M. Nissinen, 2011

CrystEngComm 13 (2011), 6531-6537. DOI:10.1039/C1CE05730H.

Packing incentives and a reliable N–H···N–pyridine synthon in co-crystallization of bipyridines with two agrochemical actives†

Elisa Nauha, Erkki Kolehmainen and Maija Nissinen*

The co-crystallization of agrochemical actives thiophanate-methyl and thiophanate-ethyl with 2,2′-bipyridine, 4,4′-bipyridine and 1,2-bis(4-pyridyl)ethane was investigated with conventional crystallization, the slurry method and liquid-assisted grinding. Co-crystals of both thiophanates with all bipyridines were found and the structures solved with single crystal X-ray diffraction. Whereas the 2,2′-bipyridine co-crystals seem to form because of a combination of weak interactions, and in the case of the thiophanate-methyl, partly because of close packing incentives, the 4,4′-bipyridine and 1,2-bis(4-pyridyl)ethane co-crystals form mainly because of a favourable N–H···N–pyridine hydrogen bonding synthon.

Introduction

The phenomenon of co-crystallization[1,2] is important for pharmaceutical,[3–5] agrochemical[6,7] and other industrial applications because of the different and sometimes improved properties of co-crystals of active ingredients compared to those of the parent molecules. For pharmaceutical applications the goal of co-crystal forms is usually to increase the solubility and bioavailability of the active ingredient while maintaining the physical stability of the dosage form, but for agrochemical actives, which are often administered as slurry formulations in water, the goal is to lower the solubility of the active to make a more stable formulation and stop the active being washed away too soon once administered.

In a simplified model co-crystallization can be seen to arise for two different reasons, either close packing or favorable hydrogen bonding interactions.[1,8] The strategy to find co-crystals that form because of close packing requires a trial and error approach since it is very hard to predict if a pair of molecules can pack tightly. For co-crystals caused by favorable hydrogen bonding interactions one can make educated guesses about possible co-crystal formers based on the knowledge about hydrogen bonding synthons[9] with, for example, the help of the CCDC database. In practice, however, packing in crystals is influenced by an intricate combination of close packing incentives, hydrogen bonding and other interactions, and therefore there is as yet no reliable way to design co-crystals.

Earlier, we investigated the polymorphism and versatile solvate formation of two agrochemical actives, thiophanate-methyl (TM)[10] and thiophanate-ethyl (TE)[11] (Scheme 1), and

now decided to examine co-crystallization with common co-crystal formers, namely 4,4′-bipyridine (44bp)[12–17] and 2,2′-bipyridine (22bp)[18] (Scheme 1) as pyridine solvates of TM and TE are also known. Due to the success with the first bipyridines, crystallizations with the similar 1,2-bis(4-pyridyl)ethane (44bpe) (Scheme 1) were also attempted. An important goal was to see how much the difference of one carbon at the end of the chains in TE, in comparison to TM, affects the crystallization behavior and packing of the molecules.

Experimental

Materials

TM (IUPAC: dimethyl 4,4′-(*o*-phenylene)bis(3-thioallophanate)) of 99.8% purity from BASF, TE (IUPAC: diethyl 4,4′-(*o*-phenylene)bis(3-thioallophanate)) of 99% purity from Chem Service, 2,2′-bipyridine from Merck, 4,4′-bipyridine from Sigma-Aldrich,
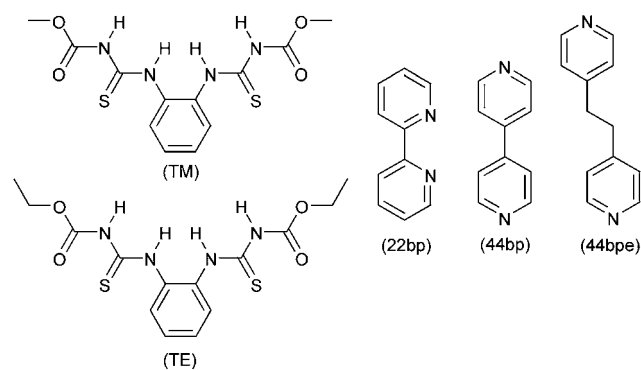
Scheme 1 Molecular structures of thiophanate-methyl (TM), thiophanate-ethyl (TE), 2,2′-bipyridine (22bp) and 4,4′-bipyridine (44bp), and 1,2-bis(4-pyridyl)ethane (44bpe).

University of Jyväskylä, Department of Chemistry, Nanoscience Center, P.O. Box 35, FI-40014 Jyväskylä, Finland. E-mail: maija.nissinen@jyu.fi; Fax: +358 14 260 4756; Tel: +358 14 260 4242

1,2-bis(4-pyridyl)ethane (99%) from Aldrich, distilled water and solvents of analytical purity (min 99%) were used in the crystallization, slurry and milling experiments.

Slurries

Slurries of TM with the 22bp and 44bp were carried out in a acetonitrile : water solution. The slurries were mixed for three days at 50 °C, filtered with suction and let dry in open vessels.

Crystallizations

Equimolar (1 : 1) amounts (<40 mg in total) of the compounds were weighed and dissolved in acetonitrile; the solutions were transferred to clean crystallization test tubes, which were covered with parafilm with a few holes and the solvent was let evaporate in room temperature. Crystallization of TM with 22bp and TE with 44bp was also attempted in ethanol with and without seeding by the grinded samples, but the crystallizations produced single crystals of the ethanol solvate of TM[10] and form I of TE,[11] respectively.

Grinding

Liquid-assisted grinding was carried out on a Retsch MM 200 ball mill in 10 ml milling vessels for 20 min with an oscillation frequency of 20 s^{-1}. 50 mg of TM/TE and a molar amount of 22bp or 44bp, according to the ratio in the co-crystal structures, were weighed and a few drops of 1 : 1 water : ethanol solution were added to the milling vessels. All but the TE–44bp mixture produced PXRD patterns similar to the calculated patterns from the structures. For the TE–44bp mixture and the TM–22bp mixture, milling was also done with 3 drops of 25% MeCN in water to confirm the results.

Thermomicroscopy

The behavior of the 22bp and 44bp co-crystals during heating was studied under polarized light with a Mettler FP82HT hot stage connected to a Mettler FP90 central processor with an Olympus BH-2 microscope. The primary heating rate used was 10 °C min^{-1} from 30 °C to melting/decomposition of the sample.

PXRD

For powder X-ray diffraction analyses the samples were pressed to a zero background silicon plate sample holder and measured on a PANalytical X'Pert Pro system in reflection mode with non-monochromated Cu-radiation. A 2θ angle range of 5–35° and a step time of 38 s were used with step resolution of 0.0167°. Figures were drawn with X'Pert HighScore Plus.[19]

Single crystal X-ray diffraction

The X-ray diffraction data were collected on a Nonius Kappa CCD diffractometer with an Apex II detector, using graphite-monochromated CuKα radiation (λ = 1.54178 Å) at 173 K. The structures were solved by direct methods, refined, and expanded by Fourier techniques with the SHELX-97 software package.[20] Absorption correction was performed with Denzo 1997.[21] All non-hydrogen atoms were refined anisotropically. Hydrogen atoms were placed in idealized positions, or in the case of hydrogen bonding hydrogens, found from the electron density map and included in structure factor calculations. The N–H hydrogen atoms found in the electron density map were restrained to a distance of 0.91 Å to give the best fit to the X-ray data and to ensure stable refinement. Pictures of the structures were drawn with Mercury.[22] Crystal data and collection parameters of the structures are presented in Table 1.

^{13}C CP/MAS NMR

The ^{13}C CP/MAS NMR spectra of the slurried TM samples were measured with a Bruker Avance 400 FT NMR spectrometer with a dual 4 mm CP/MAS probehead. The sample was packed in a 4 mm diameter ZrO_2 rotor, which was spun at 10 kHz rate at 296 or 373 K. The contact time for CP was 4 ms, pulse interval 4 s, time domain 2 K, which was zero filled to 8 K in the frequency domain. Exponential window function with 5 Hz line broadening was used. 20 000 scans were acquired. [13]C shifts are referenced to the CO-signal of glycine (176.03 ppm) measured before the TM sample.

Results and discussion

The formation of the TM co-crystals with 4,4′-bipyridine and 2,2′-bipyridine was first observed in slurry experiments, with the results confirmed by PXRD and ^{13}C CP/MAS NMR, after which they were also found to crystallize from solution. Co-crystals for TE were acquired directly with solution crystallization and also used in the liquid-assisted grinding and thermomicroscopy experiments. The 1,2-bis(4-pyridyl)ethane co-crystals were later acquired by solution crystallization for structural comparison.

^{13}C CP/MAS NMR results

High resolution solid state NMR and especially ^{13}C CP/MAS is nowadays often used as an aid or complementary technique in polymorph, solvate and co-crystal characterization.[10,23] In this work ^{13}C CP/MAS spectra were measured for the TM–22bp and TM–44bp co-crystals, acquired by the slurry method, as well as for pure TM alone (Fig. 1). The assignment of the spectra is based on the comparison with liquid state NMR spectra.

In the TM spectrum its C=O resonance is at 153.8 ppm and the aromatic carbons give three resonances as expected by symmetry reasons at 135.8, 131.9 and 126.3 ppm, respectively. C=S resonances are at 180.9 and 174.2 ppm, respectively. The tentative assignments of 2,2′-bipyridine resonances in the TM–22bp co-crystal spectrum are at 154.7 ppm (carbons 1,1′), 149.4 (carbons 3,3′), 137.1 ppm (carbons 5,5′), 126.1 ppm (carbons 4,4′) and 120.8 ppm (carbons 6,6′), respectively. In the spectrum of TM–44bp, 4,4′-bipyridine signals are easy to find and assign at 149.9 ppm (carbons 3,3′, 5,5′), 143.7 ppm (carbons 1,1′) and 121.3 ppm (carbons 2,2′, 6,6′). Differing from the TM sample in this co-crystal TM's CH_3O-signals exist as a doublet at 55.0 and 53.7 ppm. In TM–22bp spectrum the CH_3O-group shows two resonances but differs from TM–44bp with nonequal intensities.

Comparison of TM–44bp and TM–22bp spectra reveals that the chemical shift differences of C=S resonances (at 182.5 and 180.5 ppm) in TM–44bp co-crystal are clearly smaller than in TM–22bp where those are at 183.3 and 175.9 ppm, respectively.

Table 1 Crystal data and collection parameters for the co-crystal structures

Compound reference	TM–22bp	TE–22bp	TM–44bp	TE–44bp	TM–44bpe	TE–44bpe
Chemical formula	$2(C_{12}H_{14}N_4O_4S_2)\cdot$ $1.5(C_{10}H_8N_2)\cdot C_2H_3N$	$C_{14}H_{18}N_4O_4S_2\cdot$ $0.5(C_{10}H_8N_2)$	$C_{12}H_{14}N_4O_4S_2\cdot$ $0.5(C_{10}H_8N_2)$	$C_{14}H_{18}N_4O_4S_2\cdot$ $C_{10}H_8N_2$	$2(C_{12}H_{14}N_4O_4S_2)\cdot$ $C_{12}H_{12}N_2$	$2(C_{14}H_{18}N_4O_4S_2)\cdot$ $C_{12}H_{12}N_2$
Formula Mass	960.11	448.54	420.48	526.63	869.02	925.12
Crystal system	Triclinic	Monoclinic	Triclinic	Triclinic	Triclinic	Triclinic
a/Å	10.6193(3)	8.3860(7)	9.0382(2)	11.8193(4)	9.0972(2)	11.9780(10)
b/Å	15.0562(4)	17.2950(12)	9.5723(2)	12.8098(5)	9.5762(2)	14.1211(12)
c/Å	16.2601(4)	15.4566(11)	12.5370(3)	26.3527(10)	23.8891(3)	14.9536(12)
α/°	108.694(4)	90.00	100.183(3)	91.574(2)	86.224(1)	107.572(4)
β/°	95.323(3)	98.93(3)	104.203(3)	95.655(2)	88.273(1)	106.503(5)
γ/°	109.312(4)	90.00	101.444(3)	100.640(3)	88.214(1)	91.062(4)
Unit cell volume Å^{-3}	2265.87(10)	2214.6(3)	1001.16(4)	3897.9(2)	2074.79(7)	2296.8(3)
Space group	P-1	$P2(1)/c$	P-1	P-1	P-1	P-1
Z	2	4	2	6	2	2
Meas. reflns	10 805	6504	4322	18 442	10 604	9982
Indep. reflns	7733	3778	3298	13 511	7144	7030
R_{int}	0.0585	0.0975	0.1194	0.1463	0.1069	0.1410
Final R_1 values ($I > 2\sigma(I)$)	0.0517	0.0713	0.0657	0.0802	0.0604	0.0688
Final w$R(F^2)$ values ($I > 2\sigma(I)$)	0.1257	0.1812	0.1788	0.2103	0.1459	0.1382
Final R_1 values (all data)	0.0722	0.1077	0.0735	0.1094	0.0832	0.1494
Final w$R(F^2)$ values (all data)	0.1394	0.2117	0.1882	0.2389	0.1628	0.1758
Goodness of fit on F^2	1.032	1.039	1.069	1.071	1.043	1.018

Taking into account the X-ray data (see below) it is quite clear to assign the TM–22bp resonance at 175.9 ppm to that one involved in hydrogen bonding. According to X-ray data C=S groups do not form hydrogen bonds in TM–44bp co-crystal, which explains the small shift difference. In pure TM sample the C=S shift difference is very close to that of TM–22bp suggesting similar hydrogen bonding behavior.

Surprisingly no trace from MeCN is visible in TM–22bp spectrum although the powder X-ray pattern of the sample is similar to the calculated pattern of a structure that contains also MeCN. This, together with the ability of the co-crystal to form also in ethanol solution, suggests that the co-crystal is still intact even without the MeCN.

Co-crystal structures with 2,2′-bipyridine

The MeCN solvate of the TM co-crystal with 2,2′-bipyridine crystallized in space group $P\bar{1}$ with a TM : 22bp : MeCN ratio of 4 : 3 : 2, containing half of this in the asymmetric unit. The TM molecules build up double chains composed of rings of four TM molecules hydrogen bonded to each other (Fig. 2a). The rings are made with two hydrogen bonding arrangements, one of which is a $R2,2(8)$ motif[24] composed of two N–H···S hydrogen bonds and the other a second order $R2,2(8)$ motif with one N–H···S and one N–H···O–C hydrogen bond. There is also a very weak C–H···O–C bond supporting the connection with this motif. The rings of TM arrange into chains with a $R2,2(12)$ motif of two N–H···O=C hydrogen bonds.

One of the 22bp molecules resides right inside the ring of TM molecules while the other 22bp molecule along with the MeCN molecules is located between the TM double chains. There are edge-to-face aromatic interactions between the benzene rings of the TM molecules and the 22bp that are located outside the rings

with ring centroid-C distances of 3.71 and 3.94 Å, and subsequent ring centroid-H distances of 2.78 and 3.03 Å.

The TE co-crystal with 2,2′-bipyridine crystallized in space group $P2_1/c$ with a molecule of TE and half a molecule of 22bp in the asymmetric unit, giving the ratio of 2 : 1. The TE molecules build up hydrogen bonded chains (Fig. 2b) with an $R2,2(8)$ motif consisting of two N–H···S hydrogen bonds. There are additionally only intramolecular N–H···O=C hydrogen bonds in an $S(6)$ motif. The chains of TM pack parallel to each other with π–π stacking interactions to neighboring chains with ring distances of approximately 3.4 Å. The 22bp molecules are located in between the arms of the TE molecules in channels running through the structure in the direction of the crystallographic a axis (Fig. 2b). There are weak hydrogen bonds between the 22bp nitrogens and the ethyl hydrogens of TE molecules in neighboring chains. The arrangement of TE molecules in the structure of this co-crystal is interestingly the same as that in the previously obtained isomorphous acetone, DCM, chloroform and dioxane solvates of TE[11] with the 22bp taking up the space of two solvent molecules.

Co-crystal structures with 4,4′-bipyridine

In the TM·4,4′-bipyridine co-crystal the TM to 44bp ratio is 2 : 1, while in the TE·4,4′-bipyridine co-crystal the TE to 44bp ratio is 1 : 1. However, there are similarities in the hydrogen bonding patterns of these co-crystals (Fig. 3a and b). The similar hydrogen bonded unit consists of two molecules of TM/TE connected with an $R2,2(12)$ motif of two N–H···O=C hydrogen bonds and two molecules of 44bp which are hydrogen bonded to this pair. The difference of the structures lies in the hydrogen bonding of these units into chains.

The TM co-crystal with 4,4′-bipyridine crystallized in space group P-1, with one molecule of TM and half a molecule of 44bp
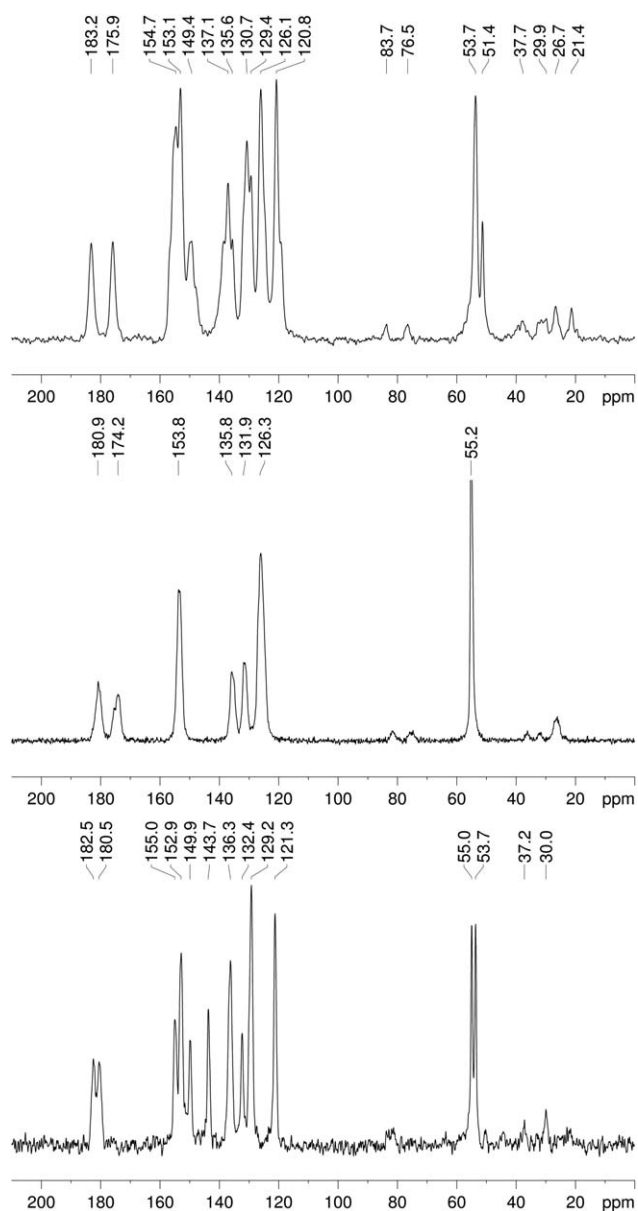
Fig. 1 CPMAS NMR of the TM–22bp co-crystal (top), TM form I (middle) and the TM–44bp co-crystal (bottom).
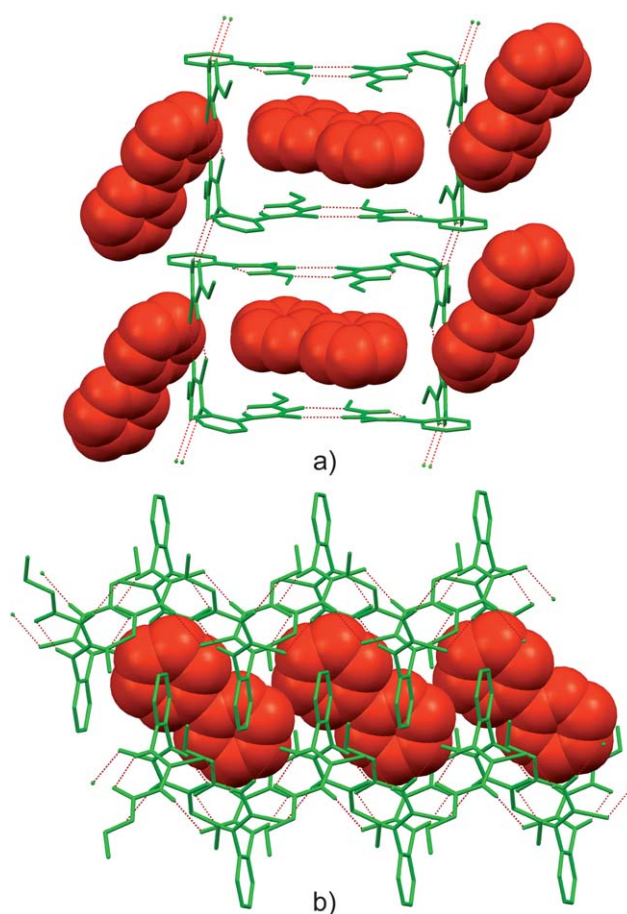

Fig. 2 (a) Rings of TM with 22bp in the MeCN solvate of the TM co-crystal with 22bp and (b) the channels of 22bp in the TE co-crystal with 22bp. MeCN molecules and C–H hydrogen atoms removed for clarity.
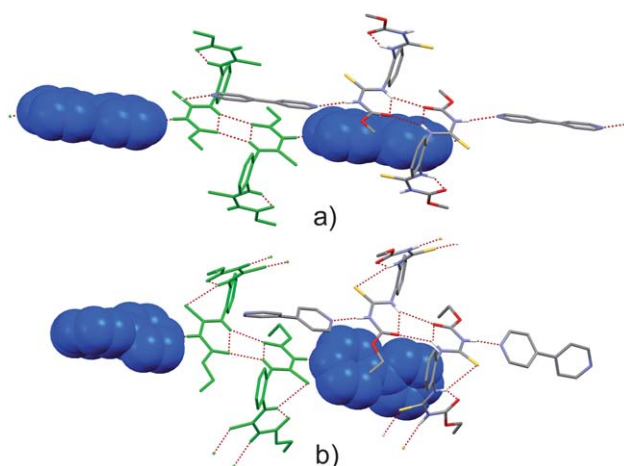

Fig. 3 Hydrogen bonding and packing in the (a) TM and (b) TE–44bp co-crystals with C–H hydrogen atoms removed for clarity.

in the asymmetric unit. The $R2,2(12)$ hydrogen bonded pairs are connected with hydrogen bonds to the 44bp molecules making up infinite parallel chains where a pair of TM molecules and a 44bp molecule alternate (Fig. 3a). Interestingly, in this structure the sulfur atoms are not involved in hydrogen bonding and one N–H hydrogen is also left without a hydrogen bond acceptor.

The TE co-crystal with 4,4′-bipyridine crystallized in space group P-1, with three molecules of TE and three molecules of 44bp in the asymmetric unit. The symmetrically different molecules of TE are fairly similar in conformation, with differences mostly in the orientation of the ethyl groups at the ends of the arms. The torsion angles of the ethyl group from the C=O groups are 170.2°, −156.1°, 165.1°, 179.2°, −88.9° and 155.1°. The symmetrically different molecules also have the same

hydrogen bonds to neighboring molecules. The reason for so many molecules in the asymmetric unit seems to be the combined influence of the flexibility of conformation of the ends of the arms of the TE molecules and in the variable conformations of the

44bp molecules. The torsion angles between the rings of the 44bp molecules are 41.3°, 43.4° and 44.9°.

The R2,2(12) hydrogen bonded pairs are connected with an R2,2(8) motif of two N–H⋯S hydrogen bonds to neighboring pairs forming hydrogen bonded chains of TE molecules in the structure (vertical direction in Fig. 3b). These chains pack parallel to each other with the 44bp molecules of the neighboring chains located partly in between the arms of the TE molecules. Unlike in the TM co-crystal, the other pyridine acceptor in the 44bp does not take part in hydrogen bonding.

Co-crystal structures with 1,2-bis(4-pyridyl)ethane

Both the 1,2-bis(4-pyridyl)ethane co-crystals crystallized in space group P-1, with a ratio of 2 : 1 (TM/TE : 44bpe). Also in these co-crystals the TM/TE molecules make pairs connected with an R2,2(12) motif of two N–H⋯O=C hydrogen bonds, and two molecules of 44bpe are hydrogen bonded to this pair.

In the TM co-crystal with 1,2-bis(4-pyridyl)ethane there are two unconnected domains in the structure consisting of the symmetry unequivalent TM molecules and half molecules of 44bpe on an inversion center. In one case the pairs are only connected with hydrogen bonds to the bipyridine, similarly to the TM co-crystal with 44bp, making up chains, but in the other case the hydrogen bonded pairs are connected with a D(2) N–H⋯S motif to other TE molecules to build up double chains which then connect into sheets *via* the bipyridine molecules (Fig. 4a). The two domains make up sheets that stack up on each other in the crystal.

In the TE co-crystal with 1,2-bis(4-pyridyl)ethane the hydrogen bonding between the TE molecules is identical to that in the TE co-crystal with 44bp, but additionally the TE chains are connected *via* the 44bpe molecules like in the TM co-crystal with 44bp (Fig. 4b). In the chains of TE pairs of the two symmetry unequivalent TE molecules connected with the R2,2(12) motif alternate.

Packing incentives

The packing coefficients[25] (Fig. 5) for co-crystal structures were calculated using the formula $C(k) = Z \times V(mol)/V(cell)$, where Z is the number of molecules in the unit cell, $V(mol)$ is the molecular volume of the molecules,[26] and $V(cell)$ is the volume of the unit cell. When compared to the packing coefficients of the two polymorphs of TM and the three polymorphs of TE,[11] the results indicate that the packing of the co-crystals is in general more loose-fitting than that of the polymorphs with the TM–22bp co-crystal being the exception. Form III of TE is left out of consideration as the structure has voids and is thus very loosely packed.

As the 2,2′-bipyridines are not hydrogen bonded to the TM/TE molecules in either of the co-crystal structures, the reason for the formation of structures is in the packing of the thiophanates and the template effect of the 22bp. The 22bp co-crystal with TM forms most likely because of the several simultaneous strong and weak hydrogen bonds between the TM molecules as well as favorable close packing. It is likely that the 22bp molecules template the formation of the rings of TM enabling this sort of clathrate packing to take place. There is some movement of the
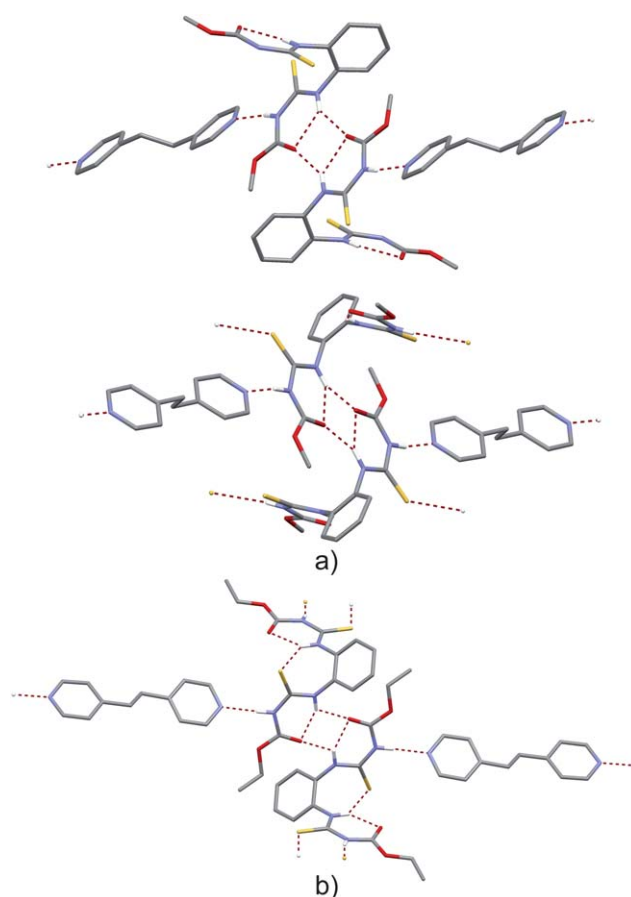

Fig. 4 Hydrogen bonded pairs in (a) the two domains of the TM·bis(4-pyridyl)ethane co-crystals and (b) the TE·1,2-bis(4-pyridyl)ethane co-crystals with C–H hydrogen atoms removed for clarity.

22bp inside the ring and the MeCN molecule, which suggests that bigger guests could fit better in the ring cavity and in place of the MeCN. The packing coefficient of the 22bp co-crystal with TE, however, is the lowest of all the co-crystal structures, which suggest that favorable weak interactions must play a major role. As the amount of hydrogen bonding is the same as in the other structures, this structure is stabilized by the aromatic stacking interactions between the TE molecules.
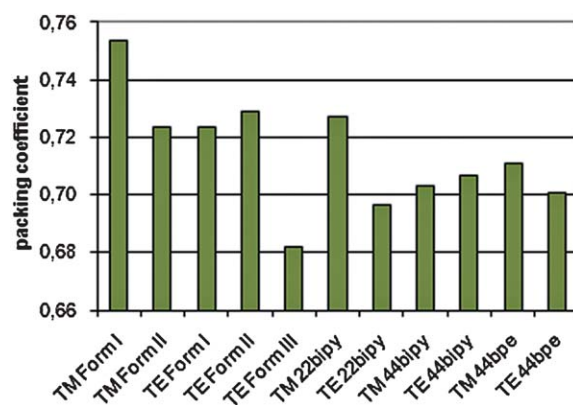

Fig. 5 Packing coefficients of the polymorphs of TM and TE and the bipyridine co-crystals.

The 4,4′-bipyridine and 1,2-bis(4-pyridyl)ethane co-crystals have low packing coefficients and are formed because of the strong hydrogen bonds between the 44bp/44bpe and thiophanate molecules. These strong hydrogen bonds are also the reason why the packing of these co-crystals of TM and TE is more similar to each other than that of the 2,2′-bipyridine co-crystals. The 44bpe co-crystal with TM is the most densely packed of all the hydrogen bonded co-crystals, likely because of the formation of the two slightly different layers. Because of the efficient use of hydrogen bonds, the 44bpe co-crystal with TE has voids of 50 Å³ and a lower packing coefficient than the other hydrogen bonded co-crystals.

Grinding

Having acquired such a group of similar co-crystals, we decided to test whether the known co-crystals could be produced with liquid-assisted grinding. Compounds were weighed in the ratios of the known co-crystals and water : ethanol was used as solvent. The TM–22bp co-crystal is known to contain MeCN, but this was disregarded partly to see if a co-crystal that does not contain acetonitrile exists.

The TM–44bp and TE–22bp mixtures formed the known co-crystals when grinded with water : ethanol, but the TE–44bp and TM–22bp mixtures did not (Fig. 6). The TE–44bp mixture PXRD does not have peaks from pure 44bp or any of the known TE polymorphs. This could indicate another co-crystal that has better packing than the original co-crystal. The crystallization of such a co-crystal was attempted from ethanol without success. The TM–22bp PXRD is similar to the calculated pattern from the MeCN solvate of the co-crystal, indicating that the formation of the co-crystal may not depend on the presence of MeCN, and that there may be a co-crystal in which ethanol takes the place of MeCN. Attempts to crystallize this were also unsuccessful. New grinding experiments of TE–44bp and TM–22bp with 3 drops of 25% MeCN in H_2O were performed to confirm the formation of the original co-crystals. Both the samples gave the pattern of the known co-crystal structure.

Thermomicroscopy

Thermomicroscopy was used to investigate the melting behavior of the co-crystals. As both TM and TE decompose upon melting,[10,11] we were unable to use melt film methods to produce the co-crystals. We wanted to know if the formation of a co-
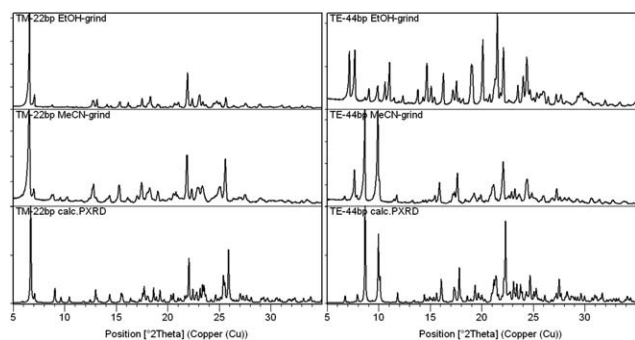

Fig. 6 PXRD patterns of the EtOH and MeCN grinding experiments of TM with 22bp (left) and TE with 44bp (right) compared to the patterns calculated from the structures.

Table 2 Approximate melting points (MP) of the compounds and co-crystals as determined by hot stage microscopy

Compound	MP (pure)	MP (22bp co-crystal)	MP (44bp co-crystal)
TM	167	110–120	160–170
TE	192	120–130	140–150
22bp	70	—	—
44bp	110	—	—

crystal could be determined with the thermomicroscope. The melting ranges for the co-crystals in Table 2 are very broad due to poor repeatability of the melting observations caused by interference from the unco-crystallized pure compounds and due to the changes in the crystallite size when the co-crystals were produced with different methods.

The melting points of the TM–22bp co-crystal and both the TE co-crystals, however, do show a clear difference to the pure compounds, all melting at temperatures in between the melting points of the pure compounds, and the formation of these co-crystals can thus be recognized with thermomicroscopic observations. The TM–44bp co-crystal, however, melts only at the temperature where TM starts to decompose and cannot be recognized in this manner from pure TM. If single crystals were not obtained to confirm the co-crystal formation, thermomicroscopy, which requires very little material, could still have been used together with powder diffraction to help verify at least three of the co-crystals.

The melting points of the found co-crystals are mostly lower than those of the pure actives, which is the opposite of what is generally preferred for agrochemical co-crystals. For TM and TE, making the melting point higher with co-crystals is unlikely because of the thermal decomposition of the actives upon melting. The co-crystals could still be viable forms for processing of formulations because of possible solubility differences and crystallite shape preferences.

Conclusions

With the discovery of these six co-crystals, we have acquired further proof that TM and TE can include a number of guest molecules in their crystal lattices. The reasons for this behavior seem to be the large amount of hydrogen bond donors coupled to weak acceptors, the flexibility of the molecules, as well as the possibility for aromatic interactions. The two arms of the molecule being *ortho*-substituted in the benzene ring may also make the packing of the molecules somewhat difficult *via* forcing the sulfur and oxygen atoms quite close to each other unless guest molecules are included between the arms.

The N–H···N–pyridine hydrogen bond was found to be a reliable synthon for co-crystal design with TM and TE. The inherent weakness of the N–H···S=C hydrogen bond commonly used in the polymorphs and solvates of TM and TE is likely the cause, as was found for a more simple dithiooxamide by Piotrkowska *et al.*[27]

An important goal was to see how much the size difference of TM and TE affects the crystallization behavior and packing of the molecules. For the hydrogen bonded co-crystals of TM and TE the size difference of the molecules was found to affect the

structures in a subtle manner. The main hydrogen bond pairing was always the same, but the size of the molecule influenced the usage of the rest of the donors and acceptors. In the TM co-crystals with 4,4′-bipyridine and 1,2-bis(4-pyridyl)ethane one N–H donor and all or most of the C=S acceptors are unused, while in the TE co-crystal with 4,4′-bipyridine only a pyridine acceptor is unused and in the TE co-crystal with 1,2-bis(4-pyridyl)ethane all donors and acceptors are in use. This is because the larger molecules have more conformational freedom and can pack well even with more hydrogen bonds in use. For the 2,2′-bipyridine co-crystals the difference is not clear while TE makes a channel structure known to also fit other molecules and TM builds a clathrate type structure templated by the 2,2′-bipyridine.

The stoichiometric diversity in the co-crystals with the same bipyridines raises the question of whether there could be more co-crystals with different molar ratios like in the work of Trask et al.[28] on caffeine co-crystals. The TE–4,4′-bipyridine sample grinded with EtOH could be an example of this, but further investigation is required. We believe there are also numerous other possibilities for co-crystals as well as solvates of TM and TE. Similar molecules with flexible chains attached ortho on a benzene ring could also be reliable co-crystal formers and we plan on further investigating these.

Acknowledgements

Notes and references

1 A. D. Bond, CrystEngComm, 2007, 9, 833–834, DOI: 10.1039/b708112j.
2 C. B. Aakeröy and D. J. Salmon, CrystEngComm, 2005, 7, 439–448, DOI: 10.1039/b505883j.
3 O. Almarsson and M. J. Zaworotko, Chem. Commun., 2004, (17), 1889–1896, DOI: 10.1039/b402150a.
4 N. Blagden, M. de Matas, P. T. Gavan and P. York, Adv. Drug Delivery Rev., 2007, 59, 617–630, DOI: 10.1016/j.addr.2007.05.011.
5 D. McNamara, S. Childs, J. Giordano, A. Iarriccio, J. Cassidy, M. Shet, R. Mannion, E. O'Donnell and A. Park, Pharm. Res., 2006, 23, 1888–1897, DOI: 10.1007/s11095-006-9032-3.
6 Pat., WO 2008/117037, 2008.
7 Pat., WO 2008/117060, 2008.
8 G. R. Desiraju, Angew. Chem., Int. Ed., 2007, 46, 8342–8356, DOI: 10.1002/anie.200700534.
9 G. R. Desiraju, Angew. Chem., Int. Ed. Engl., 1995, 34, 2311–2327, DOI: 10.1002/anie.199523111.
10 E. Nauha, H. Saxell, M. Nissinen, E. Kolehmainen, A. Schäfer and R. Schlecker, CrystEngComm, 2009, 11, 2536–2547, DOI: 10.1039/b905511h.
11 E. Nauha, A. Ojala, M. Nissinen and H. Saxell, CrystEngComm, 2011, 13, 4956–4964, DOI: 10.1039/c1ce05077j.
12 I. D. H. Oswald, W. D. S. Motherwell and S. Parsonsa, Acta Crystallogr., Sect. B: Struct. Sci., 2005, 61, 46–57, DOI: 10.1107/S0108768104028605.
13 H. W. Roesky and M. Andruh, Coord. Chem. Rev., 2003, 236, 91–119, DOI: 10.1016/S0010-8545(02)00218-7.
14 I. D. H. Oswald, D. R. Allan, P. A. McGregor, W. D. S. Motherwell, S. Parsons and C. R. Pulham, Acta Crystallogr., Sect. B: Struct. Sci., 2002, 58, 1057–1066, DOI: 10.1107/S0108768102015987.
15 A. Ranganathan, V. R. Pedireddi, G. Sanjayan, K. N. Ganesh and C. N. R. Rao, J. Mol. Struct., 2000, 522, 87–94, DOI: 10.1016/S0022-2860(99)00356-7.
16 S. Varughese and V. R. Pedireddi, Chem.–Eur. J., 2006, 12, 1597–1609, DOI: 10.1002/chem.200500570.
17 T.-F. Tan, J. Han, M.-L. Pang, H.-B. Song, Y.-X. Ma and J.-B. Meng, Cryst. Growth Des., 2006, 6, 1186–1193, DOI: 10.1021/cg060009y.
18 B. Ye, M. Tong and X. Chen, Coord. Chem. Rev., 2005, 249, 545–565, DOI: 10.1016/j.ccr.2004.07.006.
19 PANalytical B.V., 2006, 2.2b.
20 G. M. Sheldrick, Acta Crystallogr., Sect. A: Found. Crystallogr., 2008, 64, 112–122, DOI: 10.1107/S0108767307043930.
21 Z. Otwinowski, D. Borek, W. Majewski and W. Minor, Acta Crystallogr., Sect. A: Found. Crystallogr., 2003, 59, 228–234, DOI: 10.1107/S0108767303005488.
22 C. F. Macrae, P. R. Edgington, P. McCabe, E. Pidcock, G. P. Shields, R. Taylor, M. Towler and J. van de Streek, J. Appl. Crystallogr., 2006, 39, 453–457, DOI: 10.1107/S002188980600731X.
23 R. K. Harris, Analyst, 2006, 131, 351–373, DOI: 10.1039/b516057j.
24 M. C. Etter and J. C. MacDonald, Acta Crystallogr., Sect. B: Struct. Sci., 1990, B46, 256–262; J. Bernstein, R. E. Davis, L. Shimoni and N.-L. Chung, Angew. Chem., Int. Ed. Engl., 1995, 34, 1555–1573.
25 A. I. Kitaĭgorodskiĭ, Organic Chemical Crystallography, Consultants Bureau, New York, 1961.
26 Calculation of Molecular Properties and Drug-likeness, Molinspiration, http://molinspiration.com/.
27 B. Piotrkowska, A. Wasilewska, M. Gdaniec and T. Polonski, CrystEngComm, 2008, 10, 1421–1428, DOI: 10.1039/b806061d.
28 A. V. Trask, J. van de Streek, W. D. S. Motherwell and W. Jones, Cryst. Growth Des., 2005, 5, 2233–2241, DOI: 10.1021/cg0501682.

IV

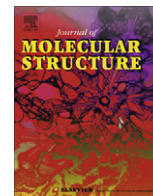## Co-crystal design using a pyridine-amine synthon for an agrochemical active containing a thioamide group

by

E. Nauha, & M. Nissinen, 2011

Co-crystals of an agrochemical active – A pyridine-amine synthon for a thioamide group

E. Nauha, M. Nissinen *

Department of Chemistry, Nanoscience Center, University of Jyväskylä, P.O. Box 35, FIN-40014 Jyväskylä, Finland

ARTICLE INFO

ABSTRACT

Five novel co-crystals of thiophanate-ethyl (TE), an agrochemical active, with di(2-pyridyl)ketone (1), 2-benzoylpyridine (2), 3-benzoylpyridine (3), 4-phenylpyridine (4) and biphenyl (5) were found and crystal structures of four of them (TE1–TE3, TE5) solved by single crystal X-ray diffraction. Three of the co-crystals (TE1–TE3) form by way of a reliable pyridine-amine hydrogen bond synthon and one (TE5) because of close packing effects. The fifth co-crystal was identified by X-ray powder diffraction. The work demonstrates the usage of a reliable supramolecular synthon for crystal engineering, while concurrently reminds that the close packing of even very similar molecules cannot be fully predicted.

© 2011 Elsevier B.V. All rights reserved.

1. Introduction

Co-crystal, i.e. multi-component molecular crystals, are of an interest to pharmaceutical and agrochemical companies as possible new and improved dosage forms [1]. The primary method of designing new co-crystals is the use of reliable supramolecular synthons [2], which are mainly composed of hydrogen bonds. Active ingredients often have many functional groups capable of hydrogen bonding, which makes this approach somewhat challenging.

We have previously investigated the polymorphism and solvate formation of an agrochemical active, thiophanate-ethyl (TE, diethyl 4,4′-(o-phenylene)bis(3-thioallophanate)) (Scheme 1), which was found to have four polymorphs and seven solvate forms [3]. TE and an analogous thiophanate-methyl [4] both have a hydrogen bonded pyridine solvate. They have also been found to make co-crystals [5] with 2,2′-bipyridine, 4,4′-bipyridine and 1,2-bis (4-pyridyl)ethane. Inspired by the success, we wanted to investigate whether the N—H···N hydrogen bond could be used further for co-crystal design and screened with a series of azaheterocycles (1–4) (Scheme 1) containing a pyridine moiety. Biphenyl (5) (Scheme 1) was selected as a comparison to investigate if it would take the place of 2,2′-bipyridine and make an arrangement also seen in several isomorphous solvates of TE.

Piotrkowska et al. [6] found dithiooxamide, a simpler compound that has some of the same functionalities as TE and TM, to be a convenient substrate for construction of two component supramolecular structures with azaheterocycles. Ellis et al. [7] used the same approach for a number of thiocarbamide derivatives and found that they formed many 2:1 co-crystals with bipyridine-type molecules. As agrochemical and pharmaceutical actives are often quite complicated molecules with a number of functionalities, we wanted to see if the pyridine-amine synthon would work well for such systems.

## 2. Experimental

2.1. Slurries and crystallizations

TE (99% Chem Service), biphenyl (99% Merck), 4-phenylpyridine (97% Aldrich), 2-benzoylpyridine (99% Aldrich), 3-benzoylpyridine (97% Aldrich), di(2-pyridyl)ketone (99% Aldrich), distilled water and solvents of analytical purity (min 99%) were used in the crystallization and slurry experiments. Screening was started with slurries (50 mg of TE and 25–150 mg of azaheterocycle/biphenyl depending on solubility and starting from a ratio of 1:1) in 2 ml of 1:4 MeCN:water, which were mixed for 1 month in RT. Evaporation crystallizations of the slurry samples in 1:1 MeCN:water or in MeCN (in the case of 2-benzoylpyridine) resulted in single crystals suitable for crystal structure determination for samples of TE with (1), (2), (3) and (5).

2.2. Powder X-ray diffraction

For powder X-ray diffraction (PXRD) analysis the original compounds and the slurries were pressed to a zero background silicon

* Corresponding author. Tel.: +358 50 428 0804; fax: +358 14 617 412.
E-mail address: maija.nissinen@jyu.fi (M. Nissinen).
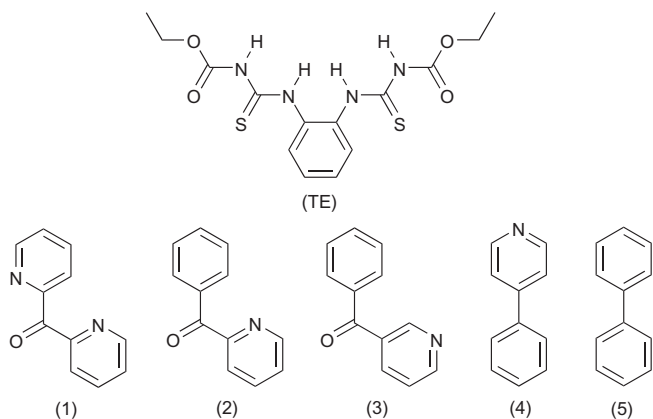
Scheme 1. Molecular structures of TE, di(2-pyridyl)ketone (1), 2-benzoylpyridine (2), 3-benzoylpyridine (3), 4-phenylpyridine (4) and biphenyl (5).

plate and measured on a PANalytical X'Pert Pro system in reflection mode with Cu Kα1-radiation. A 2θ-angle range of 3–35° and a step time of 60 s were used with step resolution of 0.0167°. Figures were drawn with X'Pert HighScore Plus [8].

2.3. Single crystal X-ray diffraction

The single crystal X-ray diffraction data was collected on Nonius Kappa CCD-diffractometer with Apex II detector at 173 K, using graphite-monochromated Cu Kα radiation (λ = 1.54178 Å). Absorption correction was performed with Denzo-SMN 1997 [9]. The structures were solved using direct methods, refined, and expanded by using Fourier techniques with the SHELX-97 software package [10]. All non-hydrogen atoms were refined anisotropically. Hydrogen atoms were placed in idealized positions or found from the electron density map (hydrogen bonding N—H hydrogens), and included in structure factor calculations. The N—H hydrogen atoms found in the electron density map were restrained to a distance of 0.91 Å for TE1 and TE2 to give the best fit to the X-ray data and to ensure stable refinement. Pictures of the structures were drawn with Mercury 2.4 [11]. Crystal data and

refinement parameters are presented in Table 1. To verify the identity of the isomorphic co-crystals, cross refinement of the differing C/N in di(2-pyridyl)ketone and 2-benzoylpyridine were done resulting in higher R-values and too small/large ellipsoids.

3. Results and discussion

3.1. Hydrogen bonded co-crystals

The isomorphic di(2-pyridyl ketone) (TE1) and 2-benzoylpyridine (TE2) co-crystals have a ratio of 1:1 TE:(1)/(2). The structures exhibit a complicated array of single and bifurcated hydrogen bonds (Fig. 1), unlike in the other TE structures [3,5], where a pairing of two donors and acceptors is often seen. The two N—H hydrogen atoms that participate in a S(6) intramolecular motif [12] are not further hydrogen bonded. However, the C=O acceptors of the same motif are additionally involved in hydrogen bonding to adjacent bifurcated N—H donors. The C1,1(4) and C1,1(11) motifs starting from the bifurcated N—H donors combine to build double chains of TE molecules running in the direction of the crystallographic b-axis. When C—H donors are taken into account, one of the C=S sulfurs and ether oxygen atoms also participate in hydrogen bonding within the TE chains. The azaheterocycles (1) and (2) are connected to one arm of TE with the pyridine-amine synthon. In addition, the C=O in (1) and (2) have a weak hydrogen bond to the methyl groups of TE of the adjacent chains. In TE1 the other pyridine nitrogen of (1) is, however, not involved in hydrogen bonding.

In TE 3-benzoylpyridine (TE3) co-crystal the ratio of TE to 3-benzoylpyridine (3) is 1:2. The 3-benzoylpyridine molecules are hydrogen bonded to both arms of the TE molecule in a second level D2,2(12) motif (Fig. 2a) containing the pyridine-amine synthon. The assembly is very symmetrical, but the symmetry is not crystallographic on a larger scale. There are weak aromatic C—H⋯O=C hydrogen bonds between adjacent 3-benzoylpyridine molecules as well as from the C=O of TE to the 3-benzoylpyridine molecules. A weak C—H⋯S=C hydrogen bond strengthens the pyridine-amine hydrogen bond. If all the weak hydrogen bonds are taken into account the molecules build up chains (Fig. 2b) that elongate in the direction of the crystallographic a-axis.

Table 1
Crystal data and refinement parameters.

	TE1ekn035	TE2ekn042	TE3ekn033	TE5ekn034
Chemical formula	$C_{14}H_{18}N_4O_4S_2$	$C_{14}H_{18}N_4O_4S_2$	$C_{14}H_{18}N_4O_4S_2$	$C_{14}H_{18}N_4O_4S_2$
	$C_{11}H_8N_2O$	$C_{12}H_9NO$	$2(C_{12}H_9NO)$	$0.5(C_{12}H_{10})$
M_r	554.64	553.65	736.85	447.54
Crystal system	Monoclinic	Monoclinic	Monoclinic	Triclinic
Space group	$P2_1/c$	$P2_1/c$	$P2_1/c$	$P-1$
Temperature (K)	173	173	173	173
a (Å)	12.7612 (7)	12.8497 (5)	10.4541 (4)	8.8861 (1)
b (Å)	8.3916 (4)	8.5996 (3)	26.8015 (11)	10.0077 (2)
c (Å)	26.3679 (14)	26.0775 (9)	13.1925 (6)	12.7746 (3)
α (°)	90	90	90	85.098 (2)
β (°)	112.022 (3)	112.182 (2)	102.607 (2)	78.793 (1)
γ (°)	90	90	90	79.930 (1)
V (Å^3)	2617.6 (2)	2668.4 (2)	3607.2 (3)	1095.65 (4)
Z	4	4	4	2
μ (mm^{-1})	2.26	2.20	1.80	2.49
Crystal size (mm)	0.15 × 0.05 × 0.05	0.12 × 0.10 × 0.06	0.30 × 0.08 × 0.06	0.22 × 0.22 × 0.20
T_{min}, T_{max}	0.728, 0.896	0.778, 0.879	0.614, 0.900	0.610, 0.635
No. of meas., indep. and obs. [$I > 2\sigma(I)$] reflections	6507, 4031, 2035	7725, 4631, 3414	11,459, 6233, 3761	5449, 3754, 3396
R_{int}	0.137	0.069	0.107	0.085
$R[F^2 > 2\sigma(F^2)]$, $wR(F^2)$, S	0.079, 0.214, 1.03	0.050, 0.126, 1.05	0.064, 0.164, 1.02	0.046, 0.126, 1.03
No. of reflections	4031	4631	6233	3754
No. of parameters	345	357	484	285
No. of restraints	4	4	0	0
$\Delta\rho_{max}$, $\Delta\rho_{min}$ (e Å^{-3})	0.39, −0.36	0.24, −0.29	0.32, −0.28	0.29, −0.28

The PXRD patterns measured from the slurry samples, except for the 2-benzoylpyridine, matched well with the calculated powder diffraction patterns of the determined structures (Fig. 3). The reason for the mismatch between the slurry powder and the
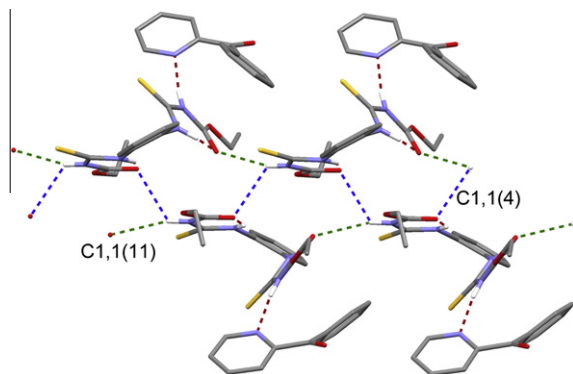

Fig. 1. Hydrogen bonding chains in the di(2-pyridyl ketone) (TE1) and 2-benzoyl-pyridine (TE2) co-crystals with C—H hydrogen atoms removed for clarity. (In the web version C1,1(4) motif hydrogen bonds are in blue, C1,1(11) motif hydrogen bonds in green and other hydrogen bonds in red.)
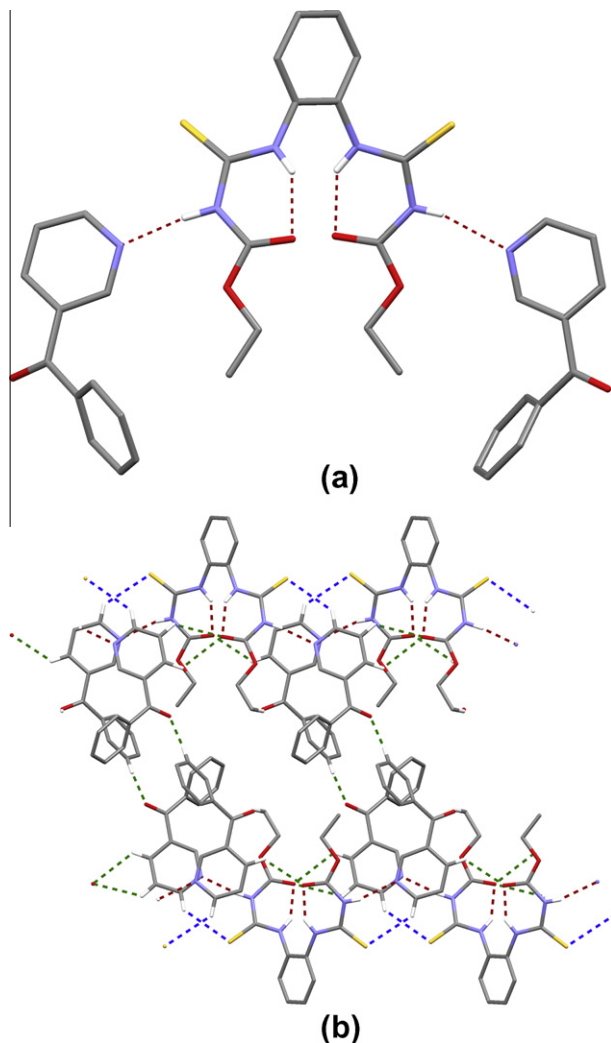
Fig. 2. (a) Strong hydrogen bonding and (b) the weakly hydrogen bonded chains in the 3-benzoylpyridine (TE3) co-crystal with non-hydrogen bonding hydrogen atoms removed for clarity. (In the web version strong hydrogen bonds in red, weak C—H···O=C hydrogen bonds in green and weak C—H···S=C hydrogen bonds in blue.)

determined structure of TE2 indicates the formation of another crystal form that, however, did not crystallize as suitably sized and quality single crystals when the slurry sample was used for the single crystal experiments. No single crystals for the TE co-crystal with 4-phenylpyridine (TE4) were acquired, but the PXRD pattern of the slurry sample was of neither 4-phenylpyridine nor any of the known TE forms, indicating the formation of a co-crystal (Fig. 4). Hydrogen bonding wise the co-crystal (TE4) is expected to be similar to the TE co-crystal with 4,4′-bipyridine [5], which only
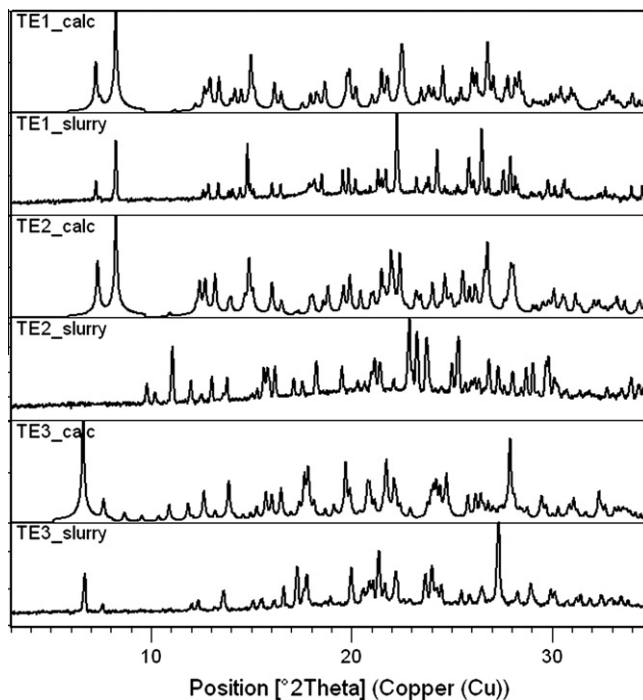

Fig. 3. Experimental slurry PXRD patterns and calculated PXRD patterns of co-crystals TE1, TE2 and TE3.
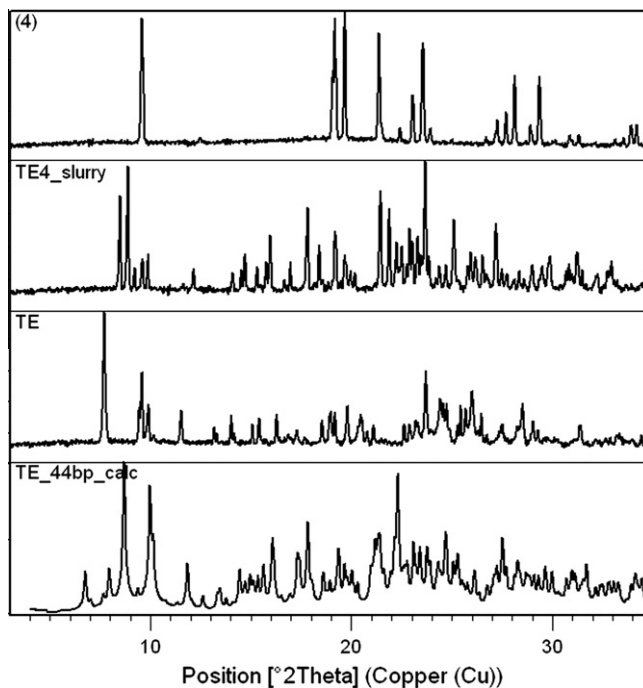

Fig. 4. PXRD patterns of 4-phenylpyridine (4), the TE4 slurry sample, TE and the calculated PXRD pattern of the TE co-crystal with 4,4′-bipyridine.

uses one of the pyridine functional groups for hydrogen bonding to TE. The PXRD patterns of these were compared, but they are not similar (Fig. 4). The TE co-crystal with 4,4′-bipyridine, however, has a Z' of 3 and is likely polymorphic, so a similar hydrogen bonding arrangement for TE4, but with different packing, is still likely.

3.2. Biphenyl

In order to explore the effect of general molecular shape vs. the effect of the N—H···N synthon we crystallized TE with biphenyl. The arrangement (Fig. 5) in the biphenyl co-crystal (TE5), however, is different to that of the 2,2′-bipyridine co-crystal [5] even though the ratio of TE to guest (2:1) is the same. The main hydrogen bonding network of TE molecules is the same with chains of TE connected with a R2,2(8) motif consisting of two N—H···S═C hydrogen bonds. The chains pack parallel to each other with the aid of π–π interactions between the TE benzene rings with ring centroid to centroid distances of 3.81 Å. There are also weak hydrogen bonds from the C═O of TE to one of the benzene ring hydrogen atoms in an adjacent chain. The biphenyl molecules are located
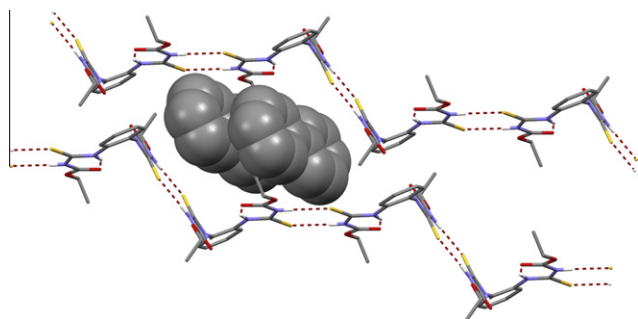

Fig. 5. Hydrogen bonding in the biphenyl co-crystal (TE5) with two biphenyl molecules between the chains shown in space fill style and C—H hydrogen atoms removed for clarity.
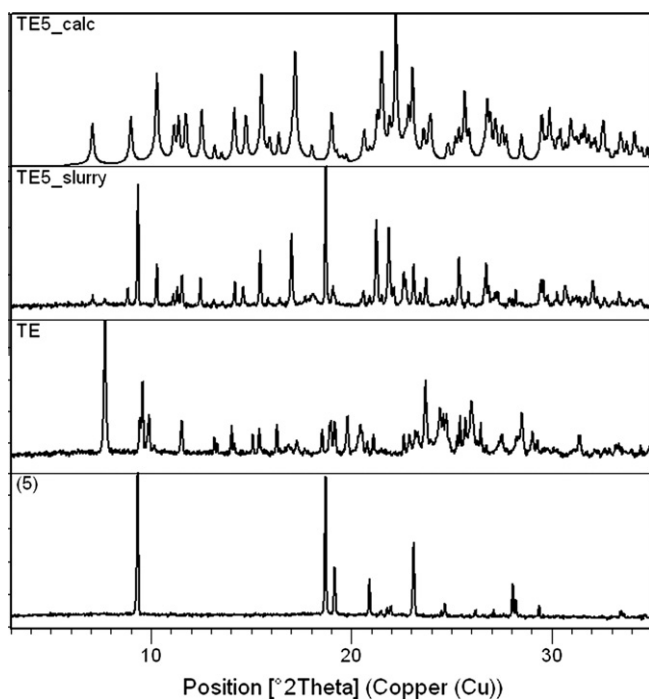

Fig. 6. PXRD patterns of biphenyl (5), TE, the TE5 slurry with peaks of (5) visible, and the calculated pattern from the structure.

between the chains in discrete cavities with no clear interactions to the TE molecules. The PXRD pattern of the slurry sample (Fig. 6) still contained peaks of pure biphenyl (5), but otherwise the pattern matched well with the pattern calculated from the single crystal structure.

4. Conclusions

Five novel co-crystal forms of TE with a selected group of pyridine containing molecules and a structurally similar biphenyl were found and the crystal structures of four of these solved with single crystal X-ray diffraction. Co-crystal design using the pyridine-amine synthon works well for TE, even though it has other functionalities, which could hinder formation of the desired synthon. The packing of the biphenyl co-crystal, however, could not be predicted even though the shape of the molecule is very similar to 2,2′-bipyridine, for which TE builds a packing arrangement containing channels of guest also seen in a number of isomorphic solvates [3]. If no strong hydrogen bonding, like the pyridine amine synthon, to a guest is formed, TE builds chains connected via a R2,2(8) motif of two N—H···S═C hydrogen bonds. These chains, which are also seen in most of the polymorphs of TE [3], can organize to leave in hydrophobic cavities that the guests can fill. The non-hydrogen bonding guest molecules, like biphenyl, likely act as templates for the packing of the chains. The strong N—H···N synthon breaks the formation of these chains and is a determining factor in the formation of the co-crystal structures of TE. The pyridine-amine synthon was found to be very useful in the design of co-crystals for molecules containing a thioamide group (—C(═S)—N(H)—), which is seen in agrochemical and pharmaceutical actives.

Supplementary material

CCDC 838991–838994 contain the supplementary crystallographic data for this paper. These data can be obtained free of charge via http://www.ccdc.cam.ac.uk/conts/retrieving.html (or from the Cambridge Crystallographic Data Centre, 12, Union Road, Cambridge CB2 1EZ, UK; fax: +44 1223 336033).

Acknowledgements

References

[1] P. Wishweshwar, J.A. McMahon, M.J. Zaworotko, Crystal engineering of pharmaceutical co-crystals, in: E.R.T. Tiekink, J.J. Vittal (Eds.), Frontiers in Crystal Engineering, John Wiley & Sons, England, 2006, pp. 25–46.
[2] G.R. Desiraju, Angew. Chem. Int. Ed. Eng. 34 (1995) 2311, doi:10.1002/anie.199523111.
[3] E. Nauha, A. Ojala, M. Nissinen, H. Saxell, CrystEngComm 13 (2011) 4956, doi:10.1039/C1CE05077J.
[4] E. Nauha, H. Saxell, M. Nissinen, E. Kolehmainen, A. Schäfer, R. Schlecker, CrystEngComm 11 (2009) 2536, doi:10.1039/b905511h.
[5] E. Nauha, E. Kolehmainen, M. Nissinen, CrystEngComm 13 (2011) 6531, doi:10.1039/C1CE05730H.
[6] B. Piotrkowska, A. Wasilewska, M. Gdaniec, T. Polonski, CrystEngComm 10 (2008) 1421.
[7] C.A. Ellis, M.A. Miller, J. Spencer, J. Zukerman-Schpector, E.R.T. Tiekink, CrystEngComm 11 (2009) 1352.
[8] PANalytical B.V., 2.2b, 2006.
[9] Z. Otwinowski, D. Borek, W. Majewski, W. Minor, Acta Cryst. A59 (2003) 228, doi:10.1107/S0108767303005488.
[10] G.M. Sheldrick, Acta Cryst. A64 (2008) 112.
[11] C.F. Macrae, P.R. Edgington, P. McCabe, E. Pidcock, G.P. Shields, R. Taylor, M. Towler, J. van de Streek, J. Appl. Cryst. 39 (2006) 453, doi:10.1107/S002188980600731X.
[12] M.C. Etter, J.C. MacDonald, Acta Cryst. B46 (1990) 256;
J. Bernstein, R.E. Davis, L. Shimoni, N-L. Chung, Angew. Chem. Int. Ed. Engl. 34 (1995) 1555.

V

Crystalline complexes of 4-hydroxy benzoic acid and selected pesticides

by

H. E. Saxell, R. Israels, A. Schäfer, M. Bratz, H. W. Höffken, I. Brode, E. Nauha, M. Nissinen, 2010

(54) **Title**: CRYSTALLINE COMPLEXES OF 4-HYDROXY BENZOIC ACID AND SELECTED PESTICIDES

(57) **Abstract**: The present invention relates to crystalline complexes of 4-hydroxy benzoic acid and selected pesticides. It also relates to agriculturally useful compositions of the complexes.

DEPARTMENT OF CHEMISTRY, UNIVERSITY OF JYVÄSKYLÄ

RESEARCH REPORT SERIES

1. Vuolle, Mikko: Electron paramagnetic resonance and molecular orbital study of radical ions generated from (2.2)metacyclophane, pyrene and its hydrogenated compounds by alkali metal reduction and by thallium(III)trifluoroacetate oxidation. (99 pp.) 1976

2. Pasanen, Kaija: Electron paramagnetic resonance study of cation radical generated from various chlorinated biphenyls. (66 pp.) 1977

3. Carbon-13 Workshop, September 6-8, 1977. (91 pp.) 1977

4. Laihia, Katri: On the structure determination of norbornane polyols by NMR spectroscopy. (111 pp.) 1979

5. Nyrönen, Timo: On the EPR, ENDOR and visible absorption spectra of some nitrogen containing heterocyclic compounds in liquid ammonia. (76 pp.) 1978

6. Talvitie, Antti: Structure determination of some sesquiterpenoids by shift reagent NMR. (54 pp.) 1979

7. Häkli, Harri: Structure analysis and molecular dynamics of cyclic compounds by shift reagent NMR. (48 pp.) 1979

8. Pitkänen, Ilkka: Thermodynamics of complexation of 1,2,4-triazole with divalent manganese, cobalt, nickel, copper, zinc, cadmium and lead ions in aqueous sodium perchlorate solutions. (89 pp.) 1980

9. Asunta, Tuula: Preparation and characterization of new organometallic compounds synthesized by using metal vapours. (91 pp.) 1980

10. Sattar, Mohammad Abdus: Analyses of MCPA and its metabolites in soil. (57 pp.) 1980

11. Bibliography 1980. (31 pp.) 1981

12. Knuuttila, Pekka: X-Ray structural studies on some divalent 3d metal compounds of picolinic and isonicotinic acid N-oxides. (77 pp.) 1981

13. Bibliography 1981. (33 pp.) 1982

14. 6th National NMR Symposium, September 9-10, 1982, Abstracts. (49 pp.) 1982

15. Bibliography 1982. (38 pp.) 1983

16. Knuuttila, Hilkka: X-Ray structural studies on some Cu(II), Co(II) and Ni(II) complexes with nicotinic and isonicotinic acid N-oxides. (54 pp.) 1983

17. Symposium on inorganic and analytical chemistry, May 18, 1984, Program and Abstracts. (100 pp.) 1984

18. Knuutinen, Juha: On the synthesis, structure verification and gas chromatographic determination of chlorinated catechols and guaiacols occuring in spent bleach liquors of kraft pulp mill. (30 pp.) 1984

19. Bibliography 1983. (47 pp.) 1984

20. Pitkänen, Maija: Addition of BrCl, B$_2$ and Cl$_2$ to methyl esters of propenoic and 2-butenoic acid derivatives and ^{13}C NMR studies on methyl esters of saturated aliphatic mono- and dichlorocarboxylic acids. (56 pp.) 1985

21. Bibliography 1984. (39 pp.) 1985

22. Salo, Esa: EPR, ENDOR and TRIPLE spectroscopy of some nitrogen heteroaromatics in liquid ammonia. (111 pp.) 1985

23. Humppi, Tarmo: Synthesis, identification and analysis of dimeric impurities of chlorophenols. (39 pp.) 1985

24. Aho, Martti: The ion exchange and adsorption properties of sphagnum peat under acid conditions. (90 pp.) 1985

25. Bibliography 1985 (61 pp.) 1986

26. Bibliography 1986. (23 pp.) 1987

27. Bibliography 1987. (26 pp.) 1988

28. Paasivirta, Jaakko (Ed.): Structures of organic environmental chemicals. (67 pp.) 1988

29. Paasivirta, Jaakko (Ed.): Chemistry and ecology of organo-element compounds. (93 pp.) 1989

30. Sinkkonen, Seija: Determination of crude oil alkylated dibenzothiophenes in environment. (35 pp.) 1989

31. Kolehmainen, Erkki (Ed.): XII National NMR Symposium Program and Abstracts. (75 pp.) 1989

32. Kuokkanen, Tauno: Chlorocymenes and Chlorocymenenes: Persistent chlorocompounds in spent bleach liquors of kraft pulp mills. (40 pp.) 1989

33. Mäkelä, Reijo: ESR, ENDOR and TRIPLE resonance study on substituted 9,10-anthraquinone radicals in solution. (35 pp.) 1990

34. Veijanen, Anja: An integrated sensory and analytical method for identification of off-flavour compounds. (70 pp.) 1990

35. Kasa, Seppo: EPR, ENDOR and TRIPLE resonance and molecular orbital studies on a substitution reaction of anthracene induced by thallium(III) in two fluorinated carboxylic acids. (114 pp.) 1990

36. Herve, Sirpa: Mussel incubation method for monitoring organochlorine compounds in freshwater recipients of pulp and paper industry. (145 pp.) 1991

37. Pohjola, Pekka: The electron paramagnetic resonance method for characterization of Finnish peat types and iron (III) complexes in the process of peat decomposition. (77 pp.) 1991

38. Paasivirta, Jaakko (Ed.): Organochlorines from pulp mills and other sources. Research methodology studies 1988-91. (120 pp.) 1992

39. Veijanen, Anja (Ed.): VI National Symposium on Mass Spectrometry, May 13-15, 1992, Abstracts. (55 pp.) 1992

40. Rissanen, Kari (Ed.): The 7. National Symposium on Inorganic and Analytical Chemistry, May 22, 1992, Abstracts and Program. (153 pp.) 1992

41. Paasivirta, Jaakko (Ed.): CEOEC'92, Second Finnish-Russian Seminar: Chemistry and Ecology of Organo-Element Compounds. (93 pp.) 1992

42. Koistinen, Jaana: Persistent polychloroaromatic compounds in the environment: structure-specific analyses. (50 pp.) 1993

43. Virkki, Liisa: Structural characterization of chlorolignins by spectroscopic and liquid chromatographic methods and a comparison with humic substances. (62 pp.) 1993

44. Helenius, Vesa: Electronic and vibrational excitations in some biologically relevant molecules. (30 pp.) 1993

45. Leppä-aho, Jaakko: Thermal behaviour, infrared spectra and x-ray structures of some new rare earth chromates(VI). (64 pp.) 1994

46. Kotila, Sirpa: Synthesis, structure and thermal behavior of solid copper(II) complexes of 2-amino-2- hydroxymethyl-1,3-propanediol. (111 pp.) 1994

47. Mikkonen, Anneli: Retention of molybdenum(VI), vanadium(V) and tungsten(VI) by kaolin and three Finnish mineral soils. (90 pp.) 1995

48. Suontamo, Reijo: Molecular orbital studies of small molecules containing sulfur and selenium. (42 pp.) 1995

49. Hämäläinen, Jouni: Effect of fuel composition on the conversion of fuel-N to nitrogen oxides in the combustion of small single particles. (50 pp.) 1995

50. Nevalainen, Tapio: Polychlorinated diphenyl ethers: synthesis, NMR spectroscopy, structural properties, and estimated toxicity. (76 pp.) 1995

51. Aittola, Jussi-Pekka: Organochloro compounds in the stack emission. (35 pp.) 1995

52. Harju, Timo: Ultrafast polar molecular photophysics of (dibenzylmethine)borondifluoride and 4-aminophthalimide in solution. (61 pp.) 1995

53. Maatela, Paula: Determination of organically bound chlorine in industrial and environmental samples. (83 pp.) 1995

54. Paasivirta, Jaakko (Ed.): CEOEC'95, Third Finnish-Russian Seminar: Chemistry and Ecology of Organo-Element Compounds. (109 pp.) 1995

55. Huuskonen, Juhani: Synthesis and structural studies of some supramolecular compounds. (54 pp.) 1995

56. Palm, Helena: Fate of chlorophenols and their derivatives in sawmill soil and pulp mill recipient environments. (52 pp.) 1995

57. Rantio, Tiina: Chlorohydrocarbons in pulp mill effluents and their fate in the environment. (89 pp.) 1997

58. Ratilainen, Jari: Covalent and non-covalent interactions in molecular recognition. (37 pp.) 1997

59. Kolehmainen, Erkki (Ed.): XIX National NMR Symposium, June 4-6, 1997, Abstracts. (89 pp.) 1997

60. Matilainen, Rose: Development of methods for fertilizer analysis by inductively coupled plasma atomic emission spectrometry. (41 pp.) 1997

61. Koistinen, Jari (Ed.): Spring Meeting on the Division of Synthetic Chemistry, May 15-16, 1997, Program and Abstracts. (36 pp.) 1997

62. Lappalainen, Kari: Monomeric and cyclic bile acid derivatives: syntheses, NMR spectroscopy and molecular recognition properties. (50 pp.) 1997

63. Laitinen, Eira: Molecular dynamics of cyanine dyes and phthalimides in solution: picosecond laser studies. (62 pp.) 1997

64. Eloranta, Jussi: Experimental and theoretical studies on some quinone and quinol radicals. (40 pp.) 1997

65. Oksanen, Jari: Spectroscopic characterization of some monomeric and aggregated chlorophylls. (43 pp.) 1998

66. Häkkänen, Heikki: Development of a method based on laser-induced plasma spectrometry for rapid spatial analysis of material distributions in paper coatings. (60 pp.) 1998

67. Virtapohja, Janne: Fate of chelating agents used in the pulp and paper industries. (58 pp.) 1998

68. Airola, Karri: X-ray structural studies of supramolecular and organic compounds. (39 pp.) 1998

69. Hyötyläinen, Juha: Transport of lignin–type compounds in the receiving waters of pulp mills. (40 pp.) 1999

70. Ristolainen, Matti: Analysis of the organic material dissolved during totally chlorine-free bleaching. (40 pp.) 1999

71. Eklin, Tero: Development of analytical procedures with industrial samples for atomic emission and atomic absorption spectrometry. (43 pp.) 1999

72. Välisaari, Jouni: Hygiene properties of resol-type phenolic resin laminates. (129 pp.) 1999

73. Hu, Jiwei: Persistent polyhalogenated diphenyl ethers: model compounds syntheses, characterization and molecular orbital studies. (59 pp.) 1999

74. Malkavaara, Petteri: Chemometric adaptations in wood processing chemistry. (56 pp.) 2000

75. Kujala Elena, Laihia Katri, Nieminen Kari (Eds.): NBC 2000, Symposium on Nuclear, Biological and Chemical Threats in the 21st Century. (299 pp.) 2000

76. Rantalainen, Anna-Lea: Semipermeable membrane devices in monitoring persistent organic pollutants in the environment. (58 pp.) 2000

77. Lahtinen, Manu: *In situ* X-ray powder diffraction studies of Pt/C, CuCl/C and Cu_2O/C catalysts at elevated temperatures in various reaction conditions. (92 pp.) 2000

78. Tamminen, Jari: Syntheses, empirical and theoretical characterization, and metal cation complexation of bile acid-based monomers and open/closed dimers. (54 pp.) 2000

79. Vatanen, Virpi: Experimental studies by EPR and theoretical studies by DFT calculations of α-amino-9,10-anthraquinone radical anions and cations in solution. (37 pp.) 2000

80. Kotilainen, Risto: Chemical changes in wood during heating at 150-260 °C. (57 pp.) 2000

81. Nissinen, Maija: X-ray structural studies on weak, non-covalent interactions in supramolecular compounds. (69 pp.) 2001

82. Wegelius, Elina: X-ray structural studies on self-assembled hydrogen-bonded networks and metallosupramolecular complexes. (84 pp.) 2001

83. Paasivirta, Jaakko (Ed.): CEOEC'2001, Fifth Finnish-Russian Seminar: Chemistry and Ecology of Organo-Element Compounds. (163 pp.) 2001

84. Kiljunen, Toni: Theoretical studies on spectroscopy and atomic dynamics in rare gas solids. (56 pp.) 2001

85. Du, Jin: Derivatives of dextran: synthesis and applications in oncology. (48 pp.) 2001

86. Koivisto, Jari: Structural analysis of selected polychlorinated persistent organic pollutants (POPs) and related compounds. (88 pp.) 2001

87. Feng, Zhinan: Alkaline pulping of non-wood feedstocks and characterization of black liquors. (54 pp.) 2001

88. Halonen, Markku: Lahon havupuun käyttö sulfaattiprosessin raaka-aineena sekä havupuun lahontorjunta. (90 pp.) 2002

89. Falábu, Dezsö: Synthesis, conformational analysis and complexation studies of resorcarene derivatives. (212 pp.) 2001

90. Lehtovuori, Pekka: EMR spectroscopic studies on radicals of ubiquinones Q-n, vitamin K_3 and vitamine E in liquid solution. (40 pp.) 2002

91. Perkkalainen, Paula: Polymorphism of sugar alcohols and effect of grinding on thermal behavior on binary sugar alcohol mixtures. (53 pp.) 2002

92. Ihalainen, Janne: Spectroscopic studies on light-harvesting complexes of green plants and purple bacteria. (42 pp.) 2002

93. Kunttu, Henrik, Kiljunen, Toni (Eds.): 4th International Conference on Low Temperature Chemistry. (159 pp.) 2002

94. Väisänen, Ari: Development of methods for toxic element analysis in samples with environmental concern by ICP-AES and ETAAS. (54 pp.) 2002

95. Luostarinen, Minna: Synthesis and characterisation of novel resorcarene derivatives. (200 pp.) 2002

96. Louhelainen, Jarmo: Changes in the chemical composition and physical properties of wood and nonwood black liquors during heating. (68 pp.) 2003

97. Lahtinen, Tanja: Concave hydrocarbon cyclophane B-prismands. (65 pp.) 2003

98. Laihia, Katri (Ed.): NBC 2003, Symposium on Nuclear, Biological and Chemical Threats – A Crisis Management Challenge. (245 pp.) 2003

99. Oasmaa, Anja: Fuel oil quality properties of wood-based pyrolysis liquids. (32 pp.) 2003

100. Virtanen, Elina: Syntheses, structural characterisation, and cation/anion recognition properties of nano-sized bile acid-based host molecules and their precursors. (123 pp.) 2003

101. Nättinen, Kalle: Synthesis and X-ray structural studies of organic and metallo-organic supramolecular systems. (79 pp.) 2003

102. Lampiselkä, Jarkko: Demonstraatio lukion kemian opetuksessa. (285 pp.) 2003

103. Kallioinen, Jani: Photoinduced dynamics of Ru(dcbpy)$_2$(NCS)$_2$ – in solution and on nanocrystalline titanium dioxide thin films. (47 pp.) 2004

104. Valkonen, Arto (Ed.): VII Synthetic Chemistry Meeting and XXVI Finnish NMR Symposium. (103 pp.) 2004

105. Vaskonen, Kari: Spectroscopic studies on atoms and small molecules isolated in low temperature rare gas matrices. (65 pp.) 2004

106. Lehtovuori, Viivi: Ultrafast light induced dissociation of Ru(dcbpy)(CO)$_2$I$_2$ in solution. (49 pp.) 2004

107. Saarenketo, Pauli: Structural studies of metal complexing schiff bases , Schiff base derived *N*-glycosides and cyclophane π-prismands. (95 pp.) 2004

108. Paasivirta, Jaakko (Ed.): CEOEC'2004, Sixth Finnish-Russian Seminar: Chemistry and Ecology of Organo-Element Compounds. (147 pp.) 2004

109. Suontamo, Tuula: Development of a test method for evaluating the cleaning efficiency of hard-surface cleaning agents. (96 pp.) 2004

110. Güneş, Minna: Studies of thiocyanates of silver for nonlinear optics. (48 pp.) 2004

111. Ropponen, Jarmo: Aliphatic polyester dendrimers and dendrons. (81 pp.) 2004

112. Vu, Mân Thi Hong: Alkaline pulping and the subsequent elemental chlorine-free bleaching of bamboo (*Bambusa procera*). (69 pp.) 2004

113. Mansikkamäki, Heidi: Self-assembly of resorcinarenes. (77 pp.) 2006

114. Tuononen, Heikki M.: EPR spectroscopic and quantum chemical studies of some inorganic main group radicals. (79 pp.) 2005

115. Kaski, Saara: Development of methods and applications of laser-induced plasma spectroscopy in vacuum ultraviolet. (44 pp.) 2005

116. Mäkinen, Riika-Mari: Synthesis, crystal structure and thermal decomposition of certain metal thiocyanates and organic thiocyanates. (119 pp.) 2006

117. Ahokas, Jussi: Spectroscopic studies of atoms and small molecules isolated in rare gas solids: photodissociation and thermal reactions. (53 pp.) 2006

118. Busi, Sara: Synthesis, characterization and thermal properties of new quaternary ammonium compounds: new materials for electrolytes, ionic liquids and complexation studies. (102 pp.) 2006

119. Mäntykoski, Keijo: PCBs in processes, products and environment of paper mills using wastepaper as their raw material. (73 pp.) 2006

120. Laamanen, Pirkko-Leena: Simultaneous determination of industrially and environmentally relevant aminopolycarboxylic and hydroxycarboxylic acids by capillary zone electrophoresis. (54 pp.) 2007

121. Salmela, Maria: Description of oxygen-alkali delignification of kraft pulp using analysis of dissolved material. (71 pp.) 2007

122. Lehtovaara, Lauri: Theoretical studies of atomic scale impurities in superfluid ^{4}He. (87 pp.) 2007

123. Rautiainen, J. Mikko: Quantum chemical calculations of structures, bonding, and spectroscopic properties of some sulphur and selenium iodine cations. (71 pp.) 2007

124. Nummelin, Sami: Synthesis, characterization, structural and retrostructural analysis of self-assembling pore forming dendrimers. (286 pp.) 2008

125. Sopo, Harri: Uranyl(VI) ion complexes of some organic aminobisphenolate ligands: syntheses, structures and extraction studies. (57 pp.) 2008

126. Valkonen, Arto: Structural characteristics and properties of substituted cholanoates and *N*-substituted cholanamides. (80 pp.) 2008

127. Lähde, Anna: Production and surface modification of pharmaceutical nano- and microparticles with the aerosol flow reactor. (43 pp.) 2008

128. Beyeh, Ngong Kodiah: Resorcinarenes and their derivatives: synthesis, characterization and complexation in gas phase and in solution. (75 pp.) 2008

129. Välisaari, Jouni, Lundell, Jan (Eds.): Kemian opetuksen päivät 2008: uusia oppimisympäristöjä ja ongelmalähtöistä opetusta. (118 pp.) 2008

130. Myllyperkiö, Pasi: Ultrafast electron transfer from potential organic and metal containing solar cell sensitizers. (69 pp.) 2009

131. Käkölä, Jaana: Fast chromatographic methods for determining aliphatic carboxylic acids in black liquors. (82 pp.) 2009

132. Koivukorpi, Juha: Bile acid-arene conjugates: from photoswitchability to cancer cell detection. (67 pp.) 2009

133. Tuuttila, Tero: Functional dendritic polyester compounds: synthesis and characterization of small bifunctional dendrimers and dyes. (74 pp.) 2009

134. Salorinne, Kirsi: Tetramethoxy resorcinarene based cation and anion receptors: synthesis, characterization and binding properties. (79 pp.) 2009

135. Rautiainen, Riikka: The use of first-thinning Scots pine (*Pinus sylvestris*) as fiber raw material for the kraft pulp and paper industry. (73 pp.) 2010

136. Ilander, Laura: Uranyl salophens: synthesis and use as ditopic receptors. (199 pp.) 2010

137. Kiviniemi, Tiina: Vibrational dynamics of iodine molecule and its complexes in solid krypton - Towards coherent control of bimolecular reactions? (73 pp.) 2010

138. Ikonen, Satu: Synthesis, characterization and structural properties of various covalent and non-covalent bile acid derivatives of N/O-heterocycles and their precursors. (105 pp.) 2010

139. Siitonen, Anni: Spectroscopic studies of semiconducting single-walled carbon nanotubes. (56 pp.) 2010

140. Raatikainen, Kari: Synthesis and structural studies of piperazine cyclophanes – Supramolecular systems through Halogen and Hydrogen bonding and metal ion coordination. (69 pp.) 2010

141. Leivo, Kimmo: Gelation and gel properties of two- and three-component Pyrene based low molecular weight organogelators. (116 pp.) 2011

142. Martiskainen, Jari: Electronic energy transfer in light-harvesting complexes isolated from *Spinacia oleracea* and from three photosynthetic green bacteria *Chloroflexus aurantiacus*, *Chlorobium tepidum*, and *Prosthecochloris aestuarii.*(55 pp.) 2011

143. Wichmann, Oula: Synthesis, characterization and structural properties of [O,N,O,X´] aminobisphenolate metal complexes. (101 pp.) 2011

144. Ilander, Aki: Development of ultrasound-assisted digestion methods for the determination of toxic element concentrations is ash samples by ICP-OES. (58 pp.) 2011

145. The Combined XII Spring Meeting of the Division of Synthetic Chemistry and XXXIII Finnish NMR Symposium. Book of Abstracts. (90 pp.) 2011

146. Valto, Piia: Development of fast analysis methods for extractives in papermaking process waters. (73 pp.) 2011

147. Andersin, Jenni: Catalytic activity of palladium-based nanostructures in the conversion of simple olefinic hydro- and chlorohydrocarbons from first principles. (78 pp.) 2011

148. Aumanen, Jukka: Photophysical properties of dansylated poly(propylene amine) dendrimers. (55 pp.) 2011

149. Kärnä, Minna: Ether-functionalized quaternary ammonium ionic liquids – synthesis, characterization and physicochemical properties. (76 pp.) 2011

150. Jurček, Ondřej: Steroid conjugates for applications in pharmacology and biology. (57 pp.) 2011